小宮研究

KOMIYA KENKYU

第 2 号「WITH THE CAMBRIDGE」

令和 5 年 11 月 22 日発行

「小宮研究」第 2 号のテーマは「WITH THE CAMBRIDGE」です。
私は、1994 年に千葉工業大学に助手として着任しました。専任講師、助教授を経て、2001 年に教授になりました。そして、2012 年から 2020 年までの 8 年間は、千葉工大の学長を務めました。来春、千葉工大に着任して 30 年目を迎えます。
私は、ケンブリッジ大学で専任教員として教えていたことがあります。千葉工大に就職して 3 年目に、突然ケンブリッジ大学から、千葉工大を辞めてケンブリッジ大学へ来て働いてくれないかという連絡が来ました。もちろん、千葉工大に着任したばかりでしたので、断ろうとしました。ところが、当時の豊田耕作理事長が、外国に行って学ぶ日本人はたくさんいるが、外国で教える日本人はほとんどいないから、イギリスの最高峰の大学に行って、イギリス人のエリートに日本の工学を教えて来いと言ってくれました。また、豊田理事長は、何年イギリスで仕事してもいいが、最後は必ず千葉工大へ帰ってきて、イギリスで経験したことを千葉工大の研究と教育に役立てて欲しいと言いました。
私は、これらの豊田理事長からの有り難い言葉を胸に、ケンブリッジ大学に専任教員として就職しました。ところが、渡英して、私にはイギリスの食事が全く合わないことが、直ぐにわかりました。美味しいものがないため食欲が湧かず、最初の 3 ヶ月間で 15 キロ位体重が減ってしまいました。食べ物が美味しくないのはケンブリッジ大学のせいではありませんが、このまま長くこの国に住んでいたら、病気になってしまうと思い、2 年間働いて日本に戻ってきました。日本に帰ってわかったことは、日本の食事は本当においしいということです。
短い間でしたが、ケンブリッジ大学では多くの研究を行い、多くの仲間と出会い親しくなることができました。これらは、私の人生で、かけがえのない宝物となって現在に至っています。本書には、私がケンブリッジ大学の仲間と一緒に発表した数多くの論文の中から、Soils and Foundations 誌掲載論文、Géotechnique 誌掲載論文と投稿時の査読意見、Géotechnique 誌掲載論文に寄せられた討議論文、ASCE Journal of Geotechnical and Geoenvironmental Engineering 誌掲載論文とそれに寄せられた討議論文を掲載します。また付録には、これらの論文を発表したことによって、約 20 年後にチュラロンコン大学で起こった素晴らしい出来事を紹介します。

令和 5 年 11 月 22 日
小 宮 一 仁

I took a job as a research associate at the Chiba Institute of Technology (CIT) in 1994. After working as a lecturer and then as an associate professor, I became a professor in 2001. And I had assumed the office of the president of CIT from 2012 to 2020. Then next spring will mark my 30th year since joining CIT.
I have taught and have conducted research full-time at the Engineering Department of University of Cambridge (CUED). During my third year working for CIT, some academic members of the University of Cambridge suddenly contacted me and they asked if I would quit my job to come work in CUED. Of course, since I had only just recently joined CIT, I turned them down first. Then Kosaku Toyota, the Chairman of the Board of Trustees at the time, told me that although many Japanese people study abroad, few Japanese teacher has taught abroad. He asked me to take advantage of this opportunity to teach Japanese engineering to elite students at the world's top university. He also told me that I could work in the UK for as many years as I wanted to, but that in the end he wanted me to be sure to return to CIT so that I could apply what I had experienced in the UK to the research and education efforts here.

After receiving these encouraging words from Chairman Toyota, I decided to accept the full-time academic position at the University of Cambridge. However, I immediately realized upon arriving in the UK that the local food did not agree with me at all. I lost around 15 kilograms during the first three months. Thinking that my body might break down if I stayed for much longer, I decided to return to Japan after about two years. After coming home, I realized just how delicious Japanese food is!
During my short few years at University of Cambridge, I was conducting a lot of research and I made many irreplaceable friends. I will never forget my experience at University of Cambridge; it's a treasure for a lifetime that I will always cherish. I have published many refereed papers in journal articles and many papers in refereed conference proceedings with my colleagues at University of Cambridge. Out of those, this book includes (i) a paper in Soils and Foundations, (ii) a paper in Géotechnique, the reviewer's opinion on the submitted paper and the corresponding discussion paper, and (iii) a paper in ASCE Journal of Geotechnical and Geoenvironmental Engineering and the corresponding discussion paper. In addition, the appendix introduces an amazing event that occurred at the Chulalongkorn University in Thailand about 20 years after the publication of these papers.

Kazuhito Komiya
22nd November 2023

Soils and Foundations
Volume 39, No.3
pp.37-52
June 1999
Japanese Geotechnical Society

SOILS AND FOUNDATIONS Vol. 39, No. 3, 37-52, June 1999
Japanese Geotechnical Society

FINITE ELEMENT MODELLING OF EXCAVATION AND ADVANCEMENT PROCESSES OF A SHIELD TUNNELLING MACHINE

KAZUHITO KOMIYA[i], KENICHI SOGA[ii], HIROKAZU AKAGI[iii], TOSHIYUKI HAGIWARA[iv] and MALCOLM D. BOLTON[v]

ABSTRACT

During shield tunnelling operation, a shield machine is driven forward by applying mechanical jack forces behind the machine tail and excavating the soil in front of the machine with its cutting face. In this study, the advancement and excavation processes of the shield tunnelling operation are modelled using the finite element method in order to investigate the effect of these construction processes on the ground response. A new excavating finite element, which models the disturbed soil in front of the cutting face, is introduced. The operation of shield advancement and of soil excavation is simulated using the finite element remeshing technique at each time step of the analysis. The accuracy of the finite element remeshing technique is discussed by analysing one-dimensional consolidation of an isotropic elastic medium. The proposed modelling techniques of shield tunnelling construction are applied to simulate a tunnelling project in Tokyo and the numerical results are compared with the field measurements. The soil deformation mechanism associated with the shield tunnelling operation is examined in detail.

Key words: cohesive soil, deformation, finite element method, stress, tunnel, water pressure (**IGC**: H5/E13)

INTRODUCTION

During shield tunnelling operations, the magnitude and distribution of the ground deformations are largely controlled by the construction process. The factors that affect the ground deformation are (Lee et al., 1992; Mair and Taylor, 1997):

(i) changes in earth pressure at the cutting face,
(ii) variation of external forces applied to the machine such as jacking forces,
(iii) shearing of soil at the shield-soil interface due to friction,
(iv) introduction of the tail void and injection of backfill between the tunnel lining and excavated tunnel cavity,
(v) overexcavation due to steering of the machine, and
(vi) long term consolidation due to excess pore pressure dissipation and changes in groundwater hydraulic conditions.

Many of the above factors are closely linked to the interaction between the soil and shield machine, which cause the stress state of the soil to change. The possible earth pressure changes due to the shield machine advancement are illustrated in Fig. 1. The figure is based on extensive earth pressure and deformation measurements of a sewer tunnel construction through soft ground in Tokyo conducted by Hashimoto (1984). The figure implies that the nature of the problem is three-dimensional and that the magnitude of earth pressure change is related to the machine characteristics, construction procedure, operator's control, etc. Therefore, when estimating the ground deformation caused by shield tunnel construction, care should be taken of how to model the character-

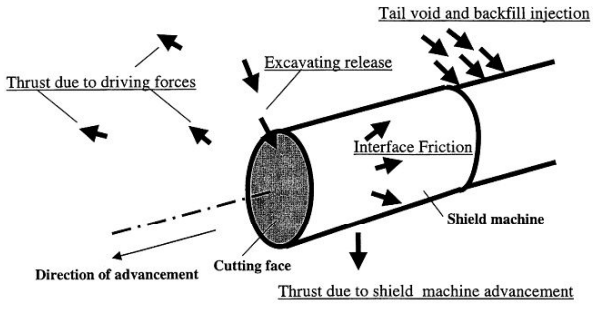

Fig. 1. Earth pressure changes due to the shield machine advancement (after Hashimoto, 1984)

[i] Associate Professor of Civil Engineering, Chiba Institute of Technology, Japan and Research Associate in Engineering, University of Cambridge, UK.
[ii] Lecturer in Engineering, University of Cambridge, UK.
[iii] Professor of Civil Engineering, Waseda University.
[iv] Chief cleak of Nishimatsu Research Institute, Nishimatsu Construction Co., LTD.
[v] Reader in Engineering, University of Cambridge, UK.
Manuscript was received for review on November 11, 1998.
Written discussions on this paper should be submitted before January 1, 2000 to the Japanese Geotechnical Society, Sugayama Bldg. 4F, Kanda Awaji-cho 2-23, Chiyoda-ku, Tokyo 101-0063, Japan. Upon request the closing date may be extended one month.

istics of the machine and the construction process.

Because of the complex boundary conditions of a shield tunnelling problem, the use of the finite element method is one of the popular methods to investigate the ground deformation behaviour. In general, the finite element analysis results reported in the literature have contributed greatly in understanding various deformation mechanisms associated with shield tunnelling (e.g. Katzenbach and Breth, 1981; Clough and Leca, 1989; Swoboda et al., 1989; Lee et al., 1992; Ohtsu et al., 1993; Addenbrooke, 1996, 1997; Addenbrooke et al., 1997; and many others). However, these past studies are often made to examine the above-mentioned factors individually. Also, many of the reported analyses use the in-situ stress condition as the initial condition of the problem without any in-depth consideration of other factors affecting the change in the stress state of the soil. For example, both the steering problem and interface friction problems are expected to influence the soil conditions around the shield machine at the same time during its advancement and their effects cannot possibly be analysed separately. Therefore, there is a need to examine the combined effect of various aspects of shield tunnelling operations on ground deformation within one analysis.

The construction process of a shield operation is often modelled by applying external forces, introducing traction, or forcing displacements at the boundary nodes of a finite element mesh under a spatially fixed tunnel configuration. In these analyses, the advancement of the shield machine is not modelled. In reality, however, the stress-strain state of the soil changes continuously as the shield machine advances and then passes the spatial point of interest. In order to fully understand the deformation mechanism associated with shield tunnelling, the stress history (or stress path) caused by shield advancement needs to be investigated.

In this study, the advancement of a shield machine and excavation at the cutting face are modelled, so that the effect of these construction processes on ground deformation and stress-strain behaviour of the soil around the tunnel can be examined. In open cut excavation problems, the finite element method has proved to be useful for design purposes, even though the actual process of excavation is not modelled in an exact manner. Therefore, an attempt was made to model the cutting operation of shield tunnelling within the framework of the finite element method.

The excavation and advancement of a shield machine are modelled by (i) remeshing the finite elements at each time step, (ii) introducing the excavating elements of a fixed size in front of the shield machine elements, and (iii) applying external forces such as jacking forces behind the shield machine and slurry (or earth) pressures at the cutting face. By doing so, it is aimed to satisfy the continuity condition as well as the boundary conditions of the problem.

The proposed modelling techniques are used to simulate shield tunnelling construction project through clayey ground in Tokyo. The results from the three dimensional coupled soil-pore water analysis were compared to the actual field measurements in order to examine the stress-deformation behaviour of the soils caused by the shield tunnelling operation.

The modelling method described in this paper originates from the doctoral dissertation by Komiya. In the present study, their method has been modified by implementing a more robust remeshing procedure for three dimensional finite element analysis of tunnel excavation. The accuracy of this new method is verified by performing one-dimensional consolidation analysis and comparing its result to the theoretical solution. A three dimensional finite element analysis of shield tunnelling in soft clayey deposits was carried out using the new method. The computed three dimensional settlement trough and the effective stress paths in the clay around a shield machine are carefully examined and reported in this study.

FINITE ELEMENT MODELLING OF EXCAVATION AND ADVANCEMENT OF A SHIELD MACHINE

EXCAVATING ELEMENT

In shield tunnelling work, the soil in front of the cutting face of a shield machine is extremely disturbed by its cutting operation. The exact operation of the cutting process is very difficult to model in the finite element method, because the excavation process itself violates the assumption of continuum mechanics used in the finite element formulation. In the past, this excavation process was commonly modelled by removing the finite elements in front of the machine and applying nodal forces at the boundary, which represents the cutting face (*see* Fig. 2). The applied nodal forces are obtained from the given (or recorded) hydraulic jack forces behind the machine and/or the earth/slurry pressures at the cutting face. Although this modelling technique satisfies the force boundary conditions, the sum of the computed nodal displacements at the cutting front and the length of the removed elements may not necessarily match the actual movement of the shield machine at a given time interval.

In this study, the excavation process is modelled by introducing new excavating finite elements of a fixed size in front of the shield machine (*see* Fig. 3). Solid finite elements are used for the excavating elements, and the presence of these elements in front of the cutting face aims to represent the disturbed area of the ground caused by the excavation process. Mathematically, the introduction of the excavating elements provides the condition where both displacement and force boundaries given by the shield machine operation are satisfied. The boundary conditions are (a) the known advancement of the machine at a given time interval, (b) the given (or recorded) external forces applied by the hydraulic jacks placed between the machine and tunnel lining, and (c) the given (or recorded) earth pressure or slurry pressure at the cutting face.

When various external forces are applied at the bound-

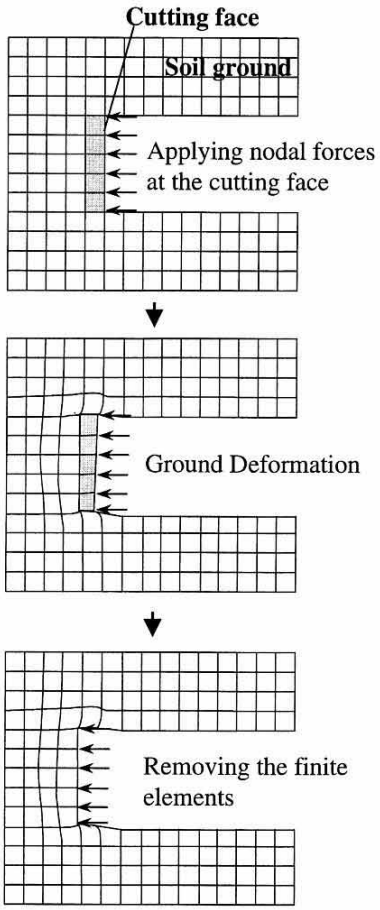

Fig. 2. Conventional excavation modelling

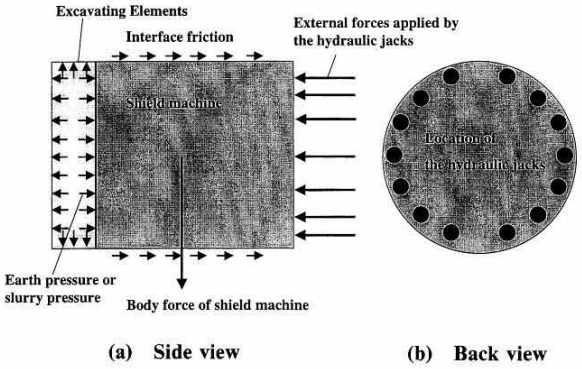

Fig. 3. Excavation modelling using the excavating element

aries of the shield machine as shown in Fig. 3, the process of excavation is represented by the (artificial) deformation of the excavating elements. The size and the constitutive model used for the excavating element are rather arbitrary. However, they need to be selected so that the calculated movement of the shield machine controlled by the given force boundary conditions matches the recorded movement of the shield machine. In this study, the isotropic elastic model was used for convenience. In practice, the size and material properties of the excavating elements are determined by trial and error, so that the computed data are compatible with the monitoring data. However, the elastic properties of the excavating element should be mainly related to the characteristics of the shield machine (shape of the cutter, etc.) and the workmanship. The method which determines the material properties of the excavating elements will be described in detail later on.

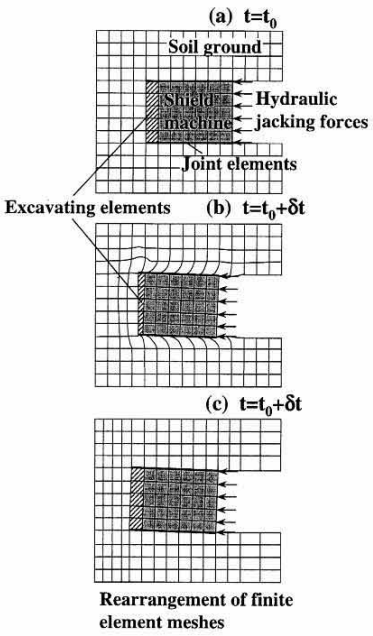

Fig. 4. Advance of shield machine simulated using excavating elements

MODELLING OF SHIELD MACHINE ADVANCEMENT

The advancement of a shield machine is modelled by (i) remeshing the finite elements at each time step, (ii) introducing the excavating elements of a fixed size in front of the shield machine elements, and (iii) applying external forces such as jacking forces behind the shield machine and slurry (or earth) pressures in front of the machine. Sequential illustrations of the finite element modelling of the excavation at the cutting face of the shield machine and the advancement of the tunnelling machine are shown in Fig. 4. The shaded area in the figure represents the proposed excavating element.

Figure 4(a) shows the status of the shield machine at reference time t_0. In order to model the hydraulic jacking forces applied to the shield machine, forces are applied at the nodes that represent the tail end of the shield machine. The applied nodal forces are given from the forces of the hydraulic jacks measured in the field at a given time. For the case of simulating slurry type shield tunnel operation, slurry and water pressures can be applied in the excavating elements, as shown in Fig. 3.

During the time interval of t_0 to $t_0+\delta t$, the excavating elements and the soil elements adjacent to the shield machine will deform by the jacking forces under undrained, partially drained conditions, or fully drained

conditions, depending on the speed of the shield machine and the permeability of the ground. The shield machine itself will act as a rigid body since a large value of stiffness is used for the elements representing the shield machine.

After obtaining a solution for $t=t_0+\delta t$, the finite elements are remeshed as shown in Fig. 4(c). The new mesh will have the same mesh geometry relative to the shield machine as $t=t_0$, but the location of the shield has shifted. Again, the excavating elements will be placed in front of the cutting face before applying external forces given for the next time step. By doing so, the advancement of the shield machine and the associated stress-strain changes of the ground are numerically simulated in a continuous manner.

UPDATING EFFECTIVE STRESSES AND PORE PRESSURES IN REARRANGED MESH

After remeshing, the values of effective stresses and pore pressures of the remeshed elements need be calculated from those obtained in the original deformed mesh. This is necessary because the equilibrium condition needs to be satisfied before conducting the next loading step. The stress interpolation procedure is summarised in the flow-chart shown in Fig. 5.

STEP 1: Element Identification

The first step of the interpolation procedure is identifying an element, which has the rearranged nodal point inside it. The three dimensional finite element used in this study is the eight-noded trilinear element. Let a rearranged nodal point n_R exist inside an element that has eight nodes of n_1 to n_8, as shown in Fig. 6(a). In this case, the volume of the element should be equal to the volume sum of the quadrangular pyramids (V_1 to V_6 as shown in Fig. 6(b)), which are formed by the side plane of the element and the rearranged nodal point n_R. When nodal displacements are small, the volume of V_1 to V_6 can be evaluated by the following vector calculations.

$$
\begin{aligned}
V_1&=(1/6)\{(\overrightarrow{n_1n_2}\times\overrightarrow{n_1n_3})+(\overrightarrow{n_1n_3}\times\overrightarrow{n_1n_4})\}\cdot\overrightarrow{n_1n_R}\\
V_2&=(1/6)\{(\overrightarrow{n_1n_5}\times\overrightarrow{n_1n_6})+(\overrightarrow{n_1n_6}\times\overrightarrow{n_1n_2})\}\cdot\overrightarrow{n_1n_R}\\
V_3&=(1/6)\{(\overrightarrow{n_2n_6}\times\overrightarrow{n_2n_7})+(\overrightarrow{n_2n_7}\times\overrightarrow{n_2n_3})\}\cdot\overrightarrow{n_2n_R}\\
V_4&=(1/6)\{(\overrightarrow{n_3n_7}\times\overrightarrow{n_3n_8})+(\overrightarrow{n_3n_8}\times\overrightarrow{n_3n_4})\}\cdot\overrightarrow{n_3n_R}\\
V_5&=(1/6)\{(\overrightarrow{n_4n_8}\times\overrightarrow{n_4n_5})+(\overrightarrow{n_4n_5}\times\overrightarrow{n_4n_1})\}\cdot\overrightarrow{n_4n_R}\\
V_6&=(1/6)\{(\overrightarrow{n_5n_6}\times\overrightarrow{n_5n_7})+(\overrightarrow{n_5n_7}\times\overrightarrow{n_7n_8})\}\cdot\overrightarrow{n_5n_R}
\end{aligned}
\tag{1}
$$

where $\times$ is the vector product and $\cdot$ is the scalor product.

If the rearranged nodal point exists outside the element, the volume sum of V_1 to V_6 will be larger than the element volume V. By doing this operation, the element, where the rearranged nodal point exists, can be identified automatically. This operation is performed for all the rearranged nodal points.

STEP 1	Identify an element, which includes the rearranged nodal point
STEP 2	Calculate the local coordinate of the rearranged nodal point in the identified element
STEP 3	Compute the incremental displacement of the rearranged nodal points
STEP 4	Evaluate the effective stresses at the Gauss-Legendre integration points of the remeshed elements
STEP 5	Evaluate the pore pressure at the centre of gravity of the remeshed elements
STEP 6	Calculate the residual forces from the equilibrium check

Fig. 5. Flow-chart of the stress interpolation procedure

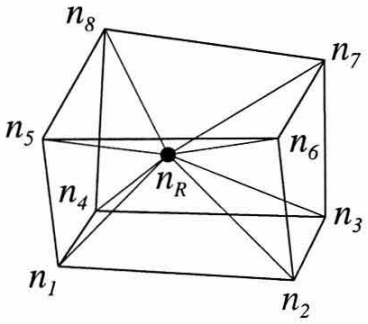

Fig. 6(a). Eight-noded trilinear element and a rearranged nodal point n_R

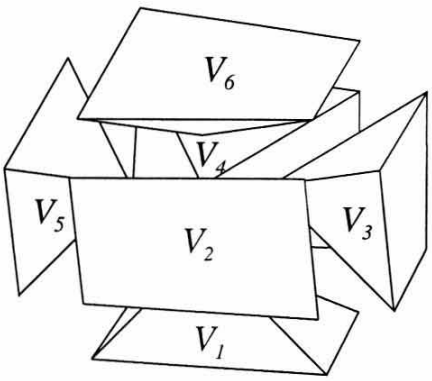

Fig. 6(b). The volume sum of the quadrangular pyramids

STEP 2: Local Coordinates Calculation

The local coordinate system of an eight-noded trilinear element is shown in Fig. 7. Assuming that the rearranged nodal point exists in an element, which has nodal point n_1 to n_8, the local coordinate (ξ, η, ζ) of the rearranged nodal point is calculated using the flow chart shown in Fig. 8. The computational algorithm shown in the figure utilises Eq. (1) to save computing time. The operation "*calc*" in the flow chart is described in Appendix A.

STEP 3: Incremental Displacement Vector Calculation

The internal incremental displacement vector $d\boldsymbol{u}_R$ at

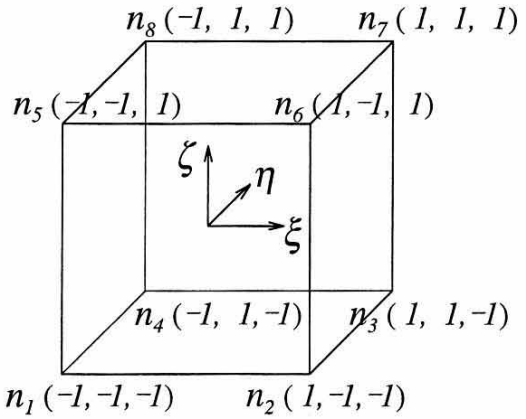

Fig. 7. Local coordinate system of eight noded trilinea element

the rearranged nodal point n_R can be computed from its local coordinate and the incremental displacement vectors of the nodal points n_1 to n_8, using the following equation

$$d\boldsymbol{u}_R = N_i(\xi, \eta, \zeta) d\boldsymbol{u}_i \tag{2}$$

where $N_i(\xi, \eta, \zeta)$ $(i=1, 8)$ is the shape function, and $d\boldsymbol{u}_i$ is the incremental displacement vector at nodal point n_i of the element.

STEP 4: Effective Stress Update

Once the incremental displacement vector of all rearranged nodal points is computed, the effective stress increment $d\boldsymbol{\sigma}'$ at the Gauss-Legendre integration points of the new remeshed finite elements are estimated using the following equation.

$$d\boldsymbol{\sigma}' = \int \boldsymbol{DB} d\boldsymbol{u}_R \tag{3}$$

where $\boldsymbol{D}$ is the stress-strain relationship of the soil skeleton at the Gauss-Legendre integration points, and $\boldsymbol{B}$ is the strain-displacement matrix. The selection of $\boldsymbol{D}$ depends on the state of the soil; so that correct stress path can be followed during the updating of the effective stresses. The effective stresses $\boldsymbol{\sigma}'$ at the Gauss-Legendre integration points of the remeshed elements at $t=t_0+\delta t$ will be

$$\boldsymbol{\sigma}' = \boldsymbol{\sigma}'_0 + d\boldsymbol{\sigma}' \tag{4}$$

where $\boldsymbol{\sigma}'_0$ is the effective stress state at $t=t_0$. Ideally, $\boldsymbol{\sigma}'_0$ should be determined from the effective stress field at $t=t_0$ obtained in the original undeformed mesh. This requires back-calculating the location of the Gauss-Legendre integration points of the remeshed elements at $t=t_0$, and interpolating $\boldsymbol{\sigma}'_0$ at these points. However, this additional calculation increases the computing time. Therefore, in this study, $\boldsymbol{\sigma}'_0$ at the Gauss-Legendre integration point of the remeshed elements is simply assumed to be equal to that of the original undeformed element, provided that the incremental displacements computed at each time step are small. The details of the effective stress updating procedure used in this study are described in Appendix B.

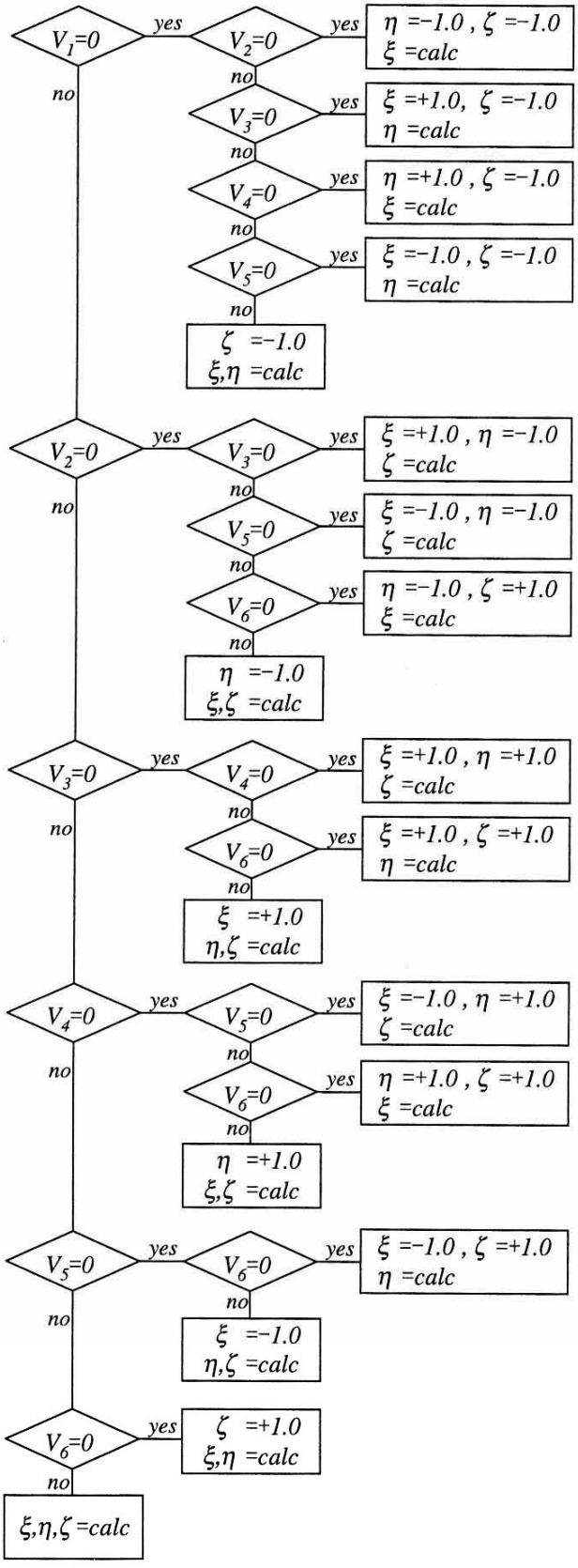

Fig. 8. Flow-chart for calculating of the local coordinate of a rearranged nodal point

STEP 5: Pore Pressure Update

In this study, the coupled stress-deformation-pore pres-

sure interaction was formulated using the method proposed by Akai and Tamura (1978). This method is similar to the one proposed by Christian and Boehmer (1970), where the pore pressure is assigned at the centre of the element. When remeshing is performed, the value of pore water pressure in the element must be updated to satisfy the total stress equilibrium condition.

In this study, it is assumed that the total stresses of the remeshed element are equal to those of the original deformed element at $t=t_0+\delta t$. With this assumption, the pore water pressure p_{wR} of a remeshed element at $t+\delta t$ becomes the sum of the pore pressure of the deformed elements before remeshing and the change in the mean effective stress σ'_m of the remeshed element, as shown in the following equation.

$$p_{wR}=p_w+\sigma'_m-\sigma'_{mR} \tag{5}$$

where p_w is the pore water pressure before remeshing, σ'_m is the mean effective stress of the element before remeshing and σ'_{mR} is that after remeshing.

STEP 6: Residual Forces Calculation

The simplified evaluation of σ'_0 and $d\sigma$ used in Step 4 and 5 will produce some errors when equilibrium is checked. These errors result in residual forces. After stress updating, the residual forces of the rearranged nodal forces $d\phi_R$ are computed using the following equation.

$$d\phi_R=\int \boldsymbol{B}d\sigma_R dV-d\boldsymbol{F} \tag{6}$$

where $d\boldsymbol{F}$ is the external incremental forces.

Further iteration of Step 4 and 5 can be made to obtain the correct stress/pore pressure field in the remeshed condition that satisfies the equilibrium condition. However, this iteration would result in a dramatic increase of computing time. Therefore, in this study, the residual forces computed at the rearranged nodal points are simply added to the loading forces of the subsequent incremental step. A similar technique is used in CRISP94 (Britto, 1994).

SIMULATION OF ONE-DIMENSIONAL CONSOLIDATION USING REMESHING TECHNIQUE

In order to verify the accuracy of the proposed remeshing technique, one-dimensional consolidation finite element analyses with and without the remeshing technique were performed, and the results were compared to Terzaghi's consolidation theory solution.

The finite element meshes and the material properties used in these analyses are shown in Fig. 9. After obtaining a solution for $t=t_0+\delta t$ (Fig. 10(b)), the finite elements were remeshed as shown in Fig. 10(c) and the stress state of each remeshed element was updated. All the remeshed elements have the same mesh geometry. The results of the analyses are compared to Terzaghi's consolidation solution for the relationship between the time factor T_v and the degree of consolidation U which is

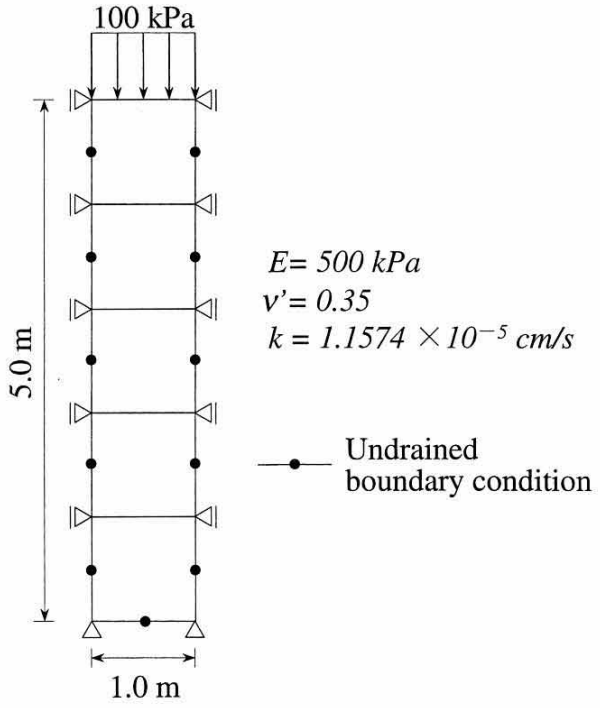

Fig. 9. Finite element model used in the one-dimensional consolidation problem

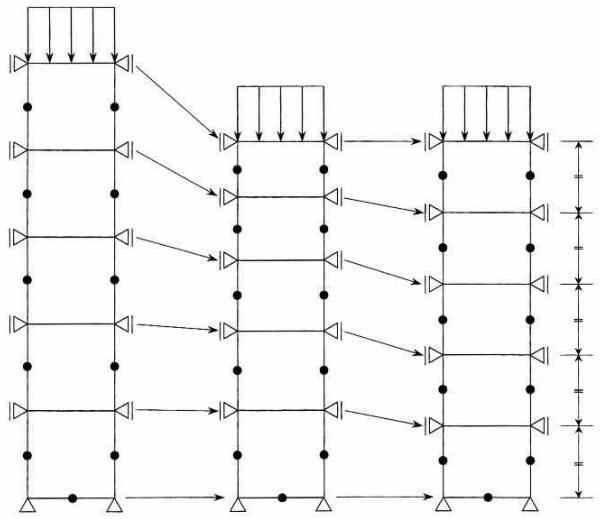

Fig. 10. Rearrangement of finite element meshes

defined as the percentage of the current surface settlement to the final surface settlement, as shown in Fig. 11. The solid circles in the figure are the results obtained by the remeshing technique, whereas the open circles are the results obtained without the remeshing technique. The numerical analysis with the remeshing technique appears to give a better match to Terzaghi's solution.

The computed isochrone curves of the excess pore water pressure are shown in Fig. 12(a) for analysis with remeshing and (b) for analysis without remeshing. The

vertical axis of the figures is the ratio of the distance from the drained surface z to the initial height of the model z_0, whereas the horizontal axis is loaded pressure p (=100 kPa). The result of the analysis with remeshing provides a better match to the theoretical solution, especially at the beginning of the consolidation and at locations close to the drainage boundary.

THREE DIMENSIONAL FINITE ELEMENT MODELLING OF SHIELD TUNNELLING

During shield tunnelling work, the position and direction of the shield machine are controlled by changing the driving forces of the hydraulic jacks installed behind the machine. Therefore, three dimensional movements of the machine, i.e. the pitching and yawing, take place in a complicated manner.

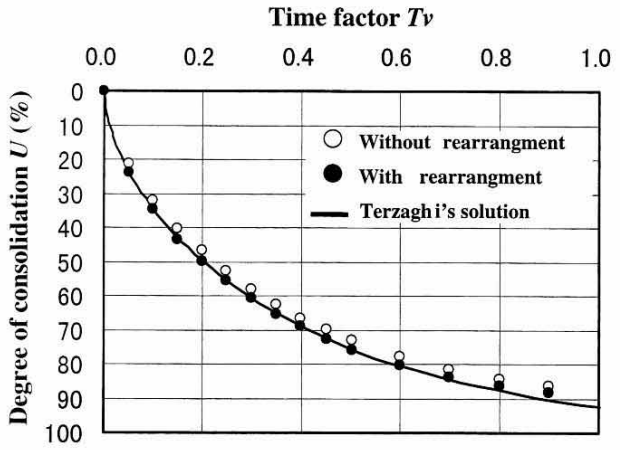

Fig. 11. Relations between the degree of consolidation U and time factor-T_v

Complicated boundary conditions exist, particularly in the case of shield tunnelling in urban areas, since the distance between the shield tunnel and the pre-existing underground structures or the foundations of superstructures frequently becomes very small. Hence, the three dimensional nature of a shield tunnelling problem must be considered carefully in order to have proper control of the construction.

The long term subsidence around a tunnel is directly related to the excess pore pressures generated during the shield machine advancement. Therefore, the coupled soil-pore water analysis is necessary to assess the time-dependent ground deformation caused by shield tunnelling construction.

With the above considerations in mind, a three dimensional coupled soil-pore water analysis was conducted to simulate the construction process of a tunnel of 3.7 m diameter in Tokyo. The tunnel was approximately 33 m deep, and 0.55 km long. The machine used was of shield type with an earth pressure balance, and air bubbles were injected in the excavation chamber to stabilise the soil and control the earth pressure in front of the shield machine.

FINITE ELEMENT MODELLING

Soil Modelling

The Sekiguchi and Ohta's model (1979) was used to model the stress-strain behaviour of the clay. The input parameters used in the analysis are listed in Table 1. Most of the input parameters were determined from the results provided by standard geotechnical tests on samples obtained at various depths. Other input parameters, which were not able to be determined from these tests, were calculated by the method suggested by Iizuka et al. (1985).

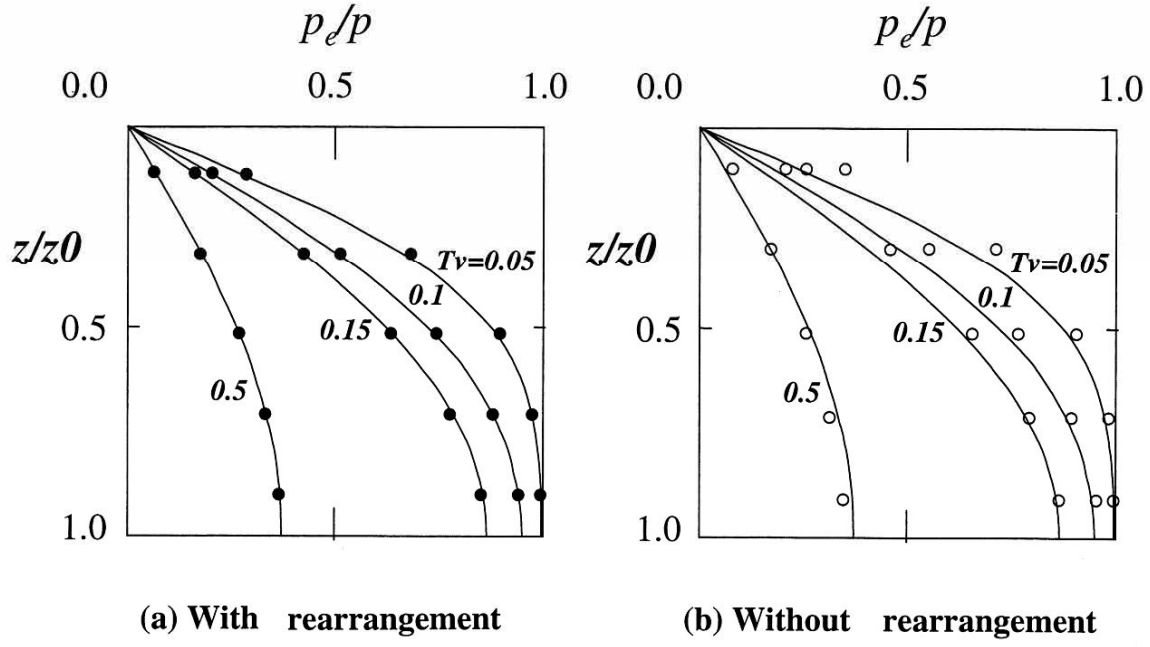

Fig. 12. Isochrone curves of excess pore water pressure

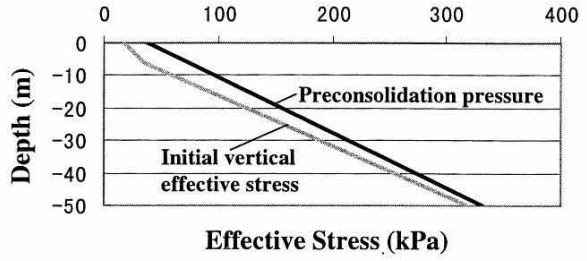

Fig. 13. Preconsolidation pressure and initial vertical effective stress

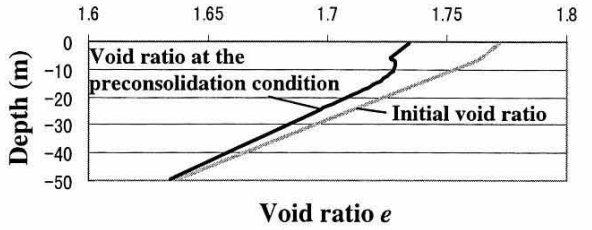

Fig. 14. Distribution of void ratio with depth

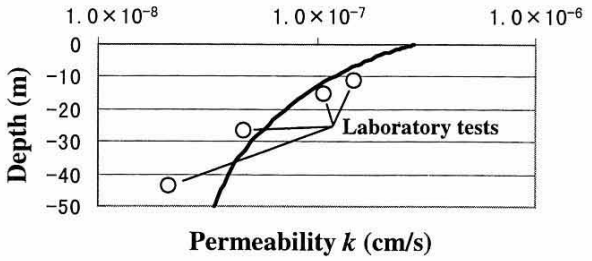

Fig. 15. Distribution of permeability with depth

The initial distribution of the preconsolidation pressure was obtained based on the results of standard oedometer consolidation tests. The variation of preconsolidation pressure versus depth used for the analysis is shown in Fig. 13.

The initial distribution of the water content was obtained from the samples taken, and the unit weight of the soil was estimated by assuming that the soil is fully saturated. The initial void ratio distribution is shown in Fig. 14. The ground water table was assumed to be at the ground surface and initially hydrostatic water condition. Accordingly, the initial vertical effective stresses were computed as shown in Fig. 13. The coefficient of lateral earth pressure was assumed to be 0.55, irrespective of the overconsolidation ratio.

The coefficient of permeability at various depths was estimated by the method proposed by Iizuka et al. (1985), which uses the preconsolidation pressure and the void ratio at the preconsolidation pressure. The distribution of the coefficient of vertical permeability is shown in Fig. 15. For comparison, the values measured from the oedometer tests are plotted in the figure. The measured values (as shown in white circle symbols in the figure) agree well with the estimated profile.

Values of coefficient of horizontal permeability were not measured in the laboratory. They were assumed to be twenty times those of vertical permeability, as it is common that the horizontal permeability is larger than the vertical.

Shield Machine Modelling

The shield machine was modelled as a rigid body by assigning a large value of elastic modulus of 2.0×10^8 (kN/m^2) and Poisson's ratio of 0.499. The weight of the machine was modelled by applying a body force. The diameter and length of the shield machine are 3.737 m and 5.67 m, respectively.

Shield Machine and Soil Interface Modelling

It has been recognized that the long-term subsidence after soft clay tunnelling is partly caused by excess pore pressure induced by disturbance associated with the interface friction between the soil and shield machine. Therefore, joint elements were placed at the interface of the elements that represent the shield machine and the adjacent soil, in order to investigate interface friction effects on ground deformations. The behaviour of the joint elements shows zero stiffness when the frictional force exceeds some critical value.

Table 1. Input parameters for shield tunnelling simulation

Shield machine	Young's modulus E	1.96×10^8 kPa
	Poisson's ratio ν	0.499
	Density ρ	3.00 g/cm^3
Excavating element	Young's modulus E	138.3 kPa
	Poisson's ratio ν	0.100
	Density ρ	1.62 g/cm^3
Cohesive soil	Specific gravity of soil particle Gs	2.680
	Compression index λ	0.320
	Swelling index κ	0.054
	Poisson's ratio ν	0.355
	Critical state parameter M	1.05
	Density of saturated soil ρ_{sat}	1.62 g/cm^3
Joint element	Yield value τ_y	4.9 kPa

Excavating Elements

The excavating elements represent the area that is disturbed by cutting and mixing of the excavated soils with slurry in front of the cutting face of the shield machine. The excavating elements are used to match the volume change and shear distortion of the elements to the actual movement of the shield machine. Therefore, the material properties of the excavating elements depend on various factors such as the method of excavation, machine characteristics, the size of the elements, etc. Hence, they need to be obtained by trial and error.

In this analysis, the excavating element was assumed to be an isotropic elastic material, and the thickness of the excavating elements was selected to be 20 cm. The air bubble pressure measured during the construction was applied as a pressure boundary within the excavating elements. The measured jacking forces were applied as nodal forces behind the shield machine. The elastic properties of the excavating elements were then determined by matching the computed advancement of the shield machine at a given time step to the measured field movement data. The initial analysis showed that a Young's modulus of 141 kPa and Poisson's ratio of 0.1 should be used in the subsequent machine advancement analysis.

Shield Machine Operation

The advancement of the shield machine was simulated by applying forces at the tail of the shield machine, where the hydraulic jacks are located, and providing pressures inside the excavating elements. The applied forces and pressures were obtained from the actual driving records of the machine. In this construction, fourteen hydraulic jacks were installed behind the machine as shown in Fig. 16(a). The jacking records are shown in Fig. 16(b), where the top column is the elapsed time. In this shield operation, each hydraulic jack did not operate independently, and the jacks were in the mode of either on or off. The solid circles in the bottom column of Fig. 16(b) show the time sequence of on/off mode of each hydraulic jack. The values in the central row of Fig. 16(b) are the combined hydraulic force of all the jacks in operation. Hence, the driving force of each jack can be computed by dividing this combined hydraulic force by the number of jacks in operation.

After the tunnel linings are installed, ground movement occurs as the earth pressure is released in the tail void, which corresponds to the space made between the excavated area of the tunnel machine and the outer surface of the tunnel lining. In order to avoid this ground movement, backfill injection is commonly made into the tail void. In this analysis, the finite element meshes adjacent to the tunnel lining were expanded in a radial direction by applying a pressure equivalent to the measured backfill pressure. Once the backfill operation was completed, the nodal displacements were fixed in position.

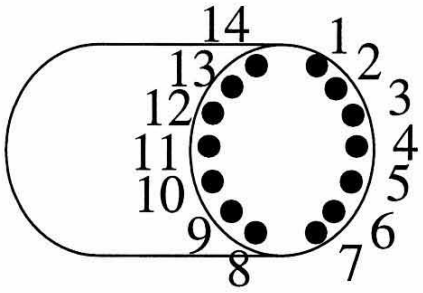

Fig. 16(a). Location of fourteen hydraulic jacks

0.000day	0.005	0.022	0.035	0.087	0.088	0.104	0.110	0.118	0.218	0.219	0.223	0.232	0.234	0.238	0.247
388kN	510	716	0	370	632	687	803	0	226	621	651	598	722	742	499
0.259day	0.264	0.405	0.411	0.412	0.417	0.418	0.419	0.421	0.423	0.426	0.429	0.431	0.432	0.434	0.436
839kN	0	386	749	673	782	704	810	649	786	675	739	754	0	595	643
0.438day	0.489	0.506	0.509	0.510	0.511	0.523	1.058	1.082	1.099	1.104	1.126	1.612	1.634	1.637	1.638
0kN	711	653	619	0	726	0	534	640	702	642	0	756	0	675	762

Fig. 16(b). The jacking record

NUMERICAL RESULTS

Ground Settlements

The three dimensional views of the computed settlement trough at 1 m above the crown of the machine at various times are shown in Fig. 17. The sequence of finite element remeshing operation with the machine advancement is illustrated in the figure.

In this case study, the subsurface displacements and pore water pressures were also measured at 1 m above the crown of the shield machine as the machine passed the measurement point. The arrow in Fig. 17 shows the measurement point. The surface settlement was also measured.

The computed vertical displacements at the ground surface and at 1 m above the crown are shown in Fig. 18. The horizontal axis of the figure is the elapsed time from the beginning of the numerical simulation. The measured data are also plotted in the figure for comparison. Although the measured data show that there is a sudden ground upheaval approximately 10 hours after the arrival of the shield machine face due to some unknown reason, both the calculated and measured vertical displacements are almost identical after the passage of the tail of the shield machine. The vertical settlement after the shield machine passed the measurement point was 6.9 mm, which corresponds to the measured displacement in the field. The vertical ground surface displacement was almost zero in this case. It is important to notice here that the field monitoring was stopped when the tail of the machine passed the measuring point. Therefore, the deformatlon related to tail void closure is not modelled in this analysis, and larger vertical displacement is expected to occur in the later stage of tunnel construction.

The contour plot of the vertical displacements at 1 m above the crown at $t=1.64$ days is shown in Fig. 19. Due to variation in the jacked forces applied to the machine, there was an upheaval of approximately 8 mm in front of the machine. Unfortunately, the field measurement started just before the machine approached to the monitoring point. Therefore, it was not possible to compare this computed result to the actual upheaval behaviour in the field.

Peck (1969) showed that the transverse surface settlement trough immediately following tunnel construction is well-described by the following Gaussian distribution curve.

$$S_v = S_{\max} \cdot \exp(-y^2/2i^2) \tag{7}$$

where S_v is the vertical settlement, $S_{\max}$ is the maximum settlement on the tunnel centre line, y is the horizontal distance from the tunnel centre line and i is the horizontal distance from the tunnel centre line to the point of inflexion of the settlement trough. The computed settlement trough at 1 m above the crown of the tunnel lining was fitted by the Peck's Gaussian distribution curve, as shown in Fig. 20. The maximum settlement at the centre of the tunnel was 6.9 mm. The shape of the computed settlement trough at 1 m above the crown of the shield tail is similar to the one suggested by Peck.

Pitching Angle of the Shield Machine

The computed vertical tilt of the shield machine, i.e. the pitching angle θ, is plotted against the elapsed time in Fig. 21. The recorded pitching angle of the machine is also plotted in the figure.

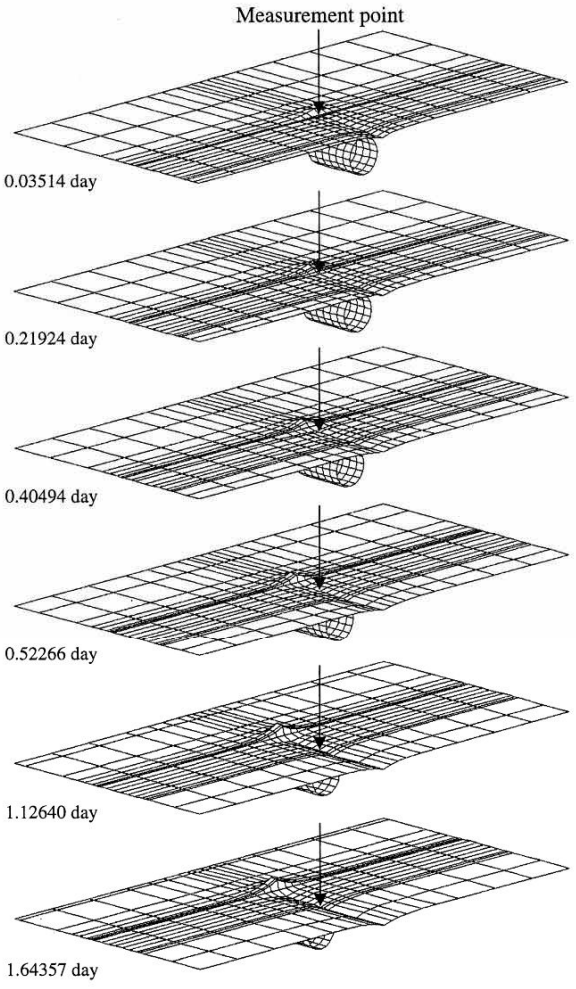

Fig. 17. Three dimensional views of the computed settlement (1 m above the crown of the machine)

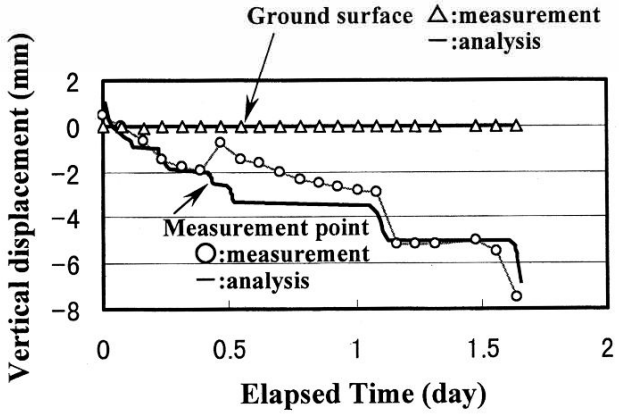

Fig. 18. Vertical displacement at the ground surface and at 1 m above the crown

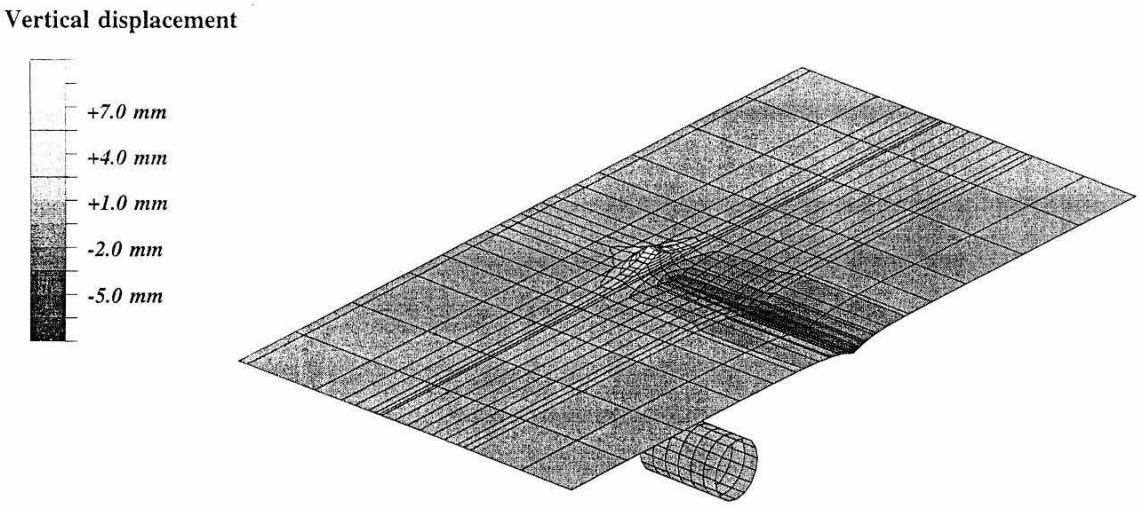

Fig. 19. Contour plot of the vertical displacements (1 m above the crown, $t=1.64$ day)

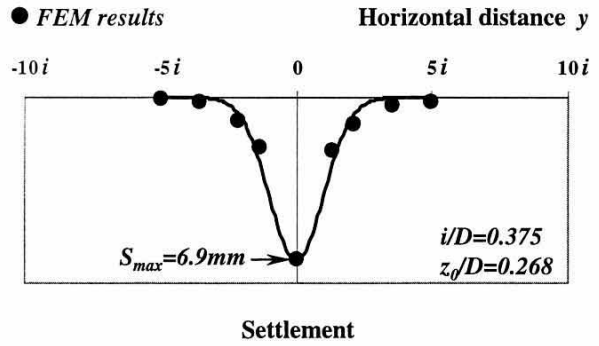

Fig. 20. Gaussian curve used to describe the transverse settlement trough

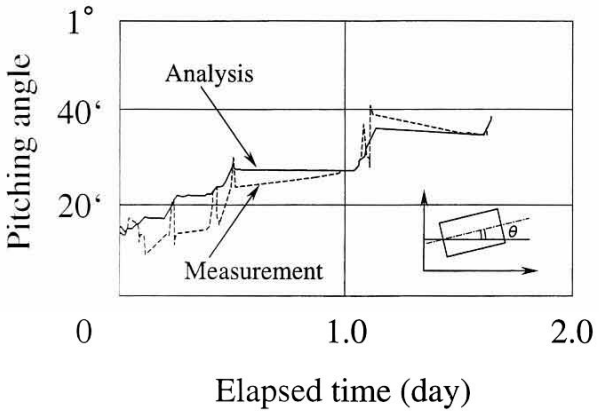

Fig. 21. Pitching angle of the shield machine

The figure shows that the pitching angle increased suddenly when the machine started to operate, implying that the machine was inclined from the horizontal level. The angle increased as the machine advanced and the increase ceased when the machine stopped. This is mainly due to the variation in the mechanical jacking forces applied behind the machine, which is controlled by the machine operator. This is one of the reasons that some upheaval ground movement was observed in front of the machine.

During the advancement, the upper tail of the machine is moving away from the tunnel linings as it excavates, providing a larger tail void space at the crown of the tunnel. On the other hand, at the invert section, the lower tail of the shield should be providing a downward force to the ground.

Stress Paths of the Soil Around the Shield Machine

The effective stress paths in the soft clay around the shield machine during the advancement are shown in Fig. 22. The stress paths are plotted in terms of mean effective stress p' and deviator stress $q=\sqrt{2J_2}$, where J_2 is the second invariant of the deviator stress tensor. Eight elements adjacent to the circumferential face of the shield machine were selected for plotting. The initial K_0 line, the critical state line and the current yield surface based on the Sekiguchi-Ohta model are also drawn in the stress path figures.

The results show that the elements around the crown of the machine (solid circles in the figure) are in a condition of unloading due to stress release as the machine passes along the element. The effective stress states move within the current yield surface, producing some elastic unloading deformation.

The positive pitching angle of the machine shown in Fig. 21 suggests that the lower tail of the shield is providing a downward force to the ground. The elements below the invert of the machine (open circles in the figure) are in the condition of loading due to the weight of the machine and the jacking operation. In this area, the yield surface of the soil expands from its initial condition, producing some plastic strains.

Excess Pore Pressure Generation

The calculated and measured excess pore water pressure changes at the measuring point above the crown of

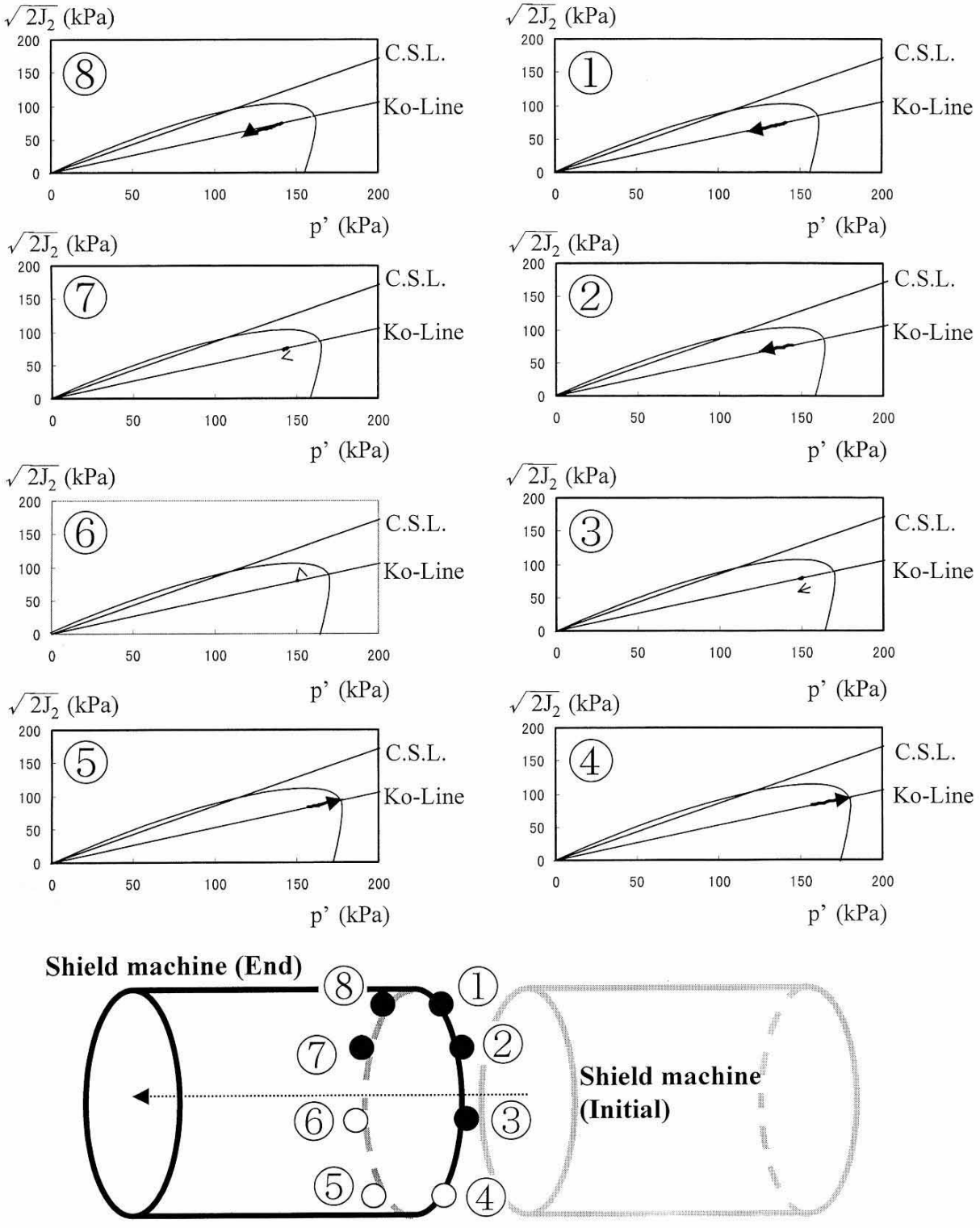

Fig. 22. Stress paths of the soil around the shield machine

the shield machine are shown in Fig. 23. The initial increase in excess pore pressure is due to stress created at the face by the jacking force. The finite element result shows that the excess pore pressures become negative as the shield machine passes the measurement point. This is due to the unloading of the soil, as illustrated in Fig. 22. The measured value, however, demonstrated a sudden increase in excess pore water pressure approximately 10 hours from the arrival of the shield machine for some unknown reason. Such a discrepancy between the measured and calculated values is similar to the sudden change in measured vertical settlement shown in Fig. 18.

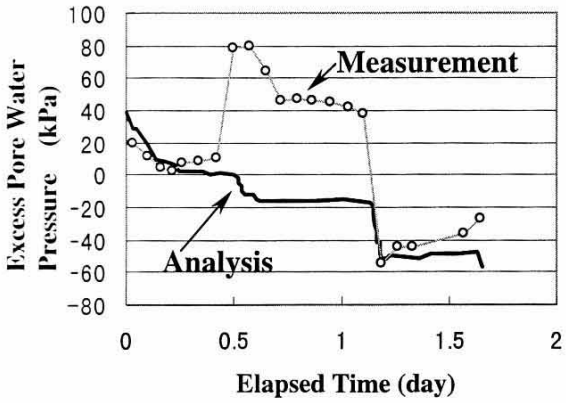

Fig. 23. Variation of excess pore water pressure at 1 m above crown

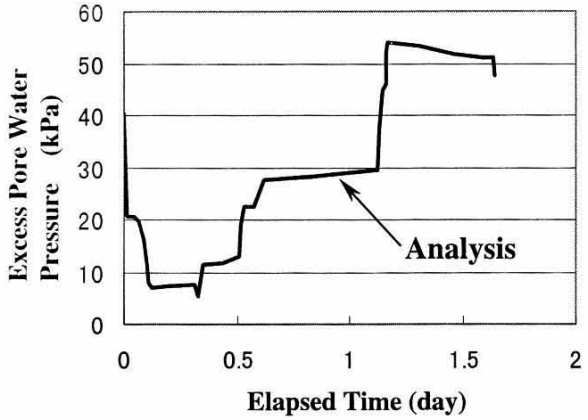

Fig. 24. Variation of excess pore water pressure at the bottom of the shield machine

The calculated excess pore water pressure at the bottom area of the shield machine is shown in Fig. 24. Again, there is an initial increase in excess pore pressure when the point of interest is in front of the machine. As the machine passes, there is an increase in excess pore pressure due to the loading condition observed at this location.

The results shown in Figs. 23 and 24 imply that the pore water pressure behaviour during shield tunnelling is closely related to loading/unloading condition of the soil caused by the positional and directional change of the shield machine. The pattern and magnitude of the excess pore pressures generated during the shield machine advancement will directly affect the long term subsidence around the tunnel, especially in the case of shield tunnelling through soft ground. Therefore, the postural change of the shield machine needs to be modelled, and controlled as accurately as possible for assessing the short and long term ground settlement due to shield tunnelling construction.

CONCLUSIONS

In this paper, the advancement and excavation processes of shield tunnelling operations were modelled using the finite element method in order to investigate the effect of these construction processes on the ground response. A new excavating finite element, which modells the disturbed soil in front of the cutting face, was proposed. The operation of shield advancement and of soil excavation was simulated using the finite element remeshing technique at each time step of the analysis.

The proposed modelling techniques of shield tunnelling construction were applied to simulate tunnelling project in soft cohesive soil in Tokyo and the results were compared with the field measurements. The soil deformation mechanism associated with the shield tunnelling operation was examined in detail. The vertical ground displacement profile, the effective stress paths in the soft clay, the excess pore water pressures, and the postural change of the shield machine, were obtained from the three-dimensional finite element simulation using the proposed modelling technique, and the results agreed with the field observations.

The cohesive soil around the crown of the machine was in a condition of unloading, due to the stress release as the machine passes. The effective stress states moved within the current yield surface, producing some elastic unloading deformation. The excess pore pressure became negative around the crown as the shield machine passes.

At the invert section, on the other hand, the lower tail of the shield was providing a downward force to the ground. The ground in this region was in a condition of loading due to the weight of the machine and the jacking operation. Therefore, the yield surface of the soil expanded from its initial condition producing some plastic strains. The excess pore pressures increased due to the loading condition at this location.

These pore pressures provide its proper input to a long-term analysis of the loading on the tunnel lining, and of ground surface displacements.

ACKNOWLEDGEMENT

The financial support of this research was provided by European Commission under the Brite Euram III program. Their support is gratefully acknowledged.

REFERENCES

1) Addenbrooke, T. I. (1996): "Numerical analysis of tunnelling in stiff clay," PhD thesis, Imperial College of Science Technology and Medicine.
2) Addenbrooke, T. I., Potts, D. M. and Puzrin, A. M. (1997): "The influence of pre-failure soil stiffness on the numerical analysis of tunnel construction," Géotechnique, Vol. 47, No. 3, pp. 693–712.
3) Akai, K. and Tamura, T. (1978): "Numerical simulations of multi-dimensional consolidation caused by elasto-plastic constitutive equation," J. of Geotech. Engrg., No. 269, Japanese Society of Civil Engineers, pp. 95–104 (in Japanese).
4) Akagi, H. and Komiya, K. (1993): "Finite element analyses of the stress ~ deformation behaviour considering the execution procedures during shield work," J. of Japan Society of Civil Engineers, No. 483/III-25, pp. 59–68 (in Japanese).
5) Britto, A. M. (1994): CRISP 94, User's and Programmer's Guide,

Cambridge University Engineering Department.
6) Christian, J. T. and Boehmer, J. W. (1970): "Plane strain consolidation by finite elements," J. of Soil Mech. Found. Div., ASCE, Vol. 94, No. SM4, pp. 1435-1457.
7) Clough, G. W. and Leca, E. (1989): "With focus on use of finite element methods for soft ground tunnelling," Review paper in Tunnels et Micro-Tunnels en Terrain Meuble-du Chantier a la Theorie, Presse de l'Ecole Natinale des Ponts et Chaussees, Paris, pp. 531-573.
8) Hashimoto, S. (1984): "Results of shield tunnelling in vertical close to existing shield tunnels," J. of Geotech. Engrg,, No. 352, III-2, Japanese Society of Civil Engineers, pp. 1-22 (in Japanese).
9) Iizuka, A., Ohta, H. and Yoshimine, T. (1985): "Input parameters of the elast-visco-plastic finite element method," Proc. of 20th Annual Meetings on Japanese Society on Soil Mechanics and Foundation Engineering, pp. 973-974 (in Japanese).
10) Katzenbach, R. and Breth, H. (1981): "Nonlinear 3D analysis for NATM in Frankfurt Clay," Proc. 10th Int. Conf. on SMFE, Stockholm, Vol. 1, pp. 315-318.
11) Lee, K. M., Rowe, R. K. and Lo, L. Y. (1992): "Subsidence owing to tunnelling. I. Estimating the gap parameter," Can. Geotech. J., Vol. 29, pp. 929-940.
12) Mair, R. J. and Taylor, R. N. (1997): "Bored tunnelling in the urban environment," Theme lecture to 14th Int. Conf. on SMFE, Hamburg, Vol. 4.
13) Ohta, H. and Sekiguchi, H. (1979): "Constitutive equations considering anisotropy and stress reorientation in clay," Proc. of 3rd Int. Conf. on Numerical Method in Geomechanics, Aachen, Vol. 1, pp. 475-484.
14) Ohtsu, H., Ohnishi, Y., Taki, H. and Kamemura, K. (1993): "A study on problems of excavation analysis based on the concept of effective stress," J. of Geotech. Engrg., No. 481, III-25, Japanese Society of Civil Engineers, p. 77-85 (in Japanese).
15) Owen, D. R. J. and Hinton, E. (1980): Finite Elements in Plasticity, Pineridge Press Limited, UK, Chapter 8.
16) Peck, R. B. (1969): "Deep excavations and tunnelling in soft ground," Proc. 7th Int. Conf. on SMFE, Mexico City, State of the Art Volume, pp. 225-290.
17) Swoboda, G., Mertz, W. and Schmid, A. (1989): "Three dimensional numerical models to simulate tunnel excavation," NUMOG III, Pande. Elsevier Science Publishers Ltd., London, pp. 536-548.

NOTATION

$\bullet$ = Scaler product
$\times$ = Vector product
$\boldsymbol{B}$ = Strain-displacement matrix
D = Diameter of shield machine
$\boldsymbol{D}$ = Stress-strain matrix
$\boldsymbol{F}$ = External force
$\boldsymbol{J}^{-1}$ = Jacobin matrix inverse
J_2 = Second invariant of the deviator stress tensor
n_i = Nodal points of finite element
n_R = Remeshed nodal point
N_i = Shape function
p_w = Pore water pressure
p' or σ'_m = Mean effective stress
q = Deviator stress
$_R$(subscript) = After remeshing
S_v = Vertical settlement
$\boldsymbol{u}_i$ = Displacement vectors at the nodal points n_i
$\boldsymbol{u}_R$ = Displacement vectors at the remeshed nodal point n_R
ξ, η, ζ = Local coordinate of the iso-parametric finite element
$\boldsymbol{\phi}$ = Residual forces of nodal forces

Appendix A

As shown in Fig. A-1, the mapping of vector $d\boldsymbol{x}$ within the finite element in the global coordinate system (x, y, z) to the vector $d\boldsymbol{r}$ with the local coordinate system of the element (ξ, η, ζ) is given by the following equation;

$$d\boldsymbol{r}=\boldsymbol{J}^{-1}d\boldsymbol{x} \tag{A1}$$

where $\boldsymbol{J}^{-1}$ is the inverse of the Jacobin matrix.

The local coordinates of the rearranged nodal point n_R can then be found from the coordinate of one nodal point. For example using the nodal coordinate of n_1.

$$(\xi_R, \eta_R, \zeta_R)=\boldsymbol{J}^{-1}(x_R-x_1, y_R-y_1, z_R-z_1) + (-1, -1, -1) \tag{A2}$$

where (ξ_R, η_R, ζ_R) is the local coordinates of the rearranged nodal point, (x_R, y_R, z_R) is the global coordinate of the rearranged nodal point, (x_1, y_1, z_1) is the global coordinates of the nodal point n_1 and $(-1, -1, -1)$ is the local coordinates of the nodal point n_1.

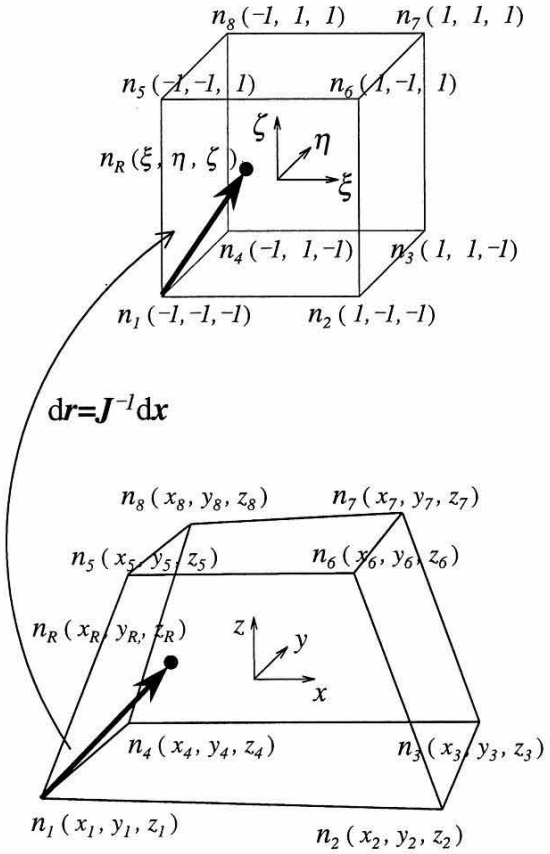

Fig. A-1. Mapping between the grobal and the local coordinate system

Appendix B

The effective stress state $\boldsymbol{\sigma}'_R$ at the Gauss-Legendre integration points of the remeshed elements at $t=t_0+\delta t$ is computed using the following equation.

$$\boldsymbol{\sigma}'_R=\boldsymbol{\sigma}'_0+d\boldsymbol{\sigma}' \tag{B1}$$

where $\boldsymbol{\sigma}'_0$ is the effective stresses estimated from the original undeformed mesh at $t=t_0$, $d\boldsymbol{\sigma}'_R$ is the effective stress increment produced within a time step δt.

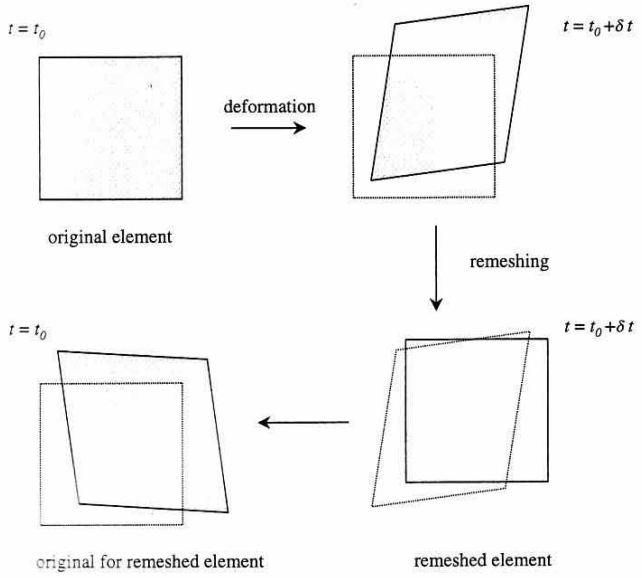

Fig. B-1. Back-calculation of the remeshed element

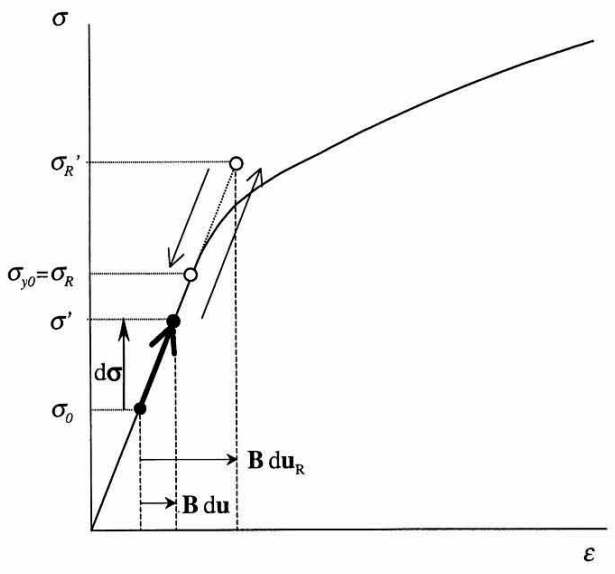

Fig. B-3.

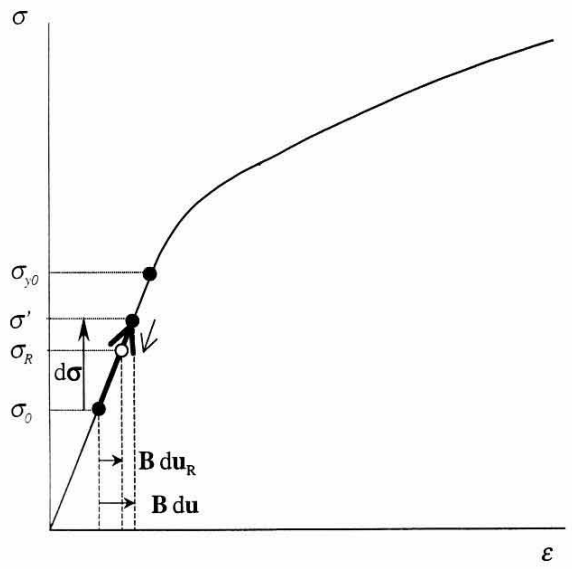

Fig. B-2.

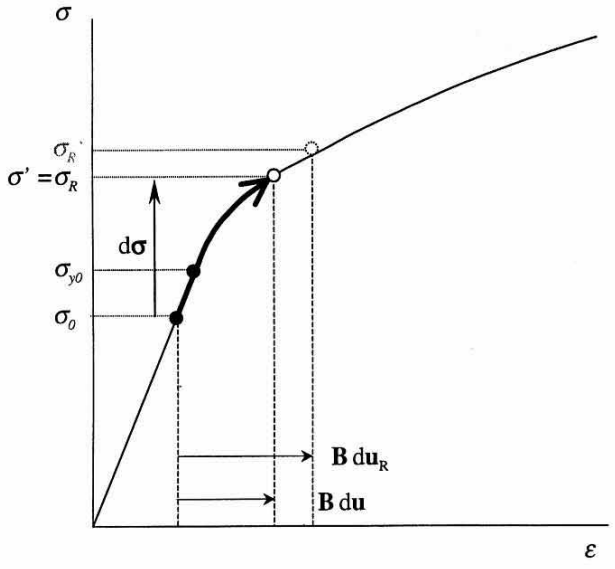

Fig. B-4.

σ_0' at the Gauss-Legendre integration points of the remeshed elements needs to be estimated from the effective stress field obtained in the original undeformed mesh at $t=t_0$. This estimation requires back-calculation of the location of the remeshed element at $t=t_0$, as shown in Fig. B-1. However, this calculation will result in large computing time, and it was considered to be uneconomical. Therefore, in this study, it is assumed that σ_0' at the Gauss-Legendre integration points of a remeshed element is the same as that of the original element.

The calculation of $d\sigma'$ requires stress-strain $\boldsymbol{D}$ matrix as shown in Eq. (3). When the soil is in plastic condition, the value of $\boldsymbol{D}$ changes with applied strain increment $d\varepsilon=\boldsymbol{B}du$. Therefore, $d\sigma$ needs to be calculated by strain integration when the soil is in a plastic condition. This integration results in additional computing time because the stress calculation should be performed twice in this analysis; (i) when the analysis is made using the original mesh and (ii) when the stress update is performed for the remeshed elements. Again, the second stress calculation was considered to be uneconomical and the stress update procedure was simplified in this study, as described below.

Hereafter, $d\varepsilon$ is the incremental strain at the Gauss points of the deformed mesh, whereas $d\varepsilon_R$ is that of the refined mesh.

Case 1 The new stress state of both original and remeshed are both in the elastic region (Fig. B-2)

In this case, σ_R' is simply calculated as follows in one

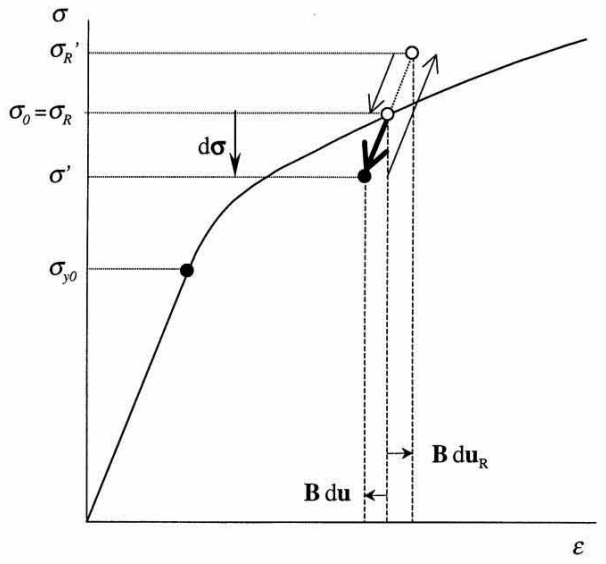

Fig. B-5.

step.

$$\sigma'_R=\sigma'_0+\boldsymbol{D}_e d\varepsilon_R \tag{B2}$$

where $\boldsymbol{D}_e$ is the elastic stiffness.

Case 2 The new stress state of the original element is in the elastic region, whereas that of the remeshed element is in the plastic region (Fig. B-3)

In this case, the stress state calculated from Eq. (B2) will be outside the current yield surface for the remeshed element and the strain integration is necessary to compute the stress state σ'_R of the remeshed element. To reduce the computing time, σ'_R is simply corrected back to the yield stress state of the current yield surface using the method proposed by Owen and Hinton (1980).

Case 3 The stress state of both the original and remeshed element are in plastic condition (Fig. B-4)

Since both increments produce plastic deformation, the strain integration is necessary to obtain the stress state σ'_R of the remeshed element. In this case, σ'_R is assumed to be equal to the stress state of the original element σ'.

Case 4 The stress states of both the original and remeshed element are unloaded into the elastic region

Similar to Case 1, σ'_R is calculated to be equal to $\sigma'_0+\boldsymbol{D}_e d\varepsilon_R$, where $\boldsymbol{D}_e$ is the elastic stiffness.

Case 5 The stress state of the original element becomes one of unloading, whereas that of the remeshed becomes one of plastic loading (Fig. B-5)

The stress state σ'_R is assumed to be equal to σ_0.

Géotechnique
Volume 51, No.10
pp.835-846
December 2001
Institution of Civil Engineers

GÉOTECHNIQUE

Thomas Telford

REPRINT

Komiya, K., Soga, K., Akagi, H., Jafari, M. R. & Bolton, M. D. (2001). *Géotechnique* **51**, No. 10, 835–846

Soil consolidation associated with grouting during shield tunnelling in soft clayey ground

K. KOMIYA,* K. SOGA,† H. AKAGI,‡ M. R. JAFARI§ and M. D. BOLTON†

The effectiveness of grouting to reduce surface settlements during underground construction in clayey ground was investigated by a field trial and laboratory tests. The field trial was carried out during shield tunnelling work conducted in alluvial clay deposits in Koto-ku, Tokyo. Grout was injected at some distance away from the tunnel, and both surface and subsurface settlements above the tunnel were monitored. Although the initial heave was achieved immediately after the grout injection, the ground continued to settle with time, owing to soil consolidation and grout shrinkage. A laboratory investigation was conducted to investigate the parameters that control the long-term behaviour of grouting in clay. It was found that better long-term grout efficiency can be achieved in overconsolidated clay than in normally consolidated clay, and the efficiency increased with increasing injection volume. Finite element analysis of the laboratory experiments confirmed that the amount and extent of excess pore pressures generated during injection govern the long-term grout efficiency. Finite element analysis of the field trial was also performed to simulate the long-term ground deformation after grout injection.

KEYWORDS: clays; consolidation; grouting; laboratory tests; numerical modelling and analysis; tunnels.

Nous étudions l'efficacité de la cimentation pour réduire le tassement de surface pendant les constructions souterraines dans des sols argileux au moyen d'essais sur le terrain et d'essais en laboratoire. Les essais sur le terrain ont été faits pendant des travaux de perçage de tunnels protecteurs effectués dans les dépôts d'argile alluviale de Koto-ku à Tokyo. Le ciment a été injecté à une certaine distance du tunnel et les tassements de surface et de sous-surface au-dessus du tunnel ont été observés. Bien que le gonflement initial se soit produit immédiatement après l'injection de ciment, le sol a continué à se tasser peu à peu en raison de sa consolidation et de la contraction du ciment. Une investigation en laboratoire a été menée pour trouver les paramètres qui commandent le comportement à long terme de la cimentation dans l'argile. On a trouvé que l'efficacité à long terme du ciment est meilleure dans une argile surconsolidée que dans une argile à consolidation normale et que l'efficacité augmentait en même temps avec le volume injecté. L'analyse d'éléments finis pratiquée sur les essais en laboratoire a confirmé que l'importance et l'étendue des pressions interstitielles excessives produites pendant l'injection gouvernent l'efficacité à long terme du ciment. Nous avons fait également des analyses d'éléments finis pour l'essai sur le terrain afin de simuler la déformation à long terme du sol après l'injection de ciment.

INTRODUCTION

The shield tunnelling method is frequently applied for constructing underground structures for railways and utility lines in urban areas. The method has been used extensively for more than 30 years, and many advances—such as the development of new excavation machines and the implementation of computer-controlled operation—have been made in order to optimise the method. Based on the large amount of experience and expertise, the sources of ground deformation associated with shield tunnelling are well investigated and widely reported (e.g. Mair & Taylor, 1997). In recent years, the magnitude of soil deformation by earth pressure balance shield tunnelling in soft ground has become remarkably small; surface settlements of less than 10 mm are common (e.g. JSSMFE, 1993).

Even with recent advances in the method, shield tunnelling in soft clayey ground, where the SPT N value is close to zero, is still a major technical challenge for tunnel engineers. Deformation in this type of ground tends to occur several months or years after the completion of tunnelling, as shown by the typical time–settlement curve in Fig. 1. This long-term settlement is due mainly to consolidation of clayey soil around the tunnel, originating from the excess pore water pressure generated during the shield tunnelling work as the ground is sheared and disturbed (e.g. Clough *et al.*, 1983; Shirlaw, 1995). Drainage into the tunnel can reduce pore pressures below their original values, and also contributes to the long-term settlement.

Manuscript received 31 January 2000; revised manuscript accepted 10 August 2001.
Discussion on this paper closes 1 May 2002. For further details see inside back cover.
* Department of Civil Engineering, Chiba Institute of Technology, Japan.
† Engineering Department, University of Cambridge, UK.
‡ Department of Civil Engineering, Waseda University, Japan.
§ Massachusetts Institute of Technology, USA.

During shield tunnelling in soft ground, grout materials can be injected around the upper part of tunnel linings to improve the strength of the soil and to reduce the magnitude of surface settlements. In recent years, compensation grouting and grout jacking have been applied successfully in many major tunnelling projects to limit ground settlements under important structures. In this operation, grout is injected at locations between the tunnel and the building foundations in order to 'compensate' for stress relief and ground loss induced by tunnel excavation. In compensation grouting, grout injection is often performed at the same time as tunnel construction (as shown by the shaded zone in Fig. 1), so that building settlements are maintained within the specified criteria. Successful applications of compensation grouting in stiff London clay have been reported for the underground construction of the Jubilee Line Extension Project (Harris *et al.*, 1996; Osborne *et al.*, 1997; Harris *et al.*, 1999). However, its effectiveness in soft clayey soils is still in question (Shirlaw *et al.*, 1999; Soga *et al.*, 1999).

In this study, grout injection tests were performed in the laboratory and in the field to investigate the short- and long-term deformations of clay around grout injection points. Finite element modelling of the laboratory grouting tests was conducted, and the parameters controlling the long-term behaviour of grouting in clay were investigated. Finite element analysis was also performed to simulate the field trial, where grout was injected in soft clayey ground at a shield tunnelling site in Tokyo. Based on the comparison between the numerical results and the laboratory/field data, soil consolidation associated with grouting is discussed in this paper.

CONCEPTUAL MODELLING OF GROUTING IN CLAYEY SOILS

The mechanism of soil–grout interaction during grout injection is a very complicated one. However, a simple conceptual model, which covers the main features of grouting process in clay, is proposed for the discussion in this paper.

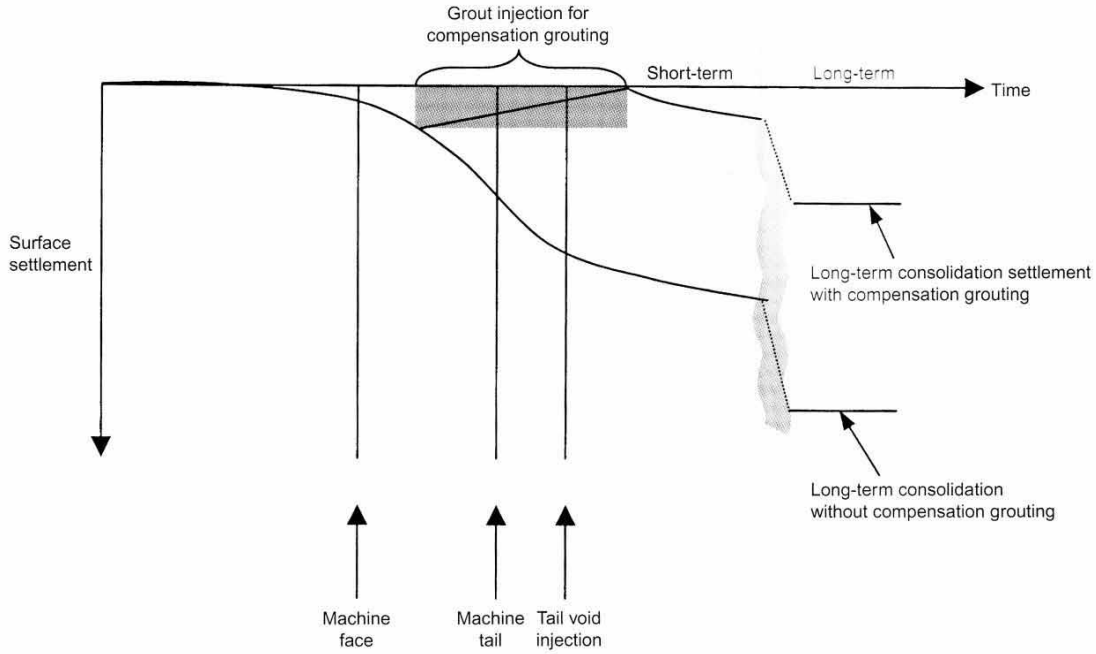

Fig. 1. Settlements associated with shield tunnelling and compensation grouting

Grouting can mainly be carried out in two different modes: (*a*) compaction grouting and (*b*) fracture grouting. Compaction grouting involves the injection of high-viscosity stiff grout (e.g. a soil–cement–water mix) into the soil mass. When this type of grout is injected, it does not penetrate into the soil pores but remains in a homogeneous mass, forming an approximately spherical bulb. The formation of a bulb displaces the surrounding soil. Fracture grouting involves the injection of lower-viscosity grout (e.g. cement and bentonite), which tends to result in a split opening the ground (often described as hydraulic fracturing). As the grout flows into the fractures, the surrounding soil is displaced. Hydraulic fracturing can happen even in compaction grouting, which results in loss of control of the grouting process. The shape of a grout body and the subsequent soil fracturing are affected by various parameters such as injection pressure, injection rate, gel time of the grout, rheology of the grout, confining pressure and permeability of the soil (e.g. Mori *et al.*, 1990, 1992; Warner, 1992, 1998).

At the initial stage of grouting, the grout pushes the soil outwards and forms a bulb, as shown in the schematic diagram of Fig. 2(a). As more grout is injected, the clay deforms plastically and the size of the grout bulb grows. It increases until the grout pressure builds up to the fracturing pressure and a plane of weakness is formed by hydraulic fracturing, as shown in Fig. 2(b). Fracture can also occur along a natural fissure, joint or bedding. As fracture occurs, the stress condition in the soil suddenly changes and the injection pressure drops. When lower-viscosity grout is used, the grout will intrude more readily into planes of weakness to form fracture grouting (Fig. 2(c)). When higher-viscosity grout is used, the grout may not able to get into planes of weakness (Fig. 2(c)). The grout bulb continues to expand, and the injection pressure starts to rise again.

The effectiveness of compensation grouting/grout jacking is often evaluated by the amount of soil heave obtained for a given injected grout volume. Ideally, if soil deformation is occurring in the undrained condition, the heave volume is equal

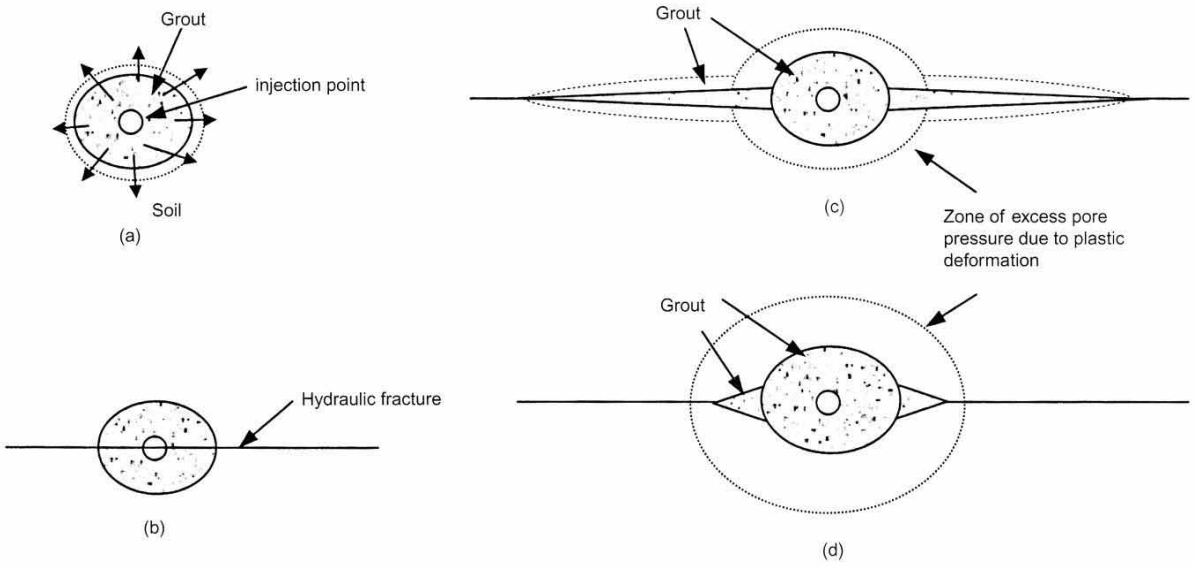

Fig. 2. Conceptual modelling of grouting in clay: (a) initial stage of grout injection; (b) initiation of fracture; (c) penetration of grout into fracture, low-viscosity grout; (d) penetration of grout into fracture, high-viscosity grout

to the injection volume. However, this is often not the case in the field, since there will be increased deformation towards the excavation and lateral subsurface displacements leading to surface heave outside the designed compensation area. Therefore injection needs to be controlled by careful monitoring of the surface deformation, so that the overall surface settlements become close to zero after tunnel construction.

Although compensation grouting and grout jacking can be an effective way to reduce surface settlements in the short term, their long-term effectiveness is still not very well known. It is likely that the clay around the grout will consolidate with time, owing to dissipation of the excess pore pressures generated during the injection (Fig. 2(c), (d)). This is especially the case for normally consolidated clays. In addition, the free water in the grout can bleed out from the designed compensation area. If lower-viscosity grout is used, it is possible that the grout escapes from the designed area through the fractures made during injection.

FIELD INVESTIGATION OF GROUTING IN ALLUVIAL CLAY

Field trial

A field trial of grout jacking was performed during shield tunnelling work conducted in alluvial clay deposits at Koto-ku, Tokyo. A tunnel 3 m diameter and 670 m long was constructed at a depth of 14·3 m using an earth pressure balance shield machine. The soil profile and the location of the tunnel are shown in Fig. 3. The thickness of the clay was approximately 30 m, and the SPT N value is reported to be close to zero throughout the layer. Some physical properties of the soils are listed in Table 1. The clay is normally consolidated with a liquidity index close to 1, and is a typical alluvial clay in Tokyo. Because of the high sensitivity values, large compressibility due to soil structure degradation can result in large long-term settlement, as discussed by Mori & Akagi (1985).

The grout injection trial was performed at three different locations, as shown in Fig. 4. In case A, mortar was injected into the gap between the tunnel lining and the excavated ground (tail void) immediately after the machine passage and installation of tunnel linings. Grout pipes were installed at the tail of the shield machine, and injection was performed when a segmental lining came out from the machine. The injected volume was approximately 120–150% of the theoretical tail void volume, and the injection pressure recorded at the invert was 300 kPa.

Instead of performing tail void grouting, grout jacking was performed above the tunnel by installing five injection pipes from the tunnel (cases B and C in Fig. 4(a)). The effectiveness was examined by injecting grout at two different distances from the tunnel: 1·0 m and 2·0 m in cases B and C respectively (see

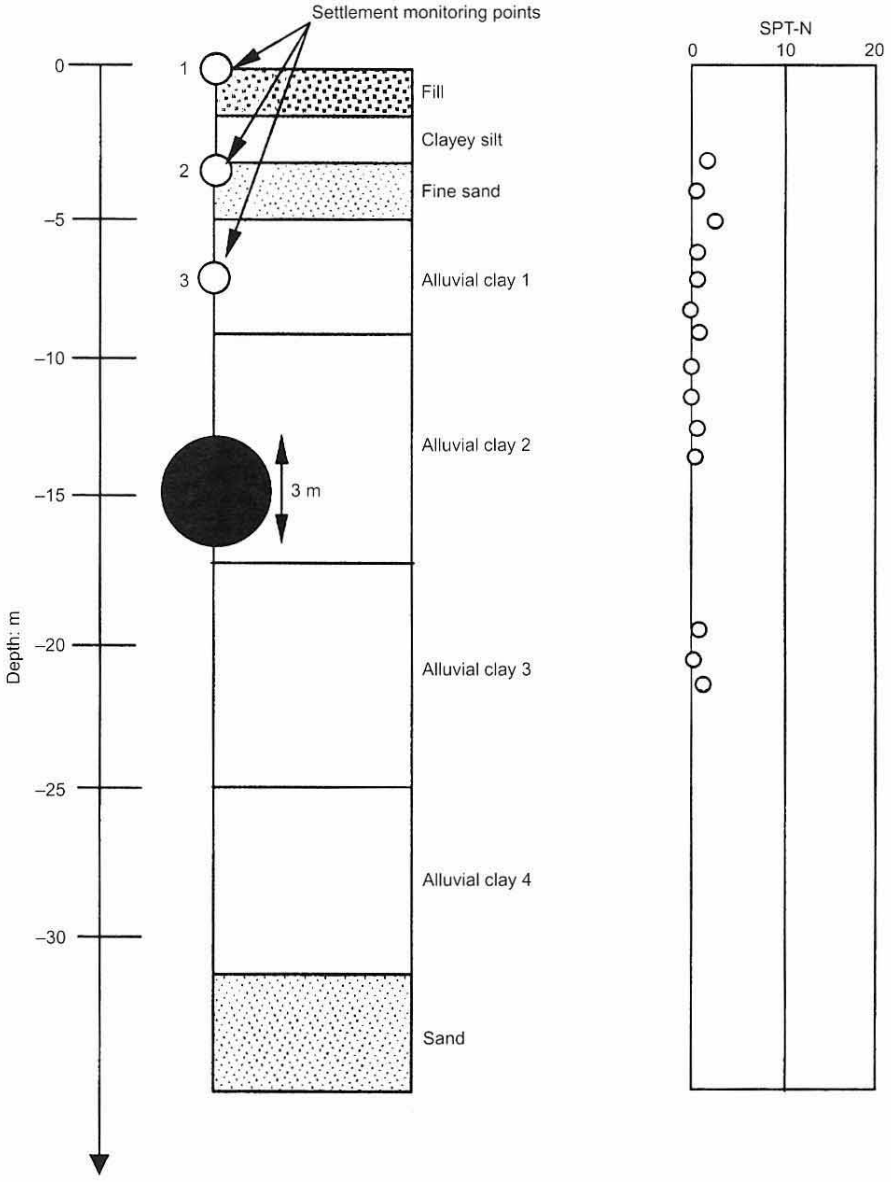

Fig. 3. Soil profile at a field trial site

Table 1. Physical properties of the soils at the field trial site

Soil	Total unit weight, γ_t:kN/m^3	Plasticity index, PI	Undrained shear strength, q_u:kPa	Sensitivity, S_t	Void ratio, e_0	Compression index, C_c
Fill	17	–	–	–	–	–
Clayey silt	15·6	23·7	30·9	10	1·70	0·94
Sand	18	–	–	–	–	–
Clay 1	15·8	38·4	49·1	16	1·62	0·87
Clay 2	15·8	40·4	66·5	23	1·56	0·86
Clay 3	17·4	39·4	116	20	1·33	0·72
Clay 4	17·4	22·2	143	41	1·33	0·49
Sand	18·0	–	–	–	–	–

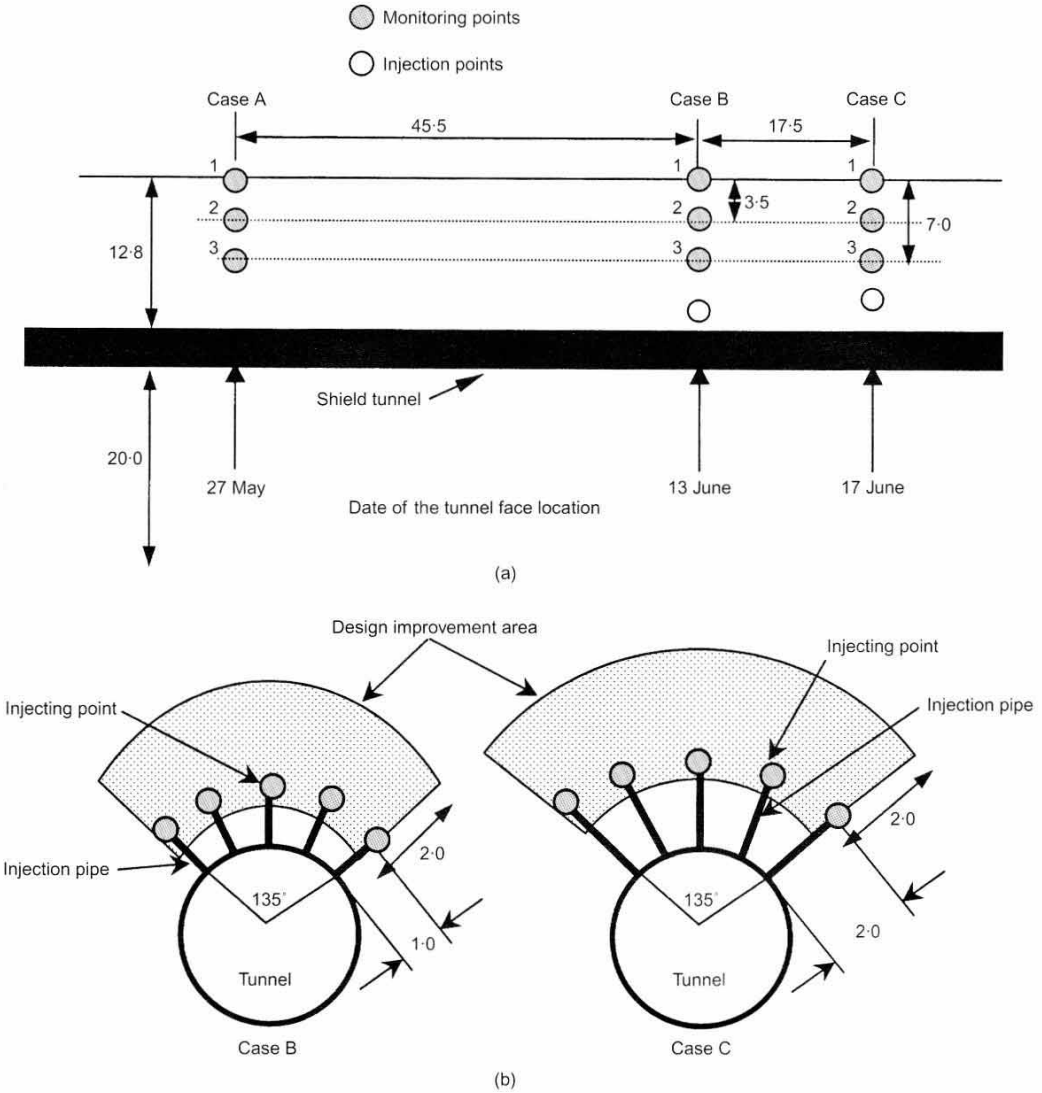

Fig. 4. Grout injection locations: (a) side view of the tunnel and grouting locations; (b) injection details for case B and case C, dimensions in metres

Fig. 4(b)). The ground settlement (or heave) was measured at three different locations above the injection points, as shown in Figs 3 and Fig 4(a). A mixture of cement, water and water-glass (Na_2O-$3SiO_2$ aq.) with gel hardening time of 20 s was used as the grout. The mass ratio of the mixture was cement : water-glass : water = 1 : 1·25 : 3·43. The use of a rapid-hardening grout was considered essential in order to avoid grout shrinkage after the injection.

The volume of injected grout was predetermined to be 3·4 m^3 (0·68 m^3 per injection tube) for case B and 6 m^3 (1·2 m^3 per injection tube) for case C. The grout was injected 8·5 h and 24 h after the machine passage in cases B and C respectively, corresponding to the time when the machine was approximately 5 m ahead of the injection points. The maximum injection pressure was recorded to be 500 kPa.

Test results

The measured ground displacements with time at the three monitoring locations are shown in Fig. 5, and the data are summarised in Table 2. In the table, the immediate deformations after machine passage and tail void grouting (S_i) and the upward displacements due to grout jacking (S_g) are listed (downward movement is taken as positive). The consolidation

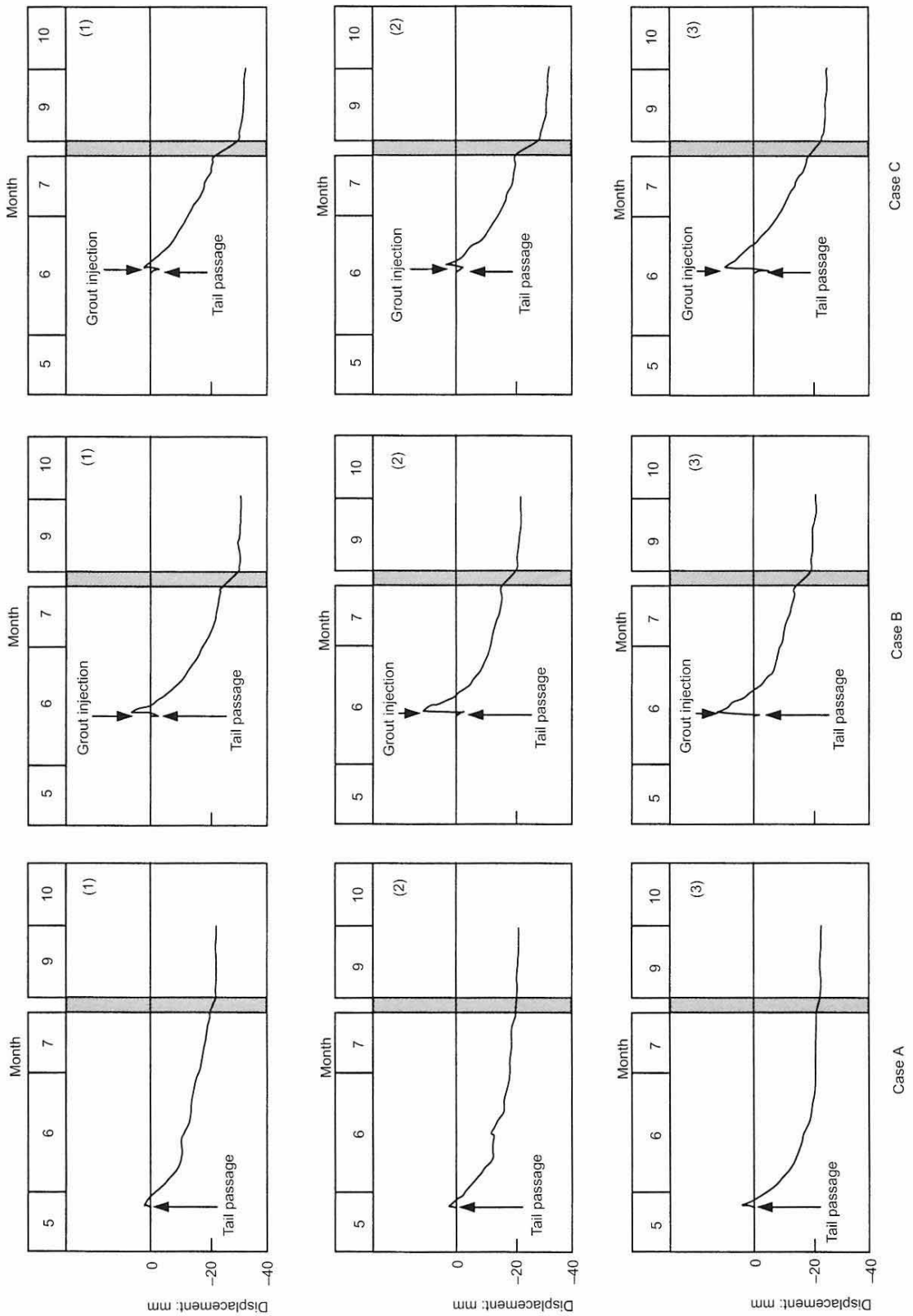

Fig. 5. Surface/subsurface settlements at the monitoring points

Table 2. Summary of ground displacements from the field trial

Case	Monitoring point	Immediate settlement, S_i: mm	Heaving due to grouting, S_g: mm	Long-term settlement, S_c: mm	Final settlement, S_f: mm
Case A	1	−1·5*	–	−24·2	+22·7
	2	−3·0*	–	−24·0	+21·0
	3	−4·0*	–	−26·0	+22·0
Case B	1	+2·5	−10·0	−37·2	+29·7
	2	+2·5	−14·0	−32·8	+21·3
	3	+2·5	−16·0	−33·3	+19·8
Case C	1	+3·0	−5·5	−33·7	+31·2
	2	+3·0	−7·0	−34·5	+30·5
	3	+4·5	−15·0	−34·3	+23·8

* Includes the effect of tail void grouting.

settlements (S_c) were measured 3 months after the grouting (at the end of month 9 in Fig. 5). The final settlement (S_f) is calculated as the sum of S_i, S_g and S_c.

Case A showed some upward displacements immediately after tunnel construction, owing to the tail void grouting operation. The displacement decreased with increase in distance from the tunnel. The consolidation settlement, S_c, was smaller than the other cases, and it was approximately the same for the three measurement points (~25 mm).

In cases B and C there were immediate settlements after machine passage owing to closure of the tail void (no tail void grouting was performed in these cases). When grout jacking was performed, the ground surface heaved more than the original level because a large amount of grout was injected. The magnitudes of the heave measured at subsurface monitoring point 3 were similar in both cases. However, a larger injection volume was required for case C to achieve this. More surface heave was obtained in case B than in case C. In case B the rigid boundary of the tunnel lining close to the injection points may have affected the soil deformation pattern. The interaction between the tunnel lining and grout injection seems to have caused more uniform upward movement of the soil above the injection points.

Both cases B and C had larger consolidation settlements, S_c, than case A; the jacking effect achieved in the short term disappeared. This is possibly due to additional large excess pore pressures generated when the clay was sheared and became plastic during the injection. Since the clay was sensitive and compressible, considerable consolidation settlement would occur during the dissipation of the excess pore pressures. Hence, although a good jacking effect was achieved immediately after the grout injection in this field trial, the grouting was not effective in terms of reducing the ground deformation in the long term.

LABORATORY INVESTIGATION OF GROUTING IN CLAYS

Test apparatus, soils and grouts

The field study highlighted the possible effect of soil consolidation on the long-term effectiveness of compensation grouting/grout jacking in clays. Laboratory tests were carried out by injecting two types of grouting material in three different clays: two normally consolidated clays (samples A and C), and one lightly overconsolidated clay (sample B). The tested clays were sampled from Tokyo alluvial clay deposits using either large-diameter, thin-wall sampling tubes (150 mm diameter) or block sampling. The physical properties of the clays are listed in Table 3.

A schematic diagram of the laboratory injection test apparatus is shown in Fig. 6. For the tests, cylindrical specimens of 150 mm diameter and 180 mm height were made from the tube or block samples. Before the specimen was placed into a mould, a 5 mm diameter hole was drilled from the bottom of the specimen into the centre, and an injection pipe was installed. The specimen was then consolidated from 9·8 kPa up to a specified pressure in stages. The drainage was allowed only from the top plate, and the consolidation stage took approximately one week. The final vertical pressures applied were 235 kPa for sample A specimens, 245 kPa for sample B

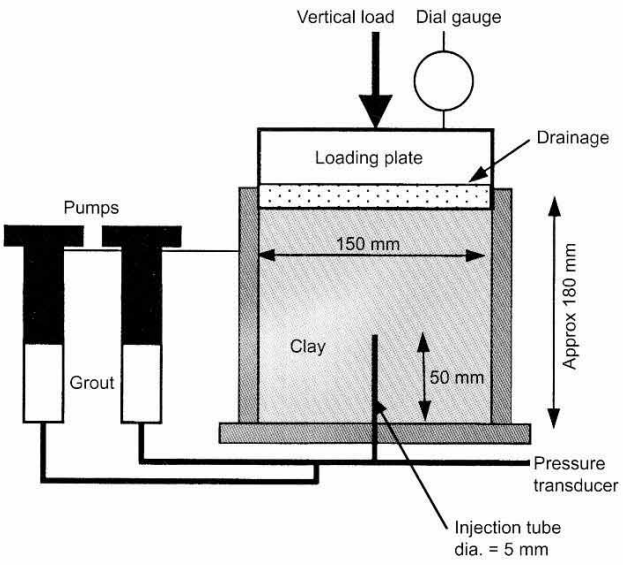

Fig. 6. Schematic diagram of laboratory injection test

Table 3. Physical properties of tested clays

Sample	A	B	C
Name	Etchujima-clay	Yashio-clay	Keihinjima-clay
Water content, w_0	78%	51%	77%
Liquid limit, LL	74%	58%	87%
Plasticity index, PI	41%	24%	49%
Preconsolidation pressure, σ_{v0}	204 kPa	392 kPa	135 kPa
OCR	1	1·6	1
Undrained strength	102 kPa	216 kPa	45 kPa
Sensitivity, S_t	17	14	8

specimens and 157 kPa for sample C specimens; sample A and C specimens were normally consolidated, whereas sample B specimens were overconsolidated (OCR = 1·6). After consolidation, grouting material was injected into the specimens using a manual injection pump.

Two types of grouting material were used in the experiment: (*a*) a mixture of cement and water-glass (type I), and (b) a mixture of cement, water-glass, chemical hardening material and bentonite (type II). The mass ratio of type I was cement : water-glass : water = 1 : 1·25 : 3·43. The gel-hardening time was 120 s, and its unconfined compressive strength was 75 kPa after 1 day curing. In type II, two liquids were prepared: (*a*) a mixture of water and water-glass (= 1 : 1) and (*b*) a mixture of cement, water, bentonite and chemical hardener (= 1 : 2·2 : 0·15 : 0·5). The liquids were placed in different pumps, as shown in Fig. 6, and were mixed immediately before the injection in order to avoid hardening inside the pump. With the chemical hardener, a shorter gel-hardening time of 20 s was achieved. Its unconfined compressive strength was 143 kPa after 1 day curing.

A total of 18 injection tests were performed. Type I grout was used in samples A and C and type II grout was used in samples B and C. The amount of injected grout varied between 7% and 26% of the volumes of the post-consolidated clay specimens. During injection, the injection pressure was measured by a pressure transducer connected to the injection pipe. The measured fracturing pressures were approximately 500 kPa for samples A and B and 400 kPa for sample C. The post-grout deformation was measured with time by a dial gauge placed on top of the loading plate.

In addition to the tests on natural clay specimens, the effect of grout shape (fracture or compaction type) on the long-term behaviour of soil after grouting was investigated. A rubber balloon was fitted to the injection point, and clay slurry originating from sample C (initial water content = 174%) was then poured into a mould. After consolidating the clay to a pressure of 49 kPa, the grout was injected into the balloon. The water content of the clay before injection was approximately 75%. The undrained shear strength was estimated to be 9·8 kPa from vane shear tests. It was considered that the use of a rubber balloon would prevent the grout from intruding into fractures and create a coherent grout bulb with no bleeding effect.

Test results

Typical cross-sectional views of grout injected specimens are shown in Fig. 7(a) and (b). In the case of small injection volume, the distribution of the grout was limited to the region adjacent to the injection point (Fig. 7(a)). The pattern of soil deformation was more or less like a compaction mode type. When more grout was injected, however, the soil fractured or deformed largely in a plastic manner, and the injected grout spread sideways to form a horizontal layer (Fig. 7(b)).

In all cases the top loading plate displaced upwards immediately after the injection as the clay heaved. The amount of volume expansion calculated from the initial displacement of the top plate was approximately equal to the injection volume, indicating that the soil deformation during injection was in the undrained condition. The vertical displacement of the top plate was continuously measured for several days until the excess pore pressure in the specimen had dissipated and the rate of settlement became negligible.

The upward displacement of the top plate was plotted against the normalised injection volume (grout volume/initial soil volume), as shown in Fig. 8. For each test, two data points are plotted: the upper value is the heave immediately after injection, whereas the lower value is the final heave after excess pore pressure dissipation. The decrease in the heave with time is due to (*a*) dissipation of the excess pore pressures in the clay generated during grout injection and (*b*) shrinkage of the grout itself by 'bleeding' its water into the surrounding soil. When a faster-setting grout was used, the long-term settlement was smaller because of reduced grout shrinkage.

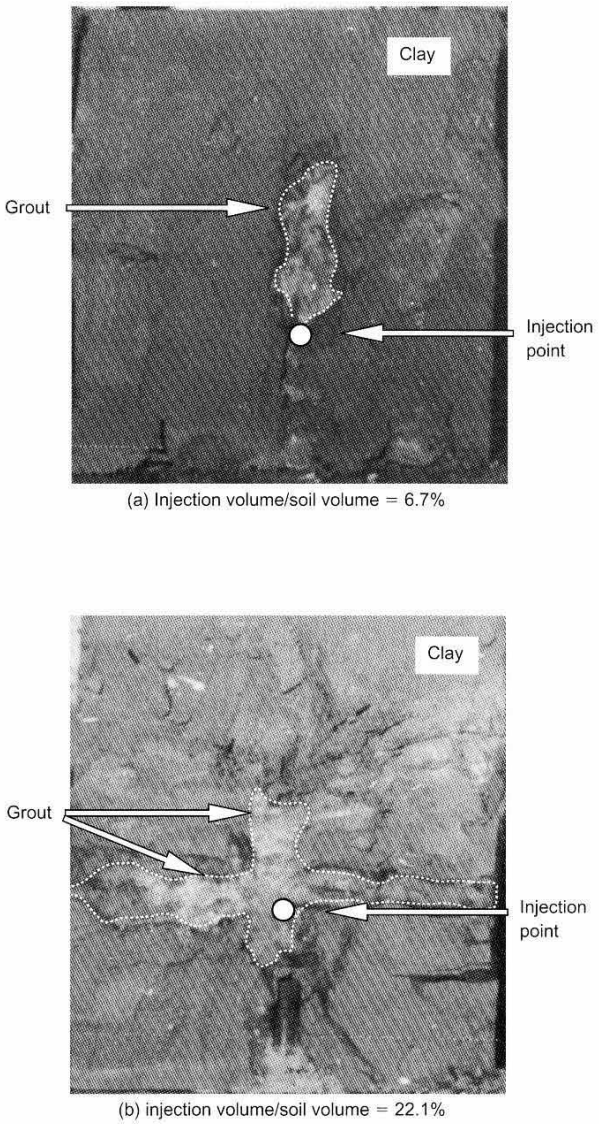

Fig. 7. Photos of sample after grout injection (sample A): injection volume/soil volume (a) 6·7%, (b) 22·1%

In this paper the grout efficiency, η_{lab}, measured in the laboratory is defined as follows:

$$\eta_{lab} = \frac{\text{Heaved volume } (V_f)}{\text{Injection volume } (V_i)} = \frac{V_i - V_c - V_G}{V_i} = 1 - \lambda_C - \lambda_G \quad (1)$$

where V_i is the injection volume, V_C is the decrease in volume due to consolidation, and V_G is the decrease in volume due to grout bleeding. The volume loss ratios of consolidation effect and grout bleeding are defined as $\lambda_C = V_C/V_i$ and $\lambda_G = V_G/V_i$ respectively.

Typical curves of grout efficiency against time are shown in Fig. 9. Immediately after injection the grout efficiency is close to 1, but it reduced with time. For example, when a small volume of grout (injection volume/soil volume = 6·7%) was injected in sample A, the grout efficiency reduced to less than 10% after 1 day. The grout efficiency of sample A increased to 60% as the injection volume increased (injection volume/soil volume = 22·1%). Better grout efficiency was obtained when the fast-setting type II grout was used.

In order to separate the soil consolidation effect from the bleeding effect, λ_G in equation (1) needs to be determined.

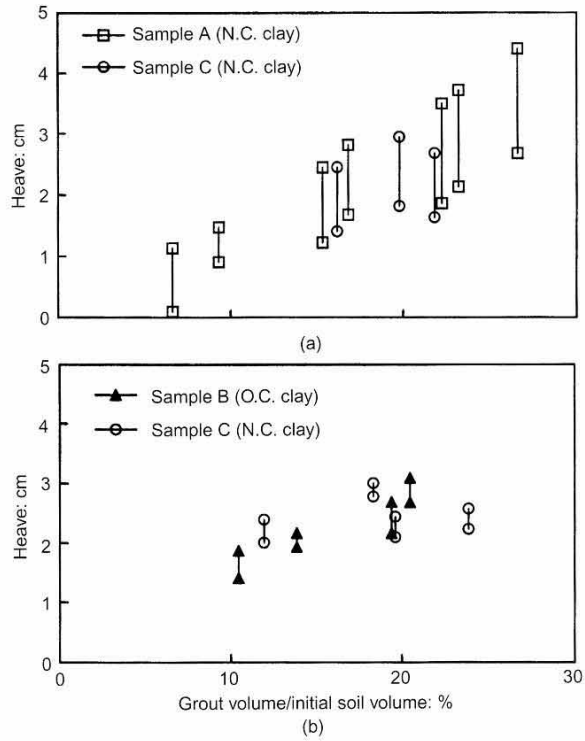

Fig. 8. Measured initial and final heaves of the upper plate: (a) type I grout; (b) type II grout

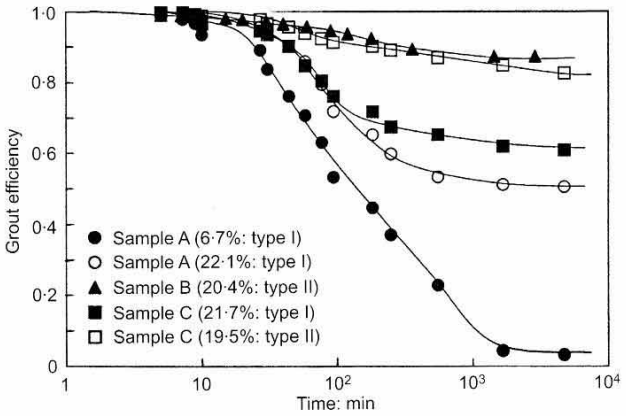

Fig. 9. Changes in grout efficiency with time

Consolidation tests were performed on the tested grouts with the same consolidation mould as used for the grouting tests. The grout was placed between two clay blocks, and a vertical stress corresponding to the injection tests was applied. Type I grout after hardening lost 30% of its original volume ($\lambda_G = 0{\cdot}30$), whereas, for type II grout, λ_G reduced to 0·07. Although it is possible that more bleeding will occur in the injection tests owing to larger injection pressure, these values were used as the volume loss due to grout bleeding (λ_G) for the subsequent discussion. However, further investigation on the compressibility of grout is needed for better characterisation of the tested grouts.

Using equation (1) with measured η_{lab} and λ_G, the implied volume loss due to consolidation (λ_C) can be estimated. The calculated values of λ_C for different injection volumes are shown in Fig. 10. For small injection volumes, there is a large loss due to soil consolidation ($\lambda_C = 0{\cdot}65$): the grout efficiency is therefore small owing to excess pore pressure development during injection and subsequent consolidation of the clay. As

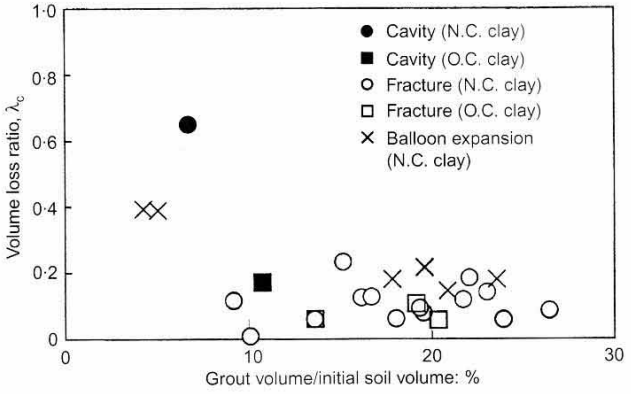

Fig. 10. Volume loss ratio due to consolidation

the injection volume increased, λ_C decreased to a value of approximately 0·10, and consequently the grout efficiency increased. The calculated volume loss ratio, λ_C, was independent of the type of grout used, suggesting that the pattern and amount of excess pore pressure development during injection were similar for both type I and II grouts.

As shown in Fig. 10, the overconsolidated clay (sample B) had a smaller volume loss than the normally consolidated clays (sample A) when the grout formed a bulb (solid symbols). This is due to the smaller excess pore pressures developed and the smaller plastic zone generated for a given injection volume compared with the normally consolidated clay.

The pattern of volume loss obtained from the grout injection into a balloon (cross symbols in Fig. 10) was similar to that without the balloon: λ_C decreased with increasing injection volume. The difference in volume loss between the balloon cases and the grout injection cases was approximately 0·1. The difference may be due to the mode of soil deformation (cavity mode rather than fracture mode) and variation in the initial conditions (natural rather than reconstituted specimens, applied vertical stresses, etc.). It was also considered that the size (or the boundary) of the mould might have affected the deformation pattern of the soil around the grout, and hence the grout efficiency. This boundary effect will be investigated in the numerical analysis described in the next section.

The boundary condition imposed in the laboratory tests needs extra consideration for any practical implications of the findings for a field scenario. In the laboratory tests, the grout cannot escape laterally because of the mould boundary; it is contained in the mould. In the field, the grout can escape laterally to any extent from the designed area. This will result in decreasing grout efficiency, especially when low-viscosity grout is used: hence the small volume losses at large injection volumes measured in the laboratory may not occur in the field.

FINITE ELEMENT MODELLING OF GROUTING IN CLAYS

Simulation of the laboratory experiments

Compensation grouting or grout jacking in the field involves a series of complex procedures and stages (for example drilling the borehole, installing tubes-a-manchettes, filling the borehole with cement bentonite, and pre-conditioning). Obviously some of these procedures are very complicated, and it is very difficult to model all the stages in great detail. However, the laboratory investigation described above highlighted the effect of the overconsolidation of clay and the boundary condition on the long-term grout efficiency. An attempt was made here to assess the finite element method's ability to model the long-term behaviour of grouting observed in the laboratory.

Several assumptions were made in the numerical investigation in order to capture the most important features of compensation grouting responsible for its long-term effectiveness. The finite element mesh used to model the laboratory tests is shown

in Fig. 11. The model geometry is the same as in the laboratory tests. The wall friction was assumed to be zero. The initial size of injection cavity was taken to be equal to the size of the injection needle diameter. Four-node axisymmetric consolidation elements (Akai & Tamura, 1978) were adopted for the analysis. The Cam-clay model (Schofield & Wroth, 1968) was used, and the material properties and the initial conditions are listed in Table 4.

At the beginning of the analysis, the initial condition of the sample (stress state and stress history) was defined. The grout injection process was simulated by applying uniform pressure at the boundary of the injection cavity; the fracturing phenomenon is not simulated. The pressure was ramped until a specific injection volume was obtained. After fixing the nodes at the cavity boundary, consolidation analysis was then performed until the excess pore pressures in the model became zero. The injection volume is fixed throughout the consolidation analysis, which means that bleeding of the grout is not modelled. The displacement of the top boundary was computed with time to calculate the volume loss ratio, λ_C. As the cavity boundary is fixed, λ_G is equal to zero in the analysis.

The volume loss ratio was computed from various injection volumes for both the normally consolidated condition (sample A) and the overconsolidated condition (sample B). As shown in Fig. 12, a trend similar to that found in the laboratory tests was obtained. Smaller volume loss ratios were obtained for the overconsolidated condition than for the normally consolidated condition, and the volume loss ratio decreased with increasing injection volume. The computed volume loss at large injection volume was close to the results of the balloon tests.

The contours of the excess pore pressures developed immediately after grout injection are shown in Fig. 13 for three different injection volumes (5%, 11% and 23% of the original soil volume) in sample A. In the figure, the calculated excess pore pressures were normalised by the maximum excess pore pressure. It is clear that the mould boundary starts to affect the pattern of excess pore pressures in the specimen as the injection volume increases. The location of the maximum excess pore pressure moves from the injection boundary into the soil. Moreover, the actual magnitudes of the excess pore pressures do not increase as much as the increase in the injection pressure or volume. This is the main reason why the volume loss due to consolidation is small in the large injection volume cases. It seems that the change from cavity expansion to fracture observed in the laboratory had only a small influence in increasing the grout efficiency.

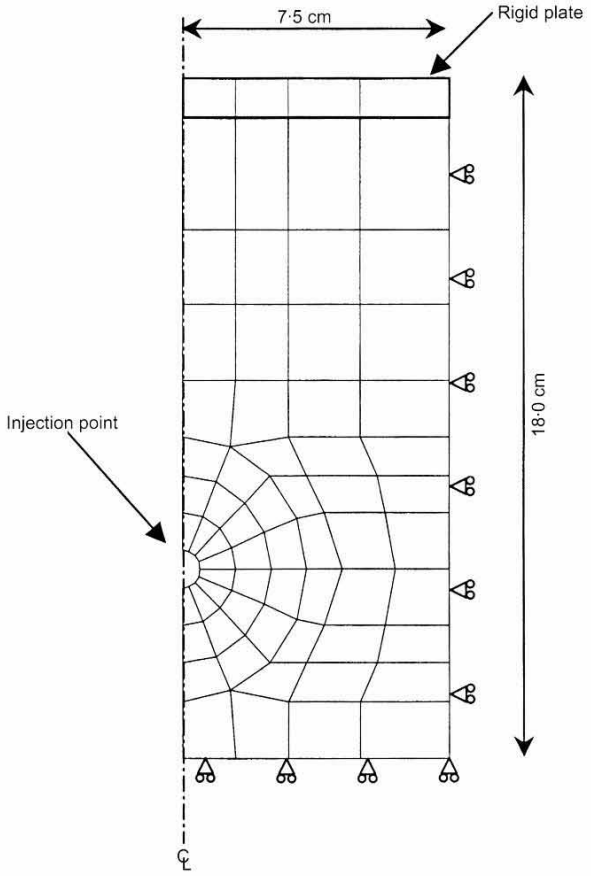

Fig. 11. FE mesh used for laboratory simulation

Simulation of the field trial

Both laboratory tests and the finite element analysis showed that soil consolidation due to the excess pore pressure generated during grout injection was responsible for reducing the grout efficiency in the long term, especially for normally consolidated clay. The finite element analysis of the laboratory tests highlighted the importance of the boundary effect when long-term grout efficiency needs to be assessed. Therefore the grout–soil interaction needs to be solved as a boundary value problem. Adopting the same modelling technique used to simulate the laboratory tests, the field trial described earlier was simulated.

The three-dimensional finite element mesh used for the analysis is shown in Fig. 14. The mesh models both case B and case C conditions. A total of 11 232 eight-noded cubic

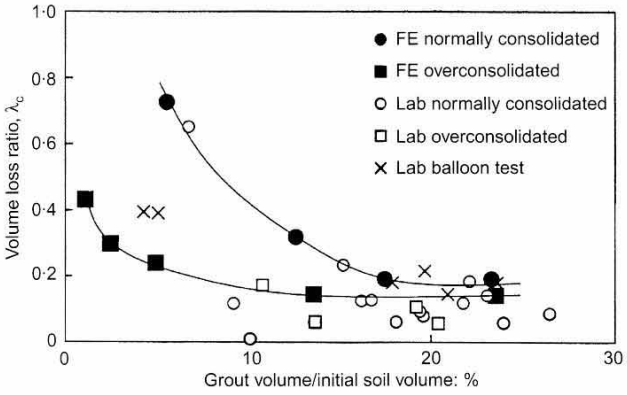

Fig. 12. Finite element results of volume loss ratio due to consolidation

Table 4. Cam-clay properties used for simulation of the laboratory experiment

Name	Normally consolidated clay	Overconsolidated clay
	Sample A	Sample B
λ	0·647	0·23
κ	0·107	0·038
M	1·02	1·17
e_0 at 1 kPa	1·8	1·25
Poisson's ratio, ν	0·361	0·338
p_0	235 kPa	402 kPa

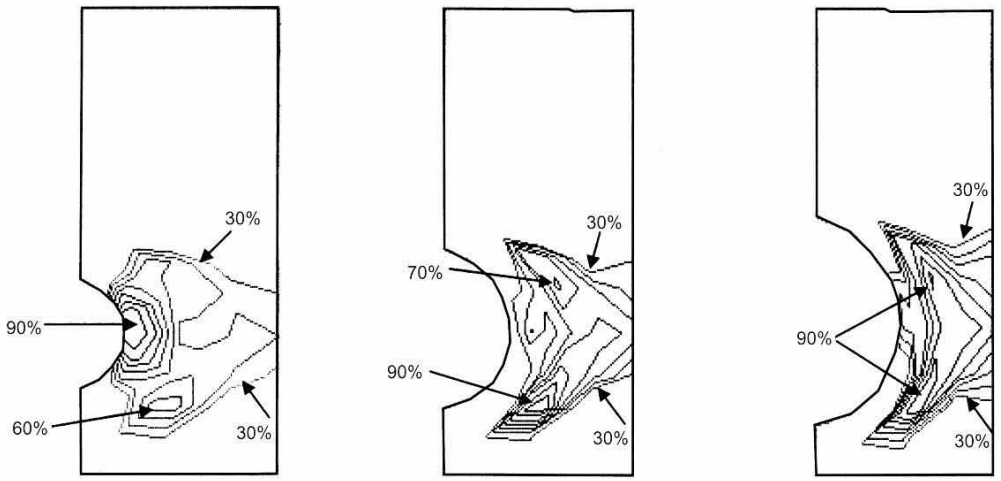

Injection volume/ initial soil volume	5%	11%	23%
Injection pressure	496 kPa	600 kPa	704 kPa
Maximum excess pore pressure	166 kPa	197 kPa	226 kPa

Fig. 13. Computed excess pore pressure development during injection; normalised excess pore pressure contours (= excess pore pressure/maximum excess pore pressure) increment of 10% from 30%

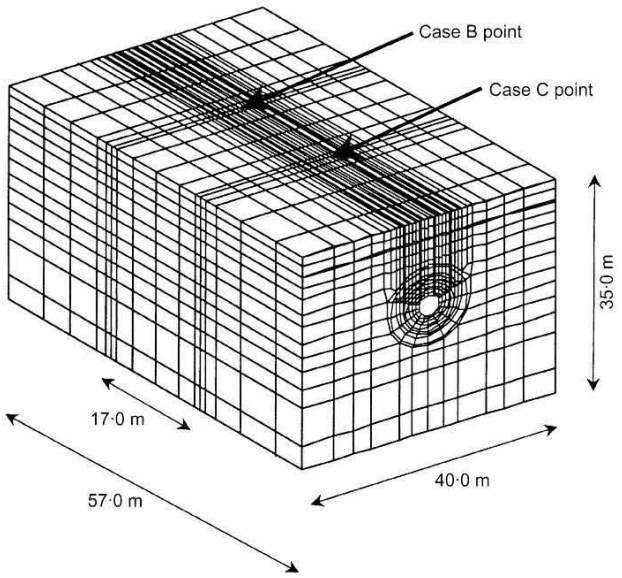

Fig. 14. FE mesh of field trial

consolidation elements were used to model the soil. The Cam-clay material properties were determined independently from conventional laboratory tests, and they are listed in Table 5. The tunnel lining was modelled using rigid beam elements, and the tunnel boundary was assumed to offer no drainage.

The injection points were modelled as an initial cavity size of 0·07 m diameter, which is the same as the injection pipe diameter. As in the laboratory test simulation, the grout injection was modelled by applying uniform pressure at the cavities. The magnitude of the applied pressure was increased until the computed heave at monitoring point 3 matched the measured one. The cavity boundaries were then fixed, and consolidation analysis was performed. It is important to note here that the construction of a tunnel is not modelled in this analysis. The geometry of the tunnel is fixed, and there is no inward movement of the soil into the tunnel: hence the computed deformation will be due to grouting operation only. The analysis was intended to investigate the long-term effect of grout jacking decoupled from the effect of tunnel construction.

Table 5. Material properties used for simulation of the field trial

	Layer		
	1	2	3
Depth	0–10 m	10–15 m	Below 15 m
λ	0·291	0·371	0·311
κ	0·049	0·062	0·052
M	1·04	1·02	1·03
e_0 at 1 kPa	1·62	1·56	1·33
ν	0·358	0·361	0·360
K_0	0·558	0·565	0·562
k	10^{-9} m/s	10^{-9} m/s	10^{-9} m/s

In order to match the heave at monitoring point 3, the volume expansion necessary for each injection point was only 0·007 23 m^3 and 0·005 12 m^3 for cases B and C respectively. These values are much smaller than the actual injected volumes (0·68 m^3 and 1·2 m^3 for cases B and C respectively). In the field, the other portion of the low-viscosity grout may have escaped into the fractures formed during injection. Unfortunately, no field inspection was conducted to confirm this.

The computed deformations with time at the three monitoring points are compared with the measured data in Figs 15 and 16 for cases B and C respectively. The computed heaves at monitoring points 1 and 2 immediately after the injection agreed reasonably well with the actual measurements. The initial heave achieved by grout jacking gradually decreased with time as the excess pore pressures generated by the cavity expansion dissipated. The final settlements were greater than the heave initially generated. The large injection pressures at the injection points sheared the surrounding normally consolidated clay, and large excess pore pressures were generated, leading to large consolidation settlements during the dissipation.

Although the trends are similar, the computed long-term displacements are smaller than the measured ones: the difference is approximately 10 to 15 mm. It is considered that this

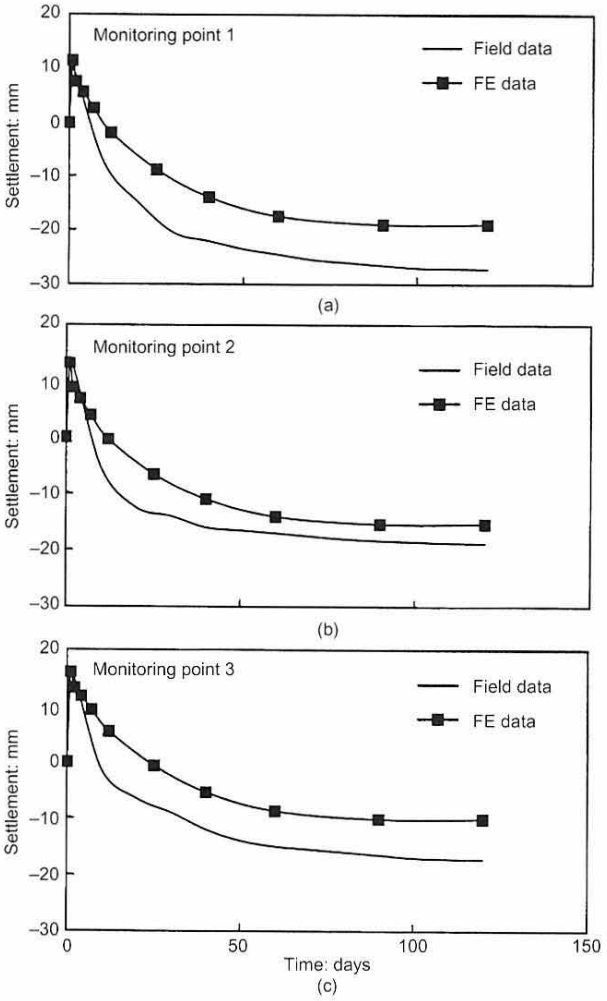

Fig. 15. Comparison between computed results and field data for case B

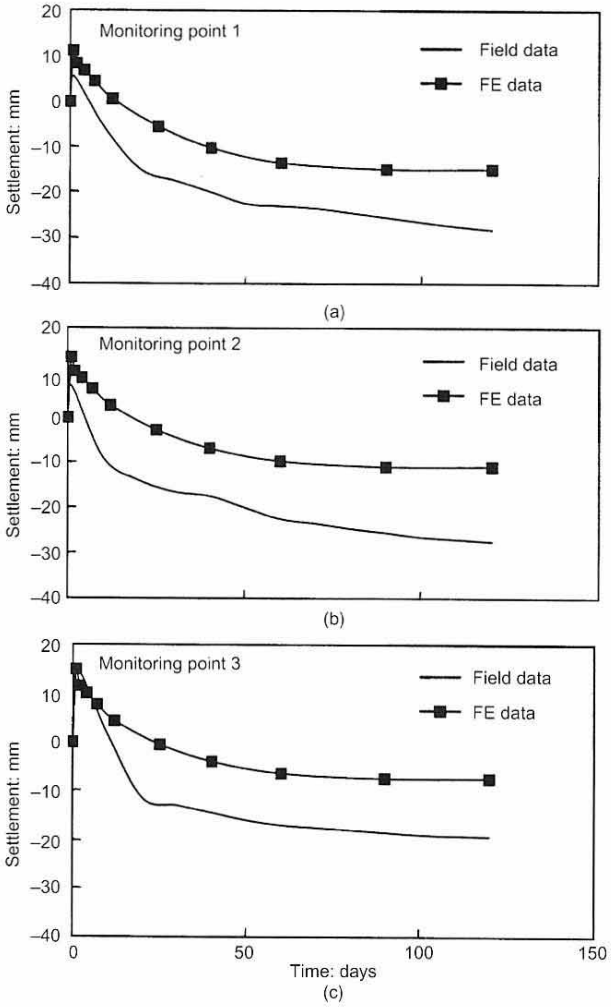

Fig. 16. Comparison between computed results and field data for case C

discrepancy is due mainly to the additional excess pore pressures generated during the shield tunnel construction and the change in drainage condition around the tunnel, which will also contribute to the long-term deformation of the surrounding soil.

Case A was also simulated by expanding the tunnel boundary radially until the computed displacement at monitoring point 3 matched the actual one. Fig. 17 shows the computed settlement curves compared with the long-term measurements at the three monitoring points. Again, the measured settlements are approximately 10–15 mm larger than the computed ones, which is similar to the results found in cases B and C. Therefore, in order to match the actual measurements, the shield machine excavation process needs to be modelled.

CONCLUSIONS

The effectiveness of grout jacking to reduce surface settlements during underground construction in clayey ground was investigated by a field trial in Tokyo. The results from the field trial showed that, although sufficient heave was achieved immediately after the grout injection, the ground continued to settle with time owing to grout shrinkage and soil consolidation associated with the excess pore pressures developed during the grout injection. Larger long-term ground settlements were observed in the grout jacking operation compared with the tail void grouting operation.

A laboratory investigation was conducted to find the parameters that reduce the long-term grouting efficiency in clays. It was found that better long-term grouting efficiency can be achieved in overconsolidated clays than in normally consolidated clays, and the efficiency increased with increasing injection volume. Finite element analysis of the laboratory experiments confirmed that the amount and extent of excess pore pressures generated during injection govern the long-term grout efficiency. When the soil deformed as an expanding cavity, the grout efficiency was as low as 10%. However, when a large amount of grout was injected, the grout efficiency increased as the clay fractured and the grout penetrated into the fractures. The finite element analysis of the laboratory tests confirmed that the mould boundary contributed to the increase in the grout efficiency.

Finite element analysis of the field trial was performed to simulate the long-term ground deformation after grout injection. Adopting the same modelling technique as used in the laboratory test simulation, it was possible to obtain a similar trend for the long-term behaviour of grout jacking as observed in the field trial. The final settlements were greater than the initial heave generated, owing to the large excess pore pressure generated in the sensitive clay around the injection points. However, the actual shield tunnel construction process needs to be modelled in order to match the field data.

ACKNOWLEDGEMENT

The authors would like to acknowledge the financial support from the Brite Euram programme of the European Commission.

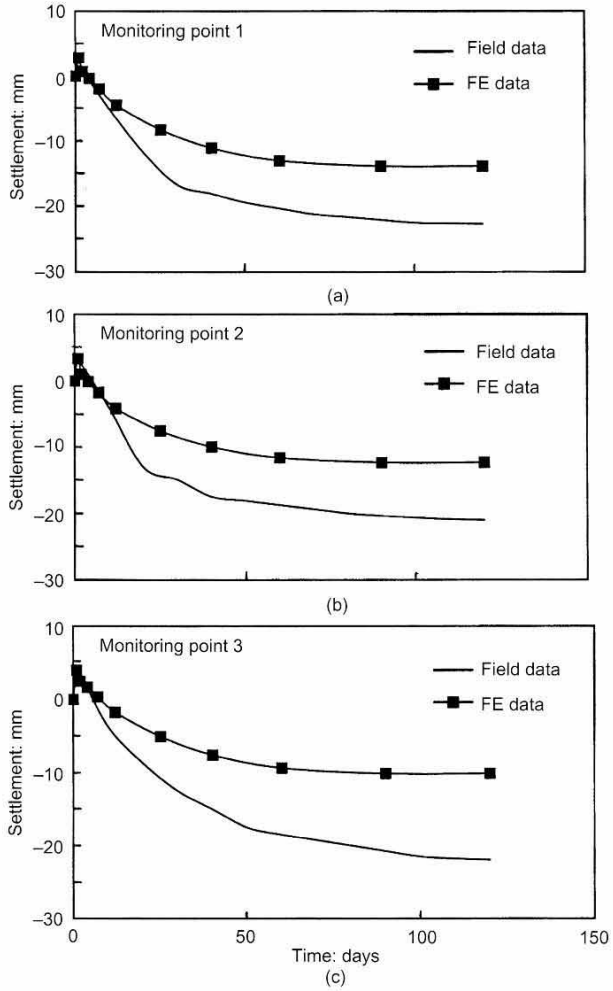

Fig. 17. Comparison between computed results and field data for case A

REFERENCES

Akai, K. & Tamura, T. (1978). Numerical simulations of multiple dimensional consolidation caused by elasto-plastic constitutive equation. *J. Geotech. Engng, Japan. Soc. Civ. Engrs*, No. 269, 95–104 (in Japanese).

Clough, G. W., Sweeny, B. P. & Finno, R. J. (1983). Measured soil response to EPB shield tunnelling. *J. Geotech. Engng, ASCE* **109**, No. 2, 131–149

Harris, D. I., Pooly, A. J., Menkiti, C. O. & Stephenson, J. A. (1996). Construction of low-level tunnels below Waterloo Station with compensation grouting for the Jubilee line. In *Geotechnical aspects of underground structures* (eds R. J. Mair and R. N. Taylor), pp. 361–366. Rotterdam: Balkema.

Harris, D. I., Mair, R. J., Burland, J. B. & Standing, J. A. (1999). (eds Kusakabe, Fujita and Miyazaki) Compensation grouting to control tilt of Big Ben clock tower. In *Geotechnical aspects of underground construction in soft ground*. (IS-Tokyo 99), pp. 225–232 Rotterdam: Balkema.

JSSMFE (1993). *Underground construction in soft ground in Japan*. JSSMFE (Japanese Society of Soil Mechanics and Foundation Engineering) Committee on Underground Construction in Soft Ground, Tokyo.

Mair, R. J. & Hight, D. W. (1994). Compensation grouting. *World Tunnelling*, Nov., 361–367.

Mair, R. J. & Taylor, R. N. (1997). Bored tunnelling in the urban environment. *Proc. 14th Int. Conf. Soil Mech. Found. Engng*, **4**, Hamburg 2353–2385.

Mori, A. and Akagi, H. (1985). Effect of backfilling at shield work in soft cohesive soil. *Proc. 11th Int. Conf. Soil Mech. Found. Engng*, **4**, San Francisco 1667–1670.

Mori, A., Tamura, M. & Fukui, Y. (1990). Fracturing pressure of soil ground by viscous materials. *Soils Found.* **30**, No. 3, 129–136.

Mori, A., Tamura, M., Shibata, H. & Hayashi, H. (1992). Some factors related to injected shape in grouting. *ASCE Proc. Grouting, Soil Improvement and Geosynthetics, New Orleans*, pp. 313–324.

Osborne, N., Murry, K., Chegini, A. & Harris, D. I. (1997). Construction of Waterloo Station upper level tunnels, Jubilee line extension project. *Proc. Tunnelling 97*, pp. 639–662. London: Institution of Mining and Metallurgy.

Schofield, A. N. & Wroth, C. P. (1968). *Critical state soil mechanics*. London, McGraw-Hill.

Shirlaw, J. N. (1995). Observed and calculated pore pressures and deformations induced by an earth pressure balance shield: Discussion. *Can. Geotech. J.* **32**, 181–189.

Shirlaw, J. N., Dazhi, W., Geneshan, V. & Hoe, C. W. (1999). A compensation grouting trail in Singapore marine clay. (eds Kusakabe, Fujita and Miyazaki) In *Geotechnical aspects of underground construction in soft ground*. (IS-Tokyo 99) pp. 149–154 Rotterdam: Balkema.

Soga, K., Bolton, M. D., Au, S. K. A., Komiya, K., Hamelin, J. P., Van Cotthem, A., Buchet, G. & Michel, J. P. (2000). (eds Kusakabe, Fujita and Miyazaki) Development of compensation grouting modelling and control system. In *Geotechnical aspects of underground construction in soft ground*. (IS-Tokyo 99) pp. 425–430 Rotterdam: Balkema.

Warner, J. (1992). Compaction grouting: rheology vs. effectiveness. *ASCE Proc. on Grouting, Soil Improvement and Geosynthetics, New Orleans*, **2**, No. 1, pp. 694–707

Warner, J. (1998). Pressure behaviour: an important monitoring tool in grouting. *Ground Improvement*, No. 2, 5–10.

The reviewer's opinion on the submitted paper for

Géotechnique, Volume 51, No.10

SOIL CONSOLIDATION ASSOCIATED WITH GROUTING DURING SHIELD TUNNELLING IN SOFT CLAYEY GROUND

OVERVIEW

a) The subject of the paper is topical and of considerable interest.

b) There is an enormous amount of information within the paper which includes a field trial and laboratory experiments together with finite element analyses of both. Perhaps inevitably with such an ambitious scope the level of detail is not great and in some instances facts which are pertinent to understanding the results are omitted. These are listed within the Specific Comments section below. Two particular instances are important: Firstly, the sensitivities of the clays are given, however, the potential influence on the observed performance of the high values quoted is not addressed. Secondly, the FE analysis of the tunnel shows settlements greater than the heave generated; it is considered that this result is of great interest and should be discussed in the paper.

c) The content or the Paper has not been published elsewhere to my knowledge.

d) Speculative material is indicated but where further deductions are made based on an assumption further reference to the original assumption would be beneficial.

e) The objectives are clearly stated.

f) The relationship between compaction grouting, compensation grouting and grout jacking should be described. The material presented pnmari1y addresses grout jacking rather than compensation grouting.

g) The information presented appears to be accurate and consistent although there appears to be an error in the units of heave on Figure 8.

h) The conclusions drawn follow from the presentation of information but some very interesting facets of the data are not discussed. (See comments under b)

i) Although the level of information given is probably sufficient, areas where further data would assist in understanding the conclusions drawn are highlighted in the Specific Comments section below.

SPECIFIC COMMENTS

INTRODUCTION

the word “lifelines” is not understood

it is not accurate to say in general terms that surface settlements due to turnnelling are typically less than 10mm. This statement needs to be qualified in some way e.g. for EPB machines in soft clay.

Figure 1 shows that majority of movement during tunnelling for the curve without compensation grouting i.e. about 70% at line indicating tail void injection. This is at variance with the statement in the text.

The role of drainage into the tunnel should be mentioned - is it the intention to state that dissipation of generated pore pressure is much more significant than reduction of pore pressures below their original values due to drainage into the tunnel? Significant long term movements can also occur for months and years after tunnelling in stiff clay, pnmari1y due to drainage.

CONCEPTUAL MODEL OF GROUTING N CLAYEY SOILS

In that the discussion relates to clayey soils it is probable that neither compaction nor fracture grout will penetrate into the soil pores – both will remain as homogeneous masses albeit with markedly different shapes. The conceptual model of grouting Within clay is that it is an undrained event and therefore no immediate densification of the ground will occur.

Fracture grouting generally exploits an existing plane of weakness to form a fracture rather than forming a plane of weakness.

If soil deformation is occurring undrained the displaced volume must equal the injected volume. The heave volume is only one component of the displaced volume, others include increased deformation towards the excavation and lateral displacements.

If water bleeds from the grout into the ground there is no immediate volume change since the ground volume would increase.

FIELD DIVESTIGATION OF COMPENSATION GROUTING IN SOFT ALLUVIAL CLAY

The soil in which the grout was infected has a sensitivity quoted as 23. Some comment on the impact of this is required.

The grout was injected after the tunnel passed and the “volume loss” settlements were small (<5mm). The grouting also induced heaves in excess of the tunnel related settlements. The process is thus grout jacking rather than compensation grouting.

There are a number of pertinent facts which are not stated for Case A:

- was the tail void routinely grouted and the volume increased for Case A?
- over what length of tunnel was Case A undertaken?
- what grout mix was used?
- what were the actual grout volumes injected?
- How were the injection tubes installed?

For Cases Band C was the tail void injected at all? How far from the TBM were the injections? Terminology such as “volume of ground to be improved” suggests that the aim of the grouting was densification by compaction (grouting) rather than controlling movements by compensation grouting.

To compare the results some discussion of potential inaccuracies is required. E.g. the tests were very localized; were 3D effects significant?; what is the natural variability of the ground response to tunnelling without compensation grouting?

Were grout volumes determined prior to injection as implied in the description of the field trial or was a specific heave of the lowest monitoring point targeted as implied in the test results section?

Figure 5 shows a flattening of the curves for Case A in the middle of month 6 which appears to be at the time of injections for Cases B and C - is this significant?

LABORATORY ひIVESTIGATION OF GROUTING IN SOFT CLAYS

The shear strengths quoted in Table 3 are not consistent with the description “soft” used in the text.

Th drainage boundary conditions could usefully be added to Figure 6.

The properties of the sample consolidated from a slurry are not given.

The heave upon injection is stated to be equal to the injection volume. Figure 8 shows significant divergence from the linear relationship determined for the nominal length of sample quoted - sample lengths would have to vary by up to 40% to account for differences. Vertical scale of both parts of Figure 8 should be in centimetres to be consistent with stated sample length and grout volume percentages.

The assumption that the oedometer measured compression of the grout would be re-produced in the grout injected within clay is not proven. The boundary conditions for drainage are very different.

The comparison of the two results for the “Cavity” mode of behaviour states that the overconsolidated sample had a "slightly smaller volume loss" [ratio]. This is not justified by the two data points given Which differ by a factor of more than 3.

It is not clear whether the “bal1oon” was successful is maintaining an approximately spherical shape of the injected grout. Did the balloon prevent bleed of the grout into the surrounding soil?

The clay used for the balloon tests was consolidated from a slurry whereas the other tests were on intact samples - a comment on the significance of this difference would be helpful.

Once the grout starts to fracture and reaches the edge of the container, uplift can continue at a pressure sufficient to overcome the overburden pressure and any friction between the soil and the container with little or no deformation or the soil. Did the results show this type or behaviour?

FIMTE ELEMENT MODELLING OF COMPENSATION GROUTING IN CLAYS

Lab Tests

Strictly the process being modelled is grout jacking rather than compensation grouting.

The boundary conditions used to model the lab apparatus are shown on Figure 11 - this should be stated. The drainage boundary conditions could also be added to this figure.

Three sets of parameters are given in Table 4. It is not clear which set were used to produce the results presented.

The OCR used in the analyses is not stated.

Are results available for all three sets of parameters?

It is stated that the analyses were pressure controlled - are the shapes of grout bulb indicated on Figure 13 therefore a result of the analyses?

Comment On the implications of the analyses results on the change in mode from cavity to fracture mechanisms observed in the lab would be of interest. Also comment on the grout efficiency ratio could be added.

Field Trial

It is interesting that the analysis re-produces the observation that settlement following grouting exceeds the heave produced. This facet of behaviour warrants further comment Particularly with respect to the potential influence of sensitivity and drainage into the tunnel. This result implies that an efficiency of greater than1 00% can be achieved by compaction grouting in non-sensitive soils. A comparison of the volume of settlement and the volume of grout would be of great interest.

Soil Consolidation Associated with Grouting During Shield Tunnelling in Soft Clayey Ground.

Komiya K. Soga K. Akagi H, Jafari M R, Bolton M D

General comments for the authors

1. I would suggest that the English is thoroughly checked by the English-speaking author.

2. Page 3 - what are “lifelines”.

3. Page 3 - could the authors refer to projects in which settlements have been less than 10mm.

4. Figure 1, most settlement appears to occur during tunnelling. Also tile kinks in the profile may not be evident a different symbol should bc used to illustrate the intention.

5. Page 5, compensation grouting my also travel along a natural fissure, joint or bedding.

6. Table 1. it would be useful to include strength data. It is noted that the clay is highly plastic and sensitive, some discussion is required on the soil properties. Is the degree of sensitivity important to the observed behaviour?

7. Page 7. over what length of tunnel is the grouting carried out.

8. Page 8. why 24% of the volume of the ground.

9. As a general point, do the authors expect drainage to occur into die tunnel?

10. Table 3, the strength of the soft clay is quite high and not compatible with the preconsolidation pressure for normally consolidated material.

11. Do the authors expect the samples of this highly sensitive clay to be of high quality and undisturved?

12. Was any attempt made to measure pore pressure in the field following compensation grouting.

13. Page - what is the effect of grout bleed on the surrounding soil?

14. Page l5. the authors arc correct to point out that the laboratory test results may not reflect the field situation. The main conclusions of relevance are the generation of pope pressure and consolidation settlement.

15. Page 17 - the OCR is not given and the parameters are not Clear.

Géotechnique
Volume 53, No.4
pp.447-448
May 2003
Institution of Civil Engineers

Komiya, K., Soga, K., Agaki, H., Jafari, M. R. & Bolton, M. D. (2003). *Géotechnique* **53**, No. 4, 447–448

DISCUSSION

Soil consolidation associated with grouting during shield tunnelling in soft clayey ground

K. KOMIYA, K. SOGA, H. AGAKI, M. R. JAFARI and M. D. BOLTON
(2001). *Géotechnique* **51**, No. 10, 835–846

J. N. Shirlaw, *Land Transport Authority, Singapore*

The authors have provided a very interesting paper, with a case study, laboratory testing and finite element analysis of the effects of grouting during EPB tunnelling. However, little detail is given on the monitoring and tunnelling in the case study, and further information would help to provide a fuller record of their work.

For the monitoring, were settlements measured using an array orthogonal to the direction of advance, to measure the width of the consolidation settlement trough? Based on my experience in Singapore with grout injected after tail void closure, I would expect the settlement troughs during consolidation for arrays B and C, and possibly A, to follow an 'error function' shape with a width similar to that of the initial settlement trough. Consolidation settlements due to this type of grouting have the effect of delaying the immediate settlement due to tunnelling, but the final effect is the same as immediate settlement. Using an i value of half the depth to tunnel axis, this would imply that the total volume loss due to tunnelling was 5·7%, 7·5% and 7·9% for cases A, B and C. These are relatively high values, but would be consistent with the closure of a gap of about 60 mm all around the tunnel. It would be useful to know the size of the tail void (the diameter cut by the machine minus the external diameter of the lining), to allow comparison with these volume loss figures.

The volume loss figures given above are high for an EPB machine operating in a firm clay. The stability number with no support pressure is 3·49. The total settlements recorded are high for such a stability number, even disregarding the support provided by the EPB machine. It would be useful to know the range of face pressures used during tunnelling, and whether the face was over-pressurised, which could lead to remoulding of the very sensitive clay.

The volume loss figures given above can also be expressed as volume losses of 0·405–0·558 m^3/m of tunnel. Trials B and C involved the injection of 3·8 and 6 m^3 of grout. Comparing these figures, I presume that the conventional tail void grouting was discontinued for several metres of the tunnel, but it is not stated over what length of tunnel the tail void grouting was replaced by the alternative grouting. This is important, because it appears that the settlement over Trials B and C was not just related to the effects of the trials. The surface settlement over the two trials would be due to the cumulative effects of tunnelling from a point about 21 m before the settlement point to about 21 m beyond the settlement point. It would therefore appear that the surface settlements over trials B and C would have included effects both from the trial injection and from the more conventional grouting as used in Trial A. I would note that the 'immediate' settlement identified in the paper does not allow for the time necessary for the full development of the immediate settlement trough, owing to this three-dimensional effect.

The conventional tail void grouting appears to have been more effective than the trial injections at controlling total surface settlement. However, the settlement was still large for this size and type of machine operating in firm clay. The authors do not state whether the tail void grouting was carried out using grout pipes laid along the tail skin, to allow grouting simultaneously with machine advance, or through the lining. The former of these has been found to be much more effective at filling the tail void before it closes (in soft clays) than the latter.

I was very interested in the high compressibility of the cement/silicate grout (Type I) used, and the significant reduction in grout compression using the Type II grout. This is clearly an area that warrants further investigation. However, I would appreciate some clarification on some of the items in the paper. The authors report a 120 s gel-hardening time for the Type I grout, but for the identical grout used in the tunnelling trial report a 20 s gel time. In the consolidation testing of the grouts, the authors report that Type I lost 30% of its original volume 'after hardening'. I am not clear whether the 30% loss was measured on hardened grout, or during the interval between injection and hardening. I also note that with Type I grout the laboratory trials show an initial volume expansion of very close to 100% of the grout volume used in all but one case. For the Type II grout the initial volume expansion is well below 100% of the grout volume used in three out of seven cases, implying some other losses in the system. The authors also do not state the mix used for grouting in trial A: it would be useful to know whether this grout was also prone to significant loss of volume.

As a final comment, I question the normalisation of the grout volume by initial soil volume in Figs 10 and 12. Within the laboratory trials the soil volume is defined by the size of the container. However, for wider application, this method of presentation is of limited value. Did the authors consider expressing the data in terms of $r+ \ni r/r$, where r is the radius of the initial injection cavity, and $r+ \ni r$ is the radius of the expanding bulb (assuming expansion as a sphere)?

Authors' reply

The authors thank Dr Shirlaw for showing his interest in the paper. The trial was performed at a site owned by the client. Owing to space constraints, unfortunately it was not possible to measure settlements orthogonal to the direction of advance. The tail void gap was approximately 50 mm all around the tunnel: therefore the estimates made by Dr Shirlaw are reasonable.

The face pressure was set to be approximately 255 kPa. This value was determined by adding 20 kPa to the total overburden pressure, which is standard practice in Japan. Because of this large pressure, it is possible that the clay in front of the machine was disturbed or remoulded, resulting

in additional consolidation settlement. Unfortunately, there is no evidence to confirm this from the limited monitoring data.

Conventional tail void grouting was not performed when the alternative grouting method was employed. The distance of the section without tail void grouting was approximately 10 m. When the tail void grouting was performed at Trial A, the monitoring points at B and C did not show any immediate settlements. However, the authors cannot confirm that the settlements at one trial site after some time were not affected by the grouting operations at the other trial sites. The data show only that Trials B and C generated larger settlements than Trial A, indicating an effect of grouting method (tail void grouting compared with alternative grouting).

No grout pipes were installed at the end of the shield machine. The tail void grouting was performed from either the first or the second lining placed outside the machine. The distance between the machine and the grouting point was about 30–50 cm. This corresponds to a time lag of about 30 min, allowing the gap possibly to close. Hence it is possible that this time lag has contributed to the large settlements observed.

In the experiment, the compressibility of the grout was evaluated separately from the grout injection tests. A given volume of grout was poured between heavily overconsolidated soil samples placed at the top and bottom of a large consolidometer. This was to create a more realistic soil–grout interface, which may affect the bleeding characteristics of grouts. After waiting for gel hardening, the composite soil–grout sample was consolidated at the same vertical pressure as used in the grout injection tests. With the knowledge of the compressibility of the overconsolidated soil sample, the volume loss of the grout due to vertical loading was measured and hence the compressibility of the grout was calculated. The 30% loss given in the paper comes from this test result.

Some initial loss observed in the Type II grout injection tests is due primarily to uncertainty in the amount of grout injected. The gel-hardening time of Type II was extremely short, and therefore it was not possible to measure the injected volume accurately. However, our experimental procedure has been improved since the presented work was performed, and injection volume is now determined more accurately. At present, grout efficiencies of close to 100% are obtained when grout is injected rapidly enough for the soil to be in undrained condition. The grout used in Trial A was a mixture of mortar and hardener; the volume reduction of this grout is considered to be small.

The authors do agree with Dr Shirlaw that the normalisations made in Figures 10 and 12 are not useful for practical application. In fact, a more extensive grout injection testing programme has been conducted at the University of Cambridge to investigate the effect of soil consolidation, grout properties, and injection method on grouting efficiency (Au, 2001), and these data are normalised in a similar manner to what Dr Shirlaw proposes.

REFERENCE

Au, S. K. A. (2001). *Fundamental study of compensation grouting in clay.* PhD thesis, University of Cambridge.

Journal of Geotechnical and Geoenvironmental Engineering
Volume 129, No.3
pp.254-262
March 2003
American Society of Civil Engineers

Factors Affecting Long-Term Efficiency of Compensation Grouting in Clays

S. K. A. Au[1]; K. Soga[2]; M. R. Jafari[3]; M. D. Bolton[4]; and K. Komiya[5]

Abstract: Compensation grouting has been attracting attention in recent years to control ground settlement caused by underground construction. A successful and effective application of compensation grouting depends not only on the use of a good monitoring system in the field but also on a fundamental understanding of grout behavior in soils. For compensation grouting in clay, there is a need to consider the long-term effectiveness of compensation grouting. Grout injection tests were conducted in the laboratory to examine soil fracturing patterns and consolidation effects in relation to compensation grouting. Both compaction and hydrofracturing modes of grouting were tested on kaolin clay specimens with different overconsolidation ratios. Finite-element analysis was also conducted to simulate the balloon expansion tests (ideal compaction grouting tests) and the results were compared with the data from the laboratory tests. Based on the research findings, new design criteria are proposed to improve the long-term efficiency of compensation grouting for clays.

DOI: 10.1061/(ASCE)1090-0241(2003)129:3(254)

CE Database keywords: Grouting; Laboratory tests; Finite element method; Fracture; Consolidation; Tunneling; Clays.

Introduction

In recent years, compensation grouting has become a popular method for settlement control during underground construction. The basic principle is that grout is injected in the zone between underground openings and building foundations to compensate for the ground loss and stress relief caused by the underground excavation. Grout injection is often undertaken simultaneously with construction in response to detailed observations so that settlement and distortions are limited to specified amounts. The use of real-time monitoring of settlement, such as by electrolevels attached to buildings, is the key to success for an effective compensation grouting operation (Mair and Hight 1994; Buchet et al. 1999; La Fonta 1999; Soga et al. 1999). In many cases, the information gathered from a real-time monitoring system has forced changes to the original grouting plan.

Successful applications of compensation grouting to tunneling are reported for the London Underground Jubilee Line extension project (Harris et al. 1996; Osborne et al. 1997; Harris et al. 1999), the Viennese subway project (Pototschnik 1992), the Saint Clair River tunnel project near the USA-Canada border (Dramer et al. 1994; Droff et al. 1995), the London Dockland extension project (Sugiyama et al. 1999; Essler et al. 2000) and the Lisbon underground line (Schweiger and Falk 1998). A summary of some of the past compensation grouting projects is listed in Table 1. The ''compensation efficiency'' in the Table 1 is defined as the ratio of the volume of heave obtained to the injected volume of grout. In general, low compensation efficiencies were calculated in soft clay conditions, whereas better compensation efficiencies were achieved in stiff clays. The field trial in Singapore soft clay reported by Shirlaw et al. (1999) showed that the heave obtained immediately after grout injection reduced with time due to soil consolidation associated with the dissipation of the excess pore pressures generated during injection. In some cases, the surface level came back close to the original condition. Similar findings were obtained in the field trials reported by Ikeda et al. (1996) and by Komiya et al. (2001), addressing the undesirable long-term effect of grouting in soft clay for settlement control purposes.

Possible Mechanisms of Decreasing Compensation Efficiency

Fig. 1 shows the conceptual modeling of compensation grouting in clays. At the initial stage of compensation grouting, the grout pushes the soil outward and deforms plastically, forming a ball. As the grouting pressure increases, the size of the ball increases rapidly until the grout pressure builds up to the fracturing pressure and a plane of weakness is formed by hydraulic fracturing as shown in Fig. 1(b). As a result, the stress condition in the soil suddenly changes and the injection pressure drops. When grout with low viscosity and/or low solid content is used, it will intrude into planes of weakness to develop grout-filled fractures. When a grout with high viscosity and/or high solid content is used, the grout would not be able to penetrate into fractures and the grout ball simply continues to expand. In Europe, fracture grouting is often used in compensation grouting because it is possible to regrout from the same grouting port.

The effectiveness of compensation grouting can be evaluated by the amount of soil heave obtained (compensation effect) for a

[1]Lecturer, City Univ. of Hong Kong, Dept. of Building and Construction, Hong Kong.

[2]Senior Lecturer, Univ. of Cambridge, Engineering Dept., Cambridge CB2 1PZ, UK. E-mail: ks@eng.cam.ac.uk

[3]Senior Geotechnical Engineer, STV Incorporated, New York.

[4]Professor, Univ. of Cambridge, Dept. of Engineering, Cambridge CB2 1PZ, UK.

[5]Professor, Chiba Institute of Technology, Dept. of Civil Engineering, Chiba, Japan.

Note. Discussion open until September 1, 2003. Separate discussions must be submitted for individual papers. To extend the closing date by one month, a written request must be filed with the ASCE Managing Editor. The manuscript for this paper was submitted for review and possible publication on December 26, 2001; approved on May 22, 2002. This paper is part of the ***Journal of Geotechnical and Geoenvironmental Engineering***, Vol. 129, No. 3, March 1, 2003. ©ASCE, ISSN 1090-0241/2003/3-254–262/$18.00.

Table 1. Case Studies of Compensation Grouting

Project	Depth (m)	Soil type	Tunneling method	Grouting method	Grout type	Compensation efficiency	Results
Viennese Subway (Pototschnik 1992)	10	Soft clay	NATM[a]	Fracture grouting	Silica gel	3%	50% settlement was reduced.
Imperial Oil's research building St. Clair River (Droff et al. 1995)	7	Soft clay	EPB[b]	Fracture grouting	Cement bentonite PFA	N/A	Soil fracture grouting proved to be an effective means of protecting the research building. The predicted settlement was reduced from 120 mm to the actual settlement about 10 mm.
Waterloo Station, London (Harris et al. 1996)	5	Stiff clay	EPB[b]	Intrusion Grouting	Cement bentonite PFA	N/A	Compensation grouting proved to be very successful in limiting settlement from 40 mm to 20 mm.
Big Ben Clock Tower (Harris et al. 1999)		Stiff clay	Open face shield	Fracture grouting	Cement bentonite	N/A	Tilt of the tower has been controlled within very fine tolerances.
Docklands Light Railway Lewishm Extension (Essler et al. 2000)	6.5	Stiff clay	EPB[b]	Fracture grouting	Cement bentonite, PFA, Silica gel	20%	Maximum settlement (predicted) was reduced from 30 mm to 0 mm (actual). Overlying structure has been protected.
Japanese Storehouse (Ikeda et al. 1996)	11	Soft clay	EPB[b]	Fracture grouting	Silica gel	3%	Compensation grouting undertaken from inside of the tunnel had been proven to be very effective in limiting settlement. The settlement was reduced from 60 mm to 14 mm heave.
Grouting trial in Singapore marine clay (Shirlaw et al. 1999)	7	Soft clay	No tunneling	Fracture grouting	Cement bentonite, PFA, Silica gel	−5%	Compensation grouting as a building protection measure within Singapore marine clay is unlikely to be successful.

[a]NATM indicates new Austrian tunneling method.

[b]EPB indicates Earth pressure balance machicne.

[c]PFA indicates pulverized fuel ash.

[d]N/A indicates not applicable.

given injected grout volume. Ideally, if an injection is rapid so that soil deformation is occurring in an undrained condition, the amount of heave is equal to the injected volume. However, this is often not the case in the field due to (1) increased deformation towards the excavation; (2) lateral subsurface displacements due to vertical fractures resulting in surface heave outside the designated compensation area; and (3) escape of the grout through extended fractures. Even if a good compensation effect is achieved immediately after injection, the effectiveness can decrease with time. The clay around the grout will consolidate due to the dissipation of excess pore pressures generated during injection [Fig. 1(c)] and the constituents of the grout can migrate into soil pores (bleeding and solid penetration).

The aim of this research was to investigate the factors affecting the long-term efficiency of compensation grouting. Grout injection tests were performed in the laboratory to examine soil fracturing patterns and consolidation effects in relation to compensation grouting. Both compaction and hydrofracturing modes of grouting were tested. During injection, the volume expansion of the specimen and the injection pressure were measured. Postinjection settlement was recorded to assess the magnitude of the consolidation effect. The factors varied in the laboratory testing program were the overconsolidation ratio (OCR) of the clay, grout materials, and the injection method (regrouting and grout spacing).

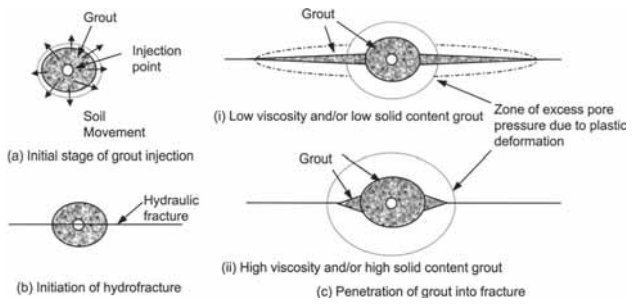

Fig. 1. Conceptual modeling of compensation grouting process

Experimental Investigation

The experimental layout of the laboratory grout injection tests is shown in Fig. 2. E-grade kaolin was consolidated in a modified consolidometer with an injection needle incorporated into the base. Two modified consolidometers with different diameters (50 cm or 100 cm) were employed. A 4 mm outer diameter (OD) and 3 mm inner diameter (ID) copper needle was used as an injection tube. The total length of the needle was 130 mm and the height above the bottom porous plate was 50 mm [see Fig. 2(a)]. In order to prevent the grout from leaking down the sides of the injection needle, a 40 mm long 4.5 mm ID copper tube was used as a retaining collar around the injection tube. As shown in Fig. 2(b), injection was made using a GDS Pressure/Volume Controller, which can control the injection rate and volume. A pressure interface chamber (PIC) was used to transmit the pressure from the hydraulic fluid in the GDS Controller to the grout during injection. Injection pressures were measured using a pressure transducer positioned between the PIC and injection needle, while surface displacements of the specimen during and after injection

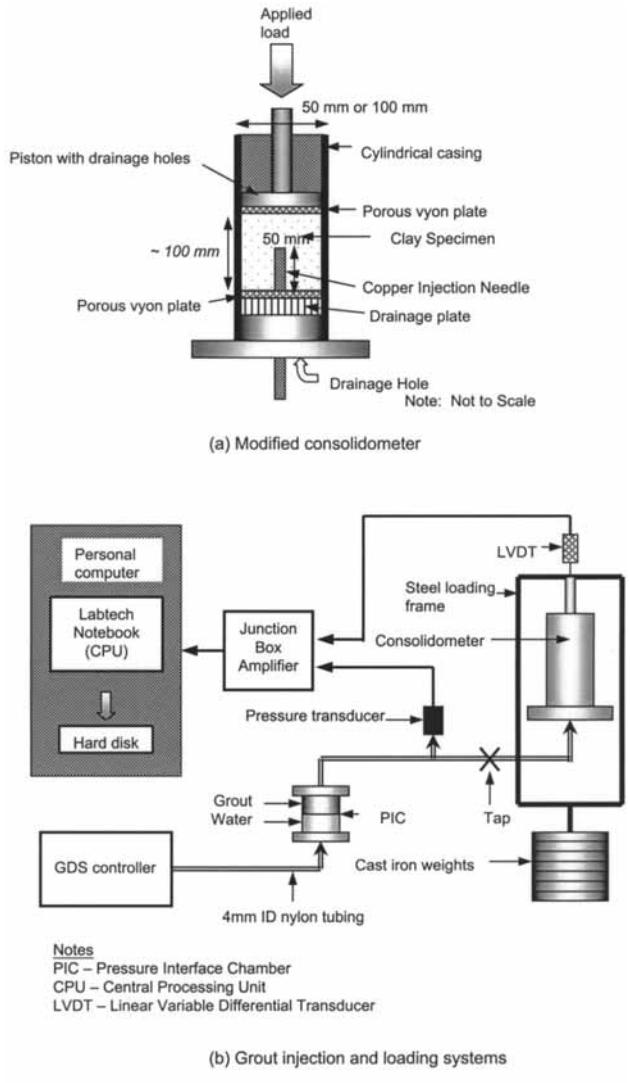

Fig. 2. Experimental setup for grout injection tests

were measured using a linear variable differential transducer attached to the top plate of the consolidometer.

In order to investigate the compensation effect under different stress histories, clay specimens were prepared at different OCR's ranging from 1 to 10. Clay slurry was made by mechanically mixing dry E-grade kaolin powder with de-aired water under a vacuum, giving a water content of 120%. The slurry was placed in a consolidometer and the volume of slurry was determined based on the condition that the specimen height before injection will be approximately 100 mm. The vertical effective stress during the injection stage was fixed to be 140 kPa.

Different injection materials were used to investigate the effect of grout bleeding and solid penetration on the long-term efficiency of compensation grouting: (1) Deaired water: Water will fracture the clay but can drain out from the fractures with time (large bleeding effect). (2) Epoxy resin: The epoxy resin used is manufactured by Sempol Surfaces Ltd. A ratio of 10:6 of resin and hardener by weight was selected to obtain the highest strength of epoxy resin. Epoxy resin does not bleed (no water), but can penetrate into clay fissures before hardening. The use of epoxy resin allowed the examination of the fracture pattern by washing the soil away after the test. (3) Laponite water mixture: Laponite is a colloidal synthetic layered silicate manufactured by Laporte Industries Ltd. A typical Laponite crystal is negatively charged and is about an order of magnitude smaller than a typical clay particle. Mixing of gel-grade Laponite with water forms a highly thixotropic gel with high viscosity at low shear. In this study, Laponite grout was prepared by mixing 3% by weight of gel-grade RD Laponite powder in 200 g de-aired water dyed red. The lack of setting properties and the small particle size mean that both bleeding of water and migration of the Laponite particles into the clay pores can occur. (4) Cement bentonite: A mixture of ordinary Portland Cement, bentonite, and water was adopted based on the grout mix used in current compensation grouting practice. The size of all of the solids is considered to be larger than the clay pores; hence, no solid penetration is expected. However, the water can bleed out from the grout with time. In order to examine the magnitude of the bleeding effect, tests were performed using three different water/cement ratios (w/c): $w/c = 0.6$, 1, and 3. Due to large wall friction through the piping, the GDS pressure controller could not inject cement bentonite grout with a water/cement ratio lower than 0.6. 3% bentonite by weight of cement was added to the mixture to increase the workability of the grout. (5) Balloon expansion: A latex balloon was placed at the tip of the injection needle and either water or epoxy was injected into the balloon to simulate an ideal compaction grouting model, where no bleeding or solid penetration could occur.

The injection volume of grout was fixed to be 5 ml. This was to ensure that the grout will be contained within the specimen and will not migrate through fractures reaching the boundaries. It was found from the preliminary tests using the smaller 50 mm diameter consolidometer that, if the grout volume is larger than 5 ml, the grout would escape from the testing boundaries through fractures, resulting in an artificial reduction in grouting efficiency. A series of regrouting tests were also conducted to investigate the effect of time lag between two injections and to find out which injection method would give the best long-term compensation effect.

Effect of Overconsolidation Ratio

The effect of OCR on grouting efficiency is shown in Fig. 3(a) for the balloon expansion tests using the 100 cm diameter consolidometer. The rate of injection was 500 mm^3/s. The grout efficiency (η) is defined as the ratio of heaved volume to the initial injection volume. The initial part of the curves immediately after injection implies that the injection process is not completely undrained. If the injection was performed in undrained conditions without grout permeation into the soil pores, the heaved volume should be equal to the injected volume resulting in 100% grout efficiency. However, it was common that the measured initial grout efficiencies (η_i) after the injection were slightly less than 100% even when the injection was done in a relatively small duration of about 10 s. This is thought to be due to the compression of tiny gas bubbles trapped in the grout materials and in the connections leading to the injection needle. Since the injection volume was only 5 ml, the effect of the compression of the air bubbles could not be neglected. In general, the amount of the initial efficiency loss was about 5% to 10% in most of the injection tests. Nevertheless, the outcome of Fig. 3(a) is clear. For the normally consolidated clay sample, negative grout efficiency was measured at the end of the consolidation stage. The final grout efficiency dramatically increased when the OCR increased from 1 to 2 and reached almost 100% for the heavily overconsolidated clay of OCR=5.

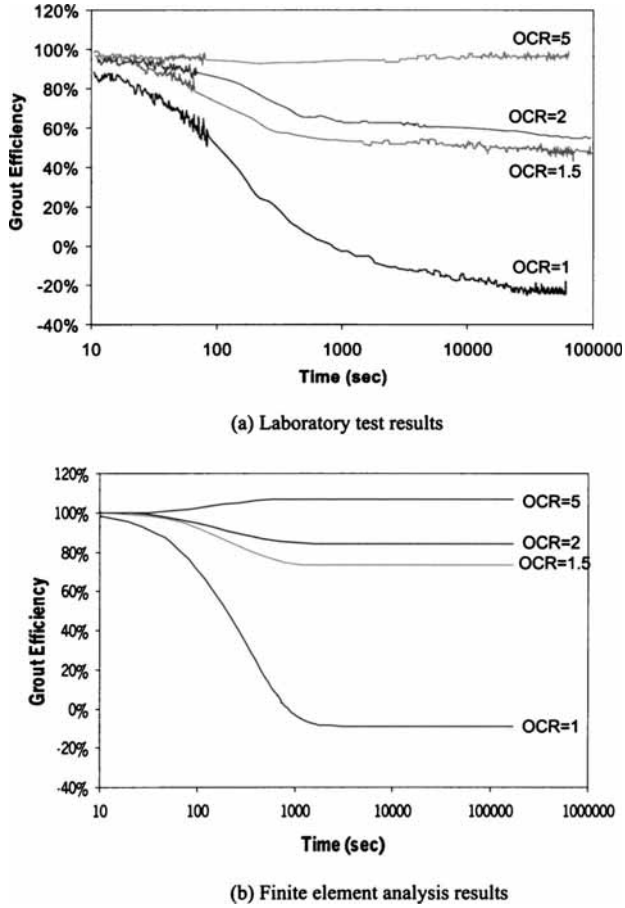

Fig. 3. Grout efficiency–time curves of balloon expansion tests

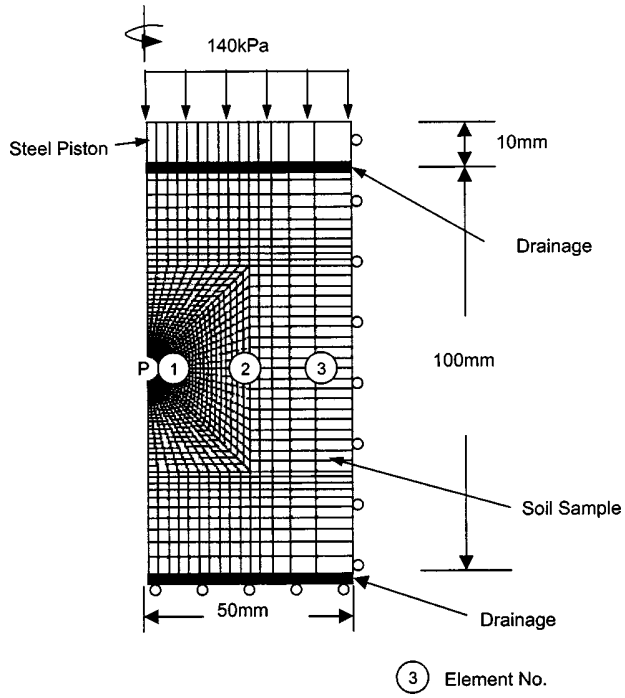

Fig. 4. Axisymmetric finite-element mesh

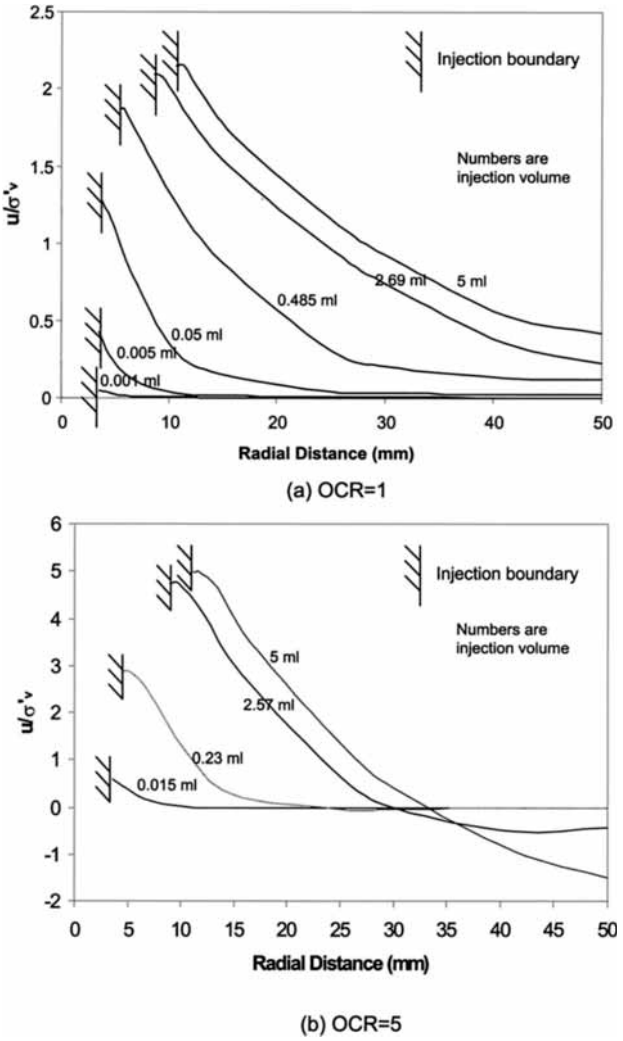

Fig. 5. Computed normalized excess pore pressure distribution within a clay specimen

Finite-element analysis of the balloon expansion tests was performed using *ABAQUS* version 5.8 with consolidation elements (HKS 1998). The axisymmetric finite-element mesh used is shown in Fig. 4. The radius of the initial cavity was assumed to be the radius of the latex balloon. The pressure was applied in the cavity until the cavity volume expanded by 5 ml. After fixing the displacements at the cavity boundary, the soil was allowed to consolidate. The modified Cam-clay model was used to simulate the deformation behavior of E-grade kaolin and the input parameters were $\lambda=0.13$, $\kappa=0.03$, $M=1.05$, $\Gamma=2.65$, $v=0.2$ and $k=2\times10^{-9}$ m/s. The details of the analysis are described in Au (2001).

The computed grout efficiency time curves with different OCR's are plotted in Fig. 3(b). Since the initial efficiency loss observed in the experiments does not exist in the finite-element analysis, the computed final grout efficiencies are consistently 10–20% higher than the experimental test results. When this initial loss is taken into account, the finite-element analyses gave good agreement with the experimental results.

The computed excess pore pressures during the injection stage along the horizontal direction from the injection point are shown in Figs. 5(a and b) for OCR=1 and 5, respectively. The computed excess pore pressures are normalized by the initial vertical effec-

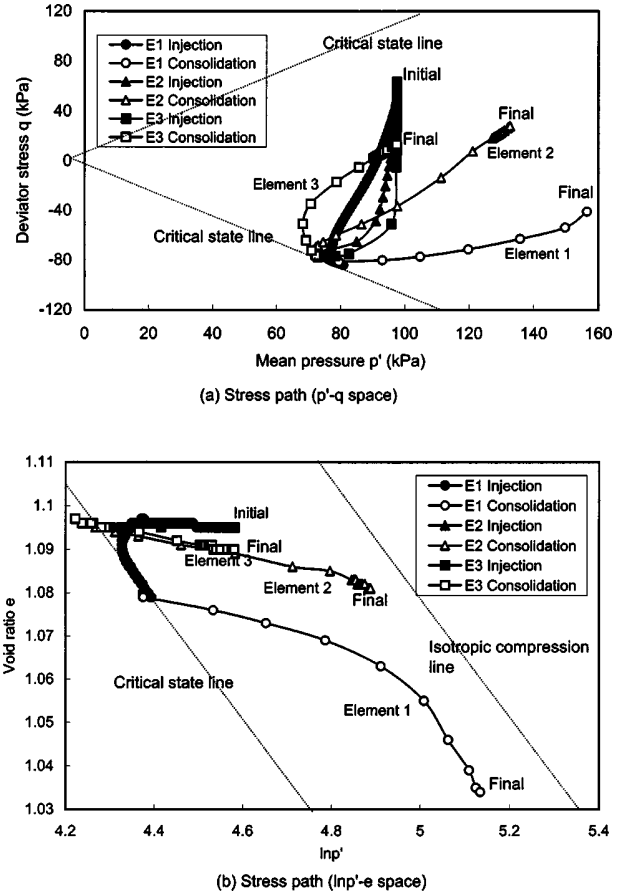

Fig. 6. State paths of selected elements for overconsolidation ratio=1 case

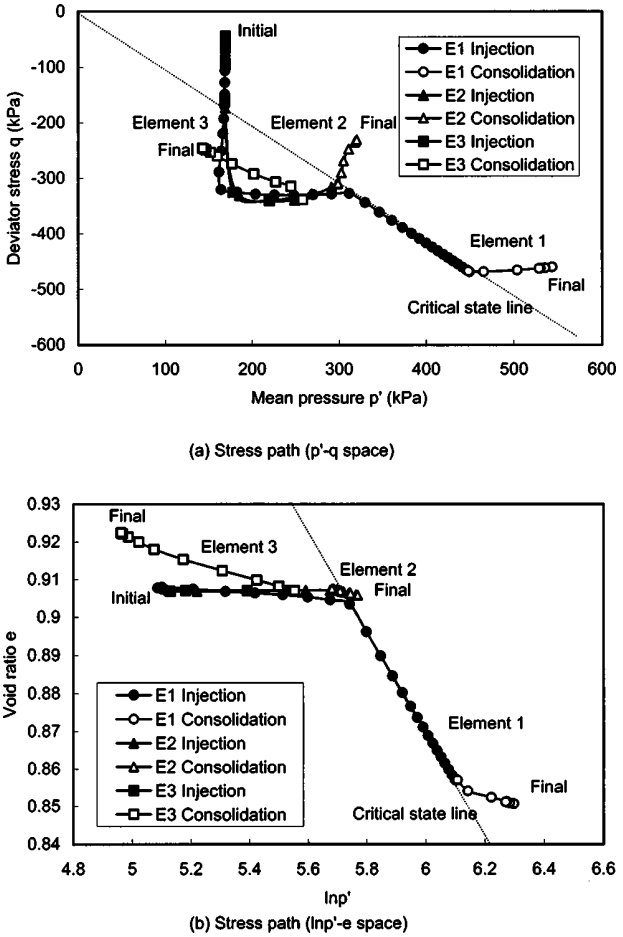

Fig. 7. State paths of selected elements for overconsolidation ratio=5 case

tive stress ($\sigma_v'=140$ kPa). In both normally consolidated and overconsolidated clay cases, the magnitude of the excess pore pressure around the injection point increased with the volume of injection.

For the normally consolidated clay, the computed excess pore pressures were all positive as shown in Fig. 5(a). Hence, the large decrease in grout efficiency with time for the normally consolidated clay specimen is due to dissipation of the positive excess pore pressures generated during injection. Fig. 6 shows the stress paths (in p'-q-e space) of the elements identified in Fig. 4. In Fig. 6, $p'(=(\sigma_v'+\sigma_r'+\sigma_\theta')/3)$ is the mean effective pressure, $q=\sigma_v'-\sigma_r'$ is the deviator stress, e is the void ratio, σ_v', σ_r', and σ_θ' are the vertical, radial, and circumferential effective stresses, respectively. The shear stress (τ_{vr}) was computed to be very small at these elements. The stress paths show that elements 2 and 3 were close to the undrained condition during the injection stage (solid symbols in Fig. 6). Element 1, which is adjacent to the injection boundary, showed partial drainage during the injection due to the large computed hydraulic gradient. During the postinjection stage (open symbols in Fig. 6), a large decrease in volume occurred due to the increase in mean effective pressure as the excess pore pressures dissipated.

For the overconsolidated clay case, the excess pore pressure was positive at the injection boundary, but it was negative at the outer boundary due to dilative behavior of the clay, as shown in Fig. 5(b). Fig. 7 shows the stress paths of the elements selected in Fig. 4. Element 1, which is adjacent to the injection boundary, decreased in volume during the injection stage along the critical state line (solid circles in Fig. 7). This is due to partial drainage caused by the large hydraulic gradient in the element. During the consolidation stage, the negative pore pressures that were generated some distance away from the injection point compensated for the excess positive pore pressures around the injection point. This resulted in a decrease in volume of element 2 (open triangles in Fig. 7) and swelling in element 3 (open squares in Fig. 7). As the excess pore pressures dissipated, the clay deformed elastically leading to a small loss in the grout efficiency as shown in Fig. 3(b).

Effect of Bleeding and Solid Penetration

The effect of bleeding and solid penetration on grout efficiency was investigated by injecting different types of grouts. The injection rate was kept as 500 mm^3/s. The 100 mm diameter consolidometer was used for the investigation.

The measured changes in the grout efficiency with time for various grouts injected into normally consolidated clay specimens are shown in Fig. 8. The injection of water resulted in the smallest final efficiency of -120%, whereas expansion of a latex balloon gave the largest final efficiency of -20%. The measured final grout efficiencies for different OCR's and different grouts are

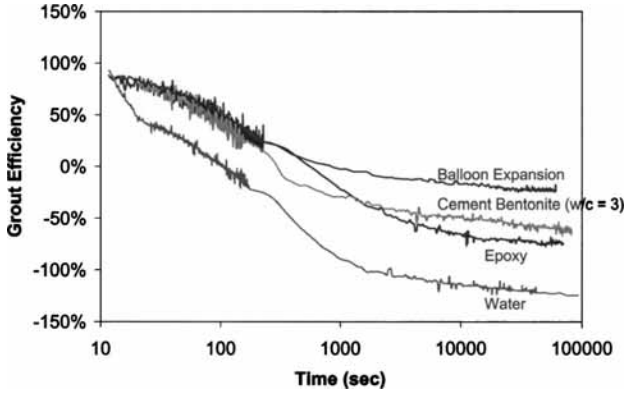

Fig. 8. Effect of grout material on grout efficiency–time curves for overconsolidation ratio=1

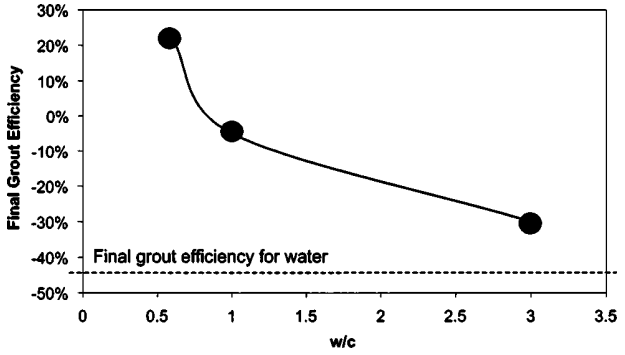

Fig. 10. Effect of water cement ratio on final grout efficiency for overconsolidation ratio=1

summarized in Fig. 9. The final grout efficiency improved dramatically when the OCR changed from 1 to 2.

The decrease in grout efficiency with time in the balloon expansion was mainly due to soil consolidation associated with excess pore pressures generated around the balloon. For the cement bentonite injection case, an additional decrease in the efficiency was caused by the bleeding of the water from the grout. From the field test result reported by Shirlaw (1990), the typical value of the w/c ratio in a fracture is about 0.3. McKinley (1994) performed laboratory tests to examine the consolidation of filter cake under the filtration pressure ranging between 5–60 kPa and found that the moisture content of the hardened grout fracture was approximately 0.35 for ordinary Portland cement. Hence, it was reasonable to assume the bleeding had occurred in the current experiments.

In order to confirm the bleeding effect, additional injection tests with different w/c ratio grouts were conducted using the 50 mm diameter consolidometer. Fig. 10 shows that the final grout efficiency increased when the w/c ratio decreased from 3 to 0.6. Hence, a high solid content grout will give good final grout efficiency owing to less bleeding effect.

Visual examination of the sectioned samples after injection indicated that the extent and thickness of fracture were different for different OCR's. Fig. 11(a) shows that a thick localized spherical ball was formed in the OCR=1 specimen. On the other hand, Fig. 11(b) shows that the grout injection in the OCR=5 specimen formed a horizontal fracture. When low solid content cement bentonite grout ($w/c=3$) was injected in an OCR=1 specimen, a thin horizontal fracture was formed across the sample as shown in Fig. 11(c). This suggests that the fracture initiation and propagation were also influenced by grout bleeding. When a grout material contains a higher solid content, filter cake is

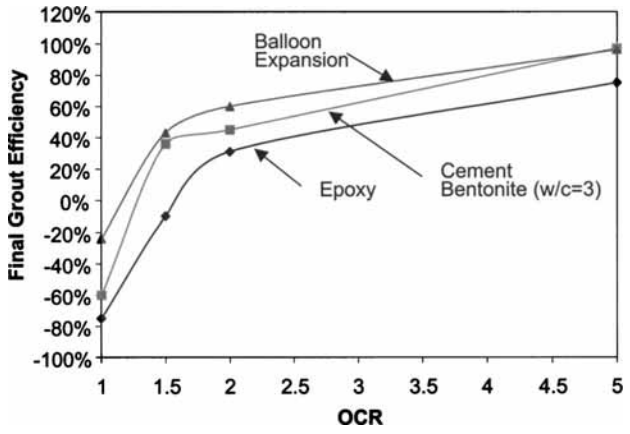

Fig. 9. Effect of grout material and overconsolidation ratio on final grout efficiency

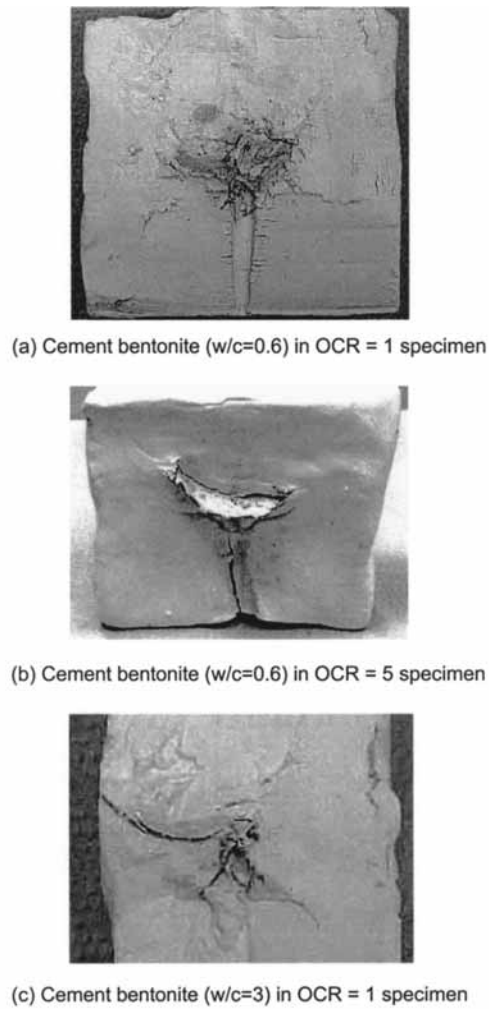

Fig. 11. Behavior of cement bentonite grout in overconsolidation ratio=1 and 5 specimens

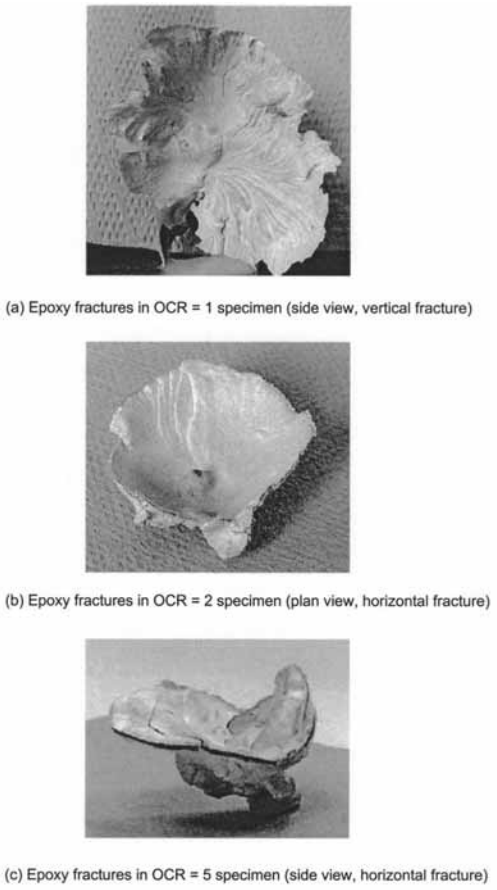

Fig. 12. Fracture patterns of epoxy injection in overconsolidation ratios=1, 2, and 5 specimens

formed rapidly around the cavity during the injection stage to block the minute cracks which developed around the injection cavity. Since the penetration of grout into fractures is less likely to occur by this blockage, further grout injection leads to shear failure around the injection cavity, similar to the balloon expansion tests.

When epoxy resin was injected into OCR=1 specimens, the fractures were thin and widespread, propagating to form a vertical fracture as shown in Fig. 12(a). Excess pore pressures were generated in a larger area, which resulted in a large decrease in grout efficiency with time. On the other hand, horizontal fractures were formed when epoxy was injected in overconsolidated clay specimens as shown in Figs. 12(b and c) for the OCR=2 and 5 specimens, respectively.

Laponite–water mixtures also resulted in low grout efficiency for normally consolidated clay specimens due both to bleeding and the solid penetration effect. The fracture generated in the OCR=1 specimen is shown in Fig. 13. The zone around the fracture was red indicating that bleeding and penetration of the grout occurred from the fracture. The injected water extensively sheared the OCR=1 specimens, creating a large zone of excess pore pressures. The large decrease in grout efficiency is due to the drainage of the injected water and the dissipation of the excess pore pressures. The post-test examination showed that the fractures propagated in different directions.

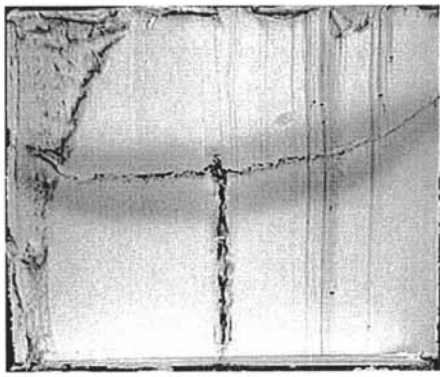

Fig. 13. Horizontal fractures by Laponite grout. Dyed Laponite grout penetrated from the fractures into the soil.

Effect of Boundary Condition

The interaction of a single-grout injection and the outer rigid boundary of the modified consolidometer is analogous to the injection of grout simultaneously at multiple points in a closely spaced grid, as shown in Fig. 14. The effect of the radial boundary condition was examined by injecting 5 ml of grout into modified consolidometers with different diameters (50 mm versus 100 mm). Fig. 15 shows that, for a given volume of grout, the reduction in the radial boundary size (i.e., grout spacing) was able to improve the final grout efficiency significantly when the OCR of the clay was between 1 and 2.

Finite-element simulations of balloon expansion tests were performed at two different radial size boundaries and Fig. 16 shows the comparison of final grout efficiencies calculated by finite element to those obtained in the experiments. Since the initial grout efficiency loss due to compression of tiny air bubbles does not occur in the finite-element analysis, the final grout efficiencies calculated by the finite-element analysis were consistently higher that the experimental data by about 10 to 20%.

Fig. 17 shows the computed excess pore pressures distributions along the horizontal line from the injection boundary for the 50 mm diameter and 100 mm diameter cases. The result indicates that a close radial boundary can limit the magnitude and extent of excess pore pressures zone effectively in normally consolidated or

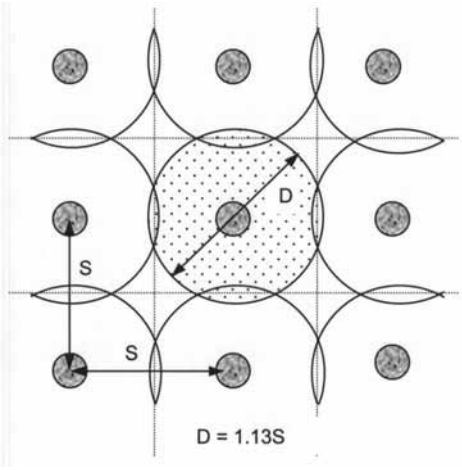

Fig. 14. Single injection with radial boundary condition

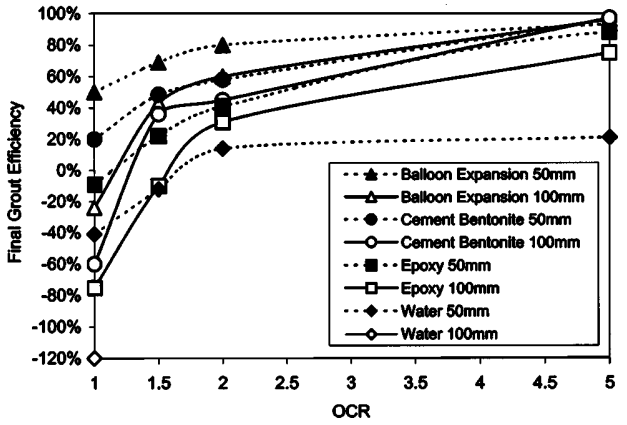

Fig. 15. Effect of radial boundary size on final grout efficiency

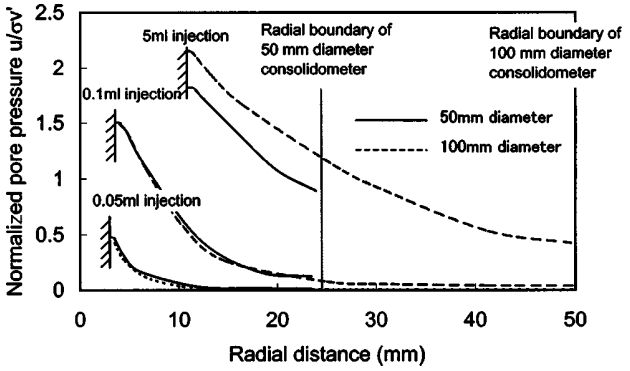

Fig. 17. Effect of radial boundary on excess pore pressure distribution

lightly overconsolidated clays which, in turn, increases the final grout efficiency. As a separate study, experiments to investigate the boundary effect as well as multiple grouting effect were performed and the discussion on these test results can be found in Au (2001).

Effect of Regrouting

It is common practice in compensation grouting to use a tube-a-manchette, which allows grout to be injected many times from the same port. If a given volume of grout is injected over a fixed area, it is possible to either regrout many times at the same point with small injection volumes, or conversely, perform a smaller number of regrouting processes but with larger injection volumes. Three tests were undertaken in normally consolidated clay specimens to investigate the effect of a waiting period on long-term grout efficiency after the regrouting process. In the experiment, an injection of 5 ml for each injection was made four times for the regrouting injection tests. The duration between each injection was varied ($T_s = 2$ min or 120 min). The test results were compared to the result of a single-injection test, which was carried out by injecting 20 ml at once. The rate of injection was fixed at 500 mm^3/s.

Fig. 18 shows that the single injection with large injection volume resulted in the best final grout efficiency. When regrouting was made, the behavior of the first injection was similar to the comparative part of the original injection. During the waiting period, consolidation occurred and more excess pore pressure was generated in the subsequent injections due to the previous consolidation effect. Therefore, the regrouting process resulted in smaller grout efficiency than for the single injection.

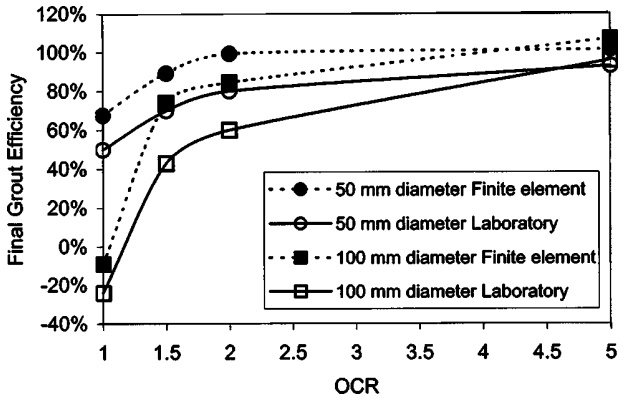

Fig. 16. Comparison of final grout efficiency computed by finite-element to that from the experiments

Conclusions

Laboratory grout injection tests were carried out to examine the effect of consolidation and grout properties on long-term grouting efficiency. The test results showed that the grout efficiency dramatically reduced with time for normally consolidated or lightly overconsolidated clays due to extensive shearing during the injection and the ultimate increase in mean effective pressure around the injection point caused by the injection pressure locked in when the grout solidified. For heavily overconsolidated clays, on the other hand, pore water migrated from the positive excess pore pressure zone around the injection point to the negative zone some distance away from the injection point, during the consolidation stage. The compression near the injection point and swelling at some distance away from the injection point resulted in a negligible consolidation effect for heavily overconsolidated clays.

The effect of bleeding and solid penetration on long-term consolidation was examined by injecting different types of grouts.

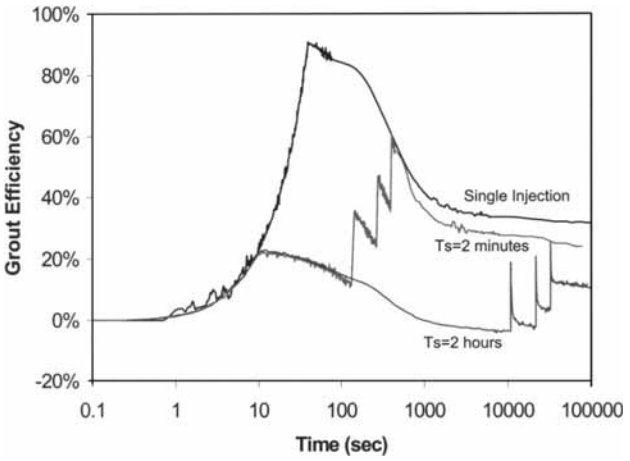

Fig. 18. Effect of waiting period (T_s) on grout efficiency

Water injection gave the lowest grout efficiency due to the drainage of the injected water as well as extensive positive pore pressures generated during the injection stage. The ideal compaction grouting tests (balloon expansion tests) resulted in the highest grout efficiency because of no bleeding/solid penetration effect. Hydrofracture grouting resulted in grout efficiency less than the balloon expansion tests due to the extensive shearing of the soil occurring around the fractures and various degrees of bleeding and solid penetration depending on the grout properties.

The effect of partial consolidation during the injection stage was examined by performing regrouting tests. The test results show that regrouting is not as effective as injecting the whole volume of grout in one effort due to extra consolidation effects. The grout efficiency increased when a smaller diameter consolidometer was used. This is because the outer radial boundary suppressed the magnitude and extent of excess pore pressure generation in the soil. This result suggests that grout efficiency can be improved if the spacing between injection ports were closer.

Although the tests identified some factors that affect the long-term efficiency of compensation grouting, the interpretation of the test data is limited by the scale of the laboratory tests. Further field trials are needed to examine the applicability of the findings to field scale conditions.

Acknowledgments

The work was supported by the European Commission under the BRITE-EURAM III program. The writers would like to thank Steve Chandler for the setup of the experimental apparatus and Professor Robert Mair (University of Cambridge) and Jean-Pierre Hamelin (Soletanche-Bachy, France) for their useful comments and suggestions.

References

Au, S. K. (2001). ''Fundamental study of compensation grouting in clay.'' PhD thesis, University of Cambridge, U.K.

Buchet, G., Soga, K., Gui, M. W., Bolton, M. D., and Hamelin, J. P. (1999). ''COSMUS; New methods for compensation grouting.'' *Proc., Association Francaise des Travaux en Souterrain (AFTES) International Conference UNDERGROUND WORKS—Ambitions and Realities*, October 25–28, 131–137.

Drammer, G. J. E., Travaes, P. D., and Drooff, E. R. (1994). ''Settlement protection works for new St. Clair river rail tunnel.'' *Can. Tunnelling*, 291–302.

Drooff, E. R., Travaes, P. D., and Forbes, J. (1995). ''Soil fracture grouting to remediate settlement due to soft ground tunnelling.'' *Proc., Rapid Excavation and Tunnelling Conf.*, Society for Mining Metallurgy and Exploration, San Francisco, 21–40.

Essler, R. D., Drooff, E. R., and Falk, E. (2000). ''Compensation grouting, concept, theory, and practice.'' Geotechnical Special Publication No. 104, American Society of Civil Engineers, 1–15.

Harris, D. I., Pooley, A. J., Menkiti, C. O., and Stephenson, J. A. (1996). ''Construction of low level tunnels below Waterloo Station with compensation grouting for Jubilee line extension.'' *Geotechnical aspects of underground construction in soft ground*, R. J. Mair and R. N. Taylor, eds., Balkema, Rotterdam, The Netherlands, 361–366.

Harris, D. I., Mair, R. J., Burland, J. B., and Standing, J. R. (1999). ''Compensation grouting to control tilt of Big Ben Clock Tower.'' *Geotechnical aspects of underground construction in soft ground*, O. Kusakabe, K. Fujita, and Y. Miyazaki, eds., Balkema, Rotterdam, The Netherlands, 225–232.

Ikeda, S., Saito, T., Huang, Y., and Mori, A. (1996). ''Settlement of storehouses during the passage of two parallel shields through.'' *Geotechnical aspects of underground construction in soft ground*, R. J. Mair and R. N. Taylor, eds., Balkema, Rotterdam, The Netherlands, 367–372.

Komiya, K., Soga, K., Akagi, H., Jafari, M. R., and Bolton, M. D. (2001). ''Soil consolidation associated with grouting during shield tunnelling in soft clayey ground.'' *Geotechnique*, 51(10), 835–847.

La Fonta, J. (1998). ''Puerto Rico real-time control of compensation grouting with the cyclops system.'' *Geotech. News*, 17(2), 27–32.

Mair, R. J., and Hight, D. W. (1994). ''Compensation grouting.'' *World Tunnelling*, November, 361–367.

McKinley, J. D. (1994). ''Grouted ground anchors and the soil mechanics aspects of cement grouting.'' PhD thesis, University of Cambridge, U.K.

Osborne, N., Murry, K., Chegini, A., and Harris, D. I. (1997). ''Construction of Waterloo Station upper level tunnels, Jubilee line extension project.'' *Proc., Tunnelling 97*, Institution of Mining and Metallurgy, London, 639–662.

Pototschnik, M. J. (1992). ''Settlement reduction of soil fracture grouting.'' *Proc., Conf., Soil Grouting, Soil improvement and Geosynthetics*, ASCE, 1, 398–409.

Schweiger, H. F., and Falk, E. (1998). ''Reduction of settlement by compensation grouting numerical studies and experience from Lisbon underground.'' *Proc., The World Tunnel Congress '98 on Tunnel and Metropolises*, Sao Paulo, April, A. Negro and A. A. Ferreira, eds., Vol. 2, 1047–1052.

Shirlaw, J. N. (1990). ''Ground treatment by injection in Hong Kong with special reference to the construction of the Hong Kong mass transit railway.'' MSc thesis, University of Bristol.

Shirlaw, J. N, Dazhi, W., Ganeshan, V., and Hoe, C. S. (1999). ''A compensation grouting trial in Singapore marine clay.'' *Geotechnical aspects of underground construction in soft ground*, O. Kusakabe, K. Fujita, and Y. Miyazaki, eds., Balkema, Rotterdam, The Netherlands, 149–154.

Soga, K., et al. (1999). ''Development of compensation grouting modelling and control system.'' *Geotechnical aspects of underground construction in soft ground*, O. Kusakabe, K. Fujita, and Y. Miyazaki, eds., Balkema, Rotterdam, The Netherlands, 425–430.

Sugiyama, T., et al. (1999). ''Compensation grouting at the Docklands Light Lewisham Extension project.'' *Geotechnical aspects of underground construction in soft ground*, O. Kusakabe, K. Fujita, and Y. Miyazaki, eds., Balkema, Rotterdam, The Netherlands, 319–324.

Journal of Geotechnical and Geoenvironmental Engineering
Volume 130, No.8
pp.883-886
August 2004
American Society of Civil Engineers

Discussion of "Factors Affecting Long-Term Efficiency of Compensation Grouting in Clays" by S. K. A. Au, K. Soga, M. R. Jafari, M. D. Bolton, and K. Komiya

March 2003, Vol. 129, No. 3, pp. 254–262.
DOI: 10.1061/(ASCE)1090-0241(2003)129:3(254)

Yu-jiong Chen[1]
[1]Senior Engineer, China Institute of Water Resources and Hydropower Research, 20 Chegongzhuangxi Rd., P.O. Box 366, Beijing 100044, China.

The discusser is very interested in the results presented in this paper, and would like to offer these comments on the authors' interpretation.

Inducement of Fracture Grouting

It is qualitatively known that thick grout tends to result in compaction grouting, and thin grout is likely to induce fracture grouting in clays. However, it is hard to define quantitatively the critical viscosity of the grout, because the mode of grouting depends upon some other factors, such as injection volume of grout per hole, rapidity of injection, overconsolidation ratio (OCR) of clay, and restriction of soil mass. Generally speaking, thin grout, large amounts of grout per hole, slow injection, high OCR, and less restriction of soil mass tend to result in fracture grouting. But it does not mean thick grout or small OCR is unable to induce fracture grouting, for instance, slowly injecting a small amount of thin grout results in fracture grouting under very small grouting pressure and fracture grouting may also occur in the same clay if a large amount of thick grout is injected into a hole.

The authors' test results, shown in their Fig. 11, evidently coincide with the previously mentioned experience. It can be seen in their Figs. 11(a and c) that thick grout resulted in compaction grouting while thin grout resulted in fracture grouting when other conditions were equal. Meanwhile, the comparison of Figs. 11(a and b) reveals that compaction grouting occurred in normally consolidated clay while fracture grouting occurred in overconsolidated clay when the same kind and amount of grout were used. It has been noticed in the field that compaction grouting sometimes becomes fracture grouting while the injection volume of grout is increasing and/or the grout viscosity is decreasing. After fracture grouting occurs, it will not change to compaction grouting again even if grout is thickened. Therefore, fracture grouting occurs more frequently in the field.

Process of Fracture Grouting

Hydraulic fracture usually occurs in the minor principal stress plane. Once fracture is induced, the grout will enter the fracture, and the rate of grout take will increase abruptly. At that time, if the rate of grout takes is larger than that of grout supply of pump, the grout pressure will drop simultaneously. However, the value of grout pressure will rebuild gradually with the increase of grout volume injected until the grout pressure acting on the fracture exceeds the original intermediate principal stress and a new fracture appears along an intermediate principal stress plane. After the grout enters the new fracture another grout vein is formed and the grout pressure drops again. As a result, a net of grout veins may form in soil mass. The lower the compressibility of the clay, the higher the restriction of soil mass, then the greater the stresses induced by the invading of grout veins and the sooner the formation of a net of grout vein.

Mechanism of Improvement

Fracture grouting is able to seal the cohesive fill of embankment dam and strengthen the foundation clay, but their mechanism is different. In dam grouting, grouting holes along the dam axis are usually drilled from the dam crest to near the bottom of the fill. When the grout pressure exceeds the minor principal stress in the dam near the hole, fracture occurs along the minor principal stress plane, which is a vertical plane parallel to the dam axis. Though the pressure of grout acting on the minor principal stress plane increases with grout take, the increment is very small because the fill of the dam is less restrained, and thus the stress increase due to the invading of a grout vein is small. Therefore, new fractures might not form along the plane other than the minor principal stress plane. If the dam is grouted in this way, a vertical mud wall consisting of overlapped grout veins will form along the dam axis (Chen and Zhang 1989). The mud wall as well as the grout intrusions in the cavities is capable of controlling seepage through the dam.

In the case of highly restrained soil mass such as foundation clay, the minor principal stress increases relatively rapidly with the increase of grout take, and a new fracture will form along the original intermediate principal stress plane. As a result, not only will the maximum shear stress decrease, but the principal stresses will increase substantially, the latter largely increases the mean normal stress and thus the stiffness of the foundation soil (Chen 1994). Meanwhile, the grout veins formed in foundation soil are not in the same orientation, the vertical component of the grout vein jack-up may compensate the foundation settlement.

Effect of Grout Viscosity and Soil Compressibility on Final Grout Efficiency

After completion of grouting work, the bleeding of the grout vein as well as the yielding and consolidation of clay near the grout veins results in not only the settlement, but also the decrease of stress in soil and thus the stiffness of foundation clay. Both reduce the grout efficiency until the stress induced by grouting reduces to a value, which could not induce further bleeding of grout and consolidation of clay. Since thick grout is less likely to bleed, the final grout efficiency should increase with the decrease of water–cement ratio, as shown in the original Fig. 10. On the other hand, since the clay, having higher OCR, is less likely to yield and consolidate, the final grout efficiency should increase with the rise of OCR, as shown in the original Fig. 15.

Effect of Stress State on Grout Vein Orientation and Final Grout Efficiency

The process of fractures formation generally depends upon the initial state of stress in a clay specimen. In a normally consolidated specimen (OCR=1), the minor principal stress plane is vertical, therefore, the grout vein formed at first is vertical, while in the overconsolidated specimen (OCR=2 or 5), the minor principal stress plane and grout vein become horizontal, as shown in Fig. 12.

The invading of a vertical grout vein significantly increases the lateral total stress because the lateral deformation is highly restricted by the rigid container of the specimen. As a result, significant consolidation and drop of grout efficiency with time occur in the normally consolidated clay specimen. While the invading of a horizontal grout vein in an overconsolidated clay specimen could only induce a small increment of the vertical stress, the vertical stress was mainly controlled by the dead weights placed at the top of the specimen and by a small amount of side friction between the specimen and the rigid container. Therefore, grouting can cause a very limited amount of consolidation and thus no significant drop in grout efficiency with time for overconsolidated clay. Though this explanation accords with the test results shown in the original Fig. 3(a), it may not be reasonable because Fig. 3(a) was based on balloon tests in which the shape of the balloon under the pressure of grout is usually considered to be spherical but not planar or nearly planar as assumed in the discusser's explanation. Therefore, the validity of the discusser's explanation depends upon the real shape of the cavity around the balloon after the test is observed by the authors. If the shape of the cavity was nearly planar or even elliptical, then the orientation of the fissure in the specimen changing gradually from horizontal to vertical, while its OCR, decreasing from 2 to 1, might be one of the factors causing the dramatic drop of final grouting efficiency between OCR 2 and 1, as shown in Figs. 9, 15, and 16.

Effect of Volume Proportion of Grout on Final Grout Efficiency

The volume proportion of grout to the soil to be treated, V_g/V_s, plays an important role in fracture grouting. High V_g/V_s may result in fracture rather than compaction grouting as discussed in the preceding paragraph. Moreover, high V_g/V_s also produces high final grout efficiency when the grouting mode is the same. In the authors' tests, the value of V_s is easily calculated and remains constant during the test. When equal amounts of grout are injected into 50 and 100 mm diameter specimens, the V_g/V_s value of a 50 mm diameter specimen is greater than that of a 100 mm diameter specimen, therefore, a 50 mm diameter specimen produces a higher final grout efficiency as shown in Fig. 15. Strictly speaking, the volume of grout V_g should indicate the volume of grout after bleeding when different grouts are used. Though the same amount of grouts was injected in the tests, the V_g of epoxy after bleeding might be the smallest, and the V_g for the balloon test would be the largest because of no bleeding. Therefore, the final grout efficiency of epoxy was the lowest and the balloon test was the highest as shown in Figs. 8 and 9.

It should be noted that the value of V_s of a single grouting hole in the field may not equal the volume of soil defined by the radial boundary of the hole as shown in Fig. 14. In other words, the values of V_s for each hole are different from each other. This is because once fracture occurs in foundation soil, the extension and widening of the fracture will not stop until the completion of grouting of the hole or formation of a new fracture. Sometimes fractures extend, far exceeding the center-to-center distance of grouting holes, especially for the initial holes that received a large amount of grout. Therefore, if an equal amount of grout is injected into each hole, the final grout efficiencies will be different, and the holes grouted in the early period usually will have a much lower efficiency.

On the contrary, the final grouting efficiency of each hole in the field may be relatively equal for compaction grouting because the V_s of each hole is nearly equal to the volume of soil defined by its radial boundary.

Negative Final Grout Efficiency

The grout efficiency was defined as the ratio of heaved volume to the initial injection volume. Therefore, the negative grout efficiency physically means grouting induces settlement instead of heave. The authors consider that the negative value of grout efficiency was caused by the compression of trapped air in the grout and by the consolidation of clay due to grouting. Since the compressibility of normally consolidated clay is higher than that of overconsolidated clay, and the consolidation pressure induced by grouting is higher in a normal consolidation clay specimen than in an overconsolidated clay specimen, the negative value is much higher for normally consolidated clay as shown in Figs. 15 and 8. This explanation is reasonable for the authors' test results, but if it is applied to the field grouting work, it will mean that fracture grouting usually causes settlement instead of heave in normally or lightly overconsolidated clay, and is only effective in heavily overconsolidated clay layers in foundation soil. This problem needs further study.

References

Chen, Y. J. (1994). "Principles and methods of compaction and fracturing grouting for foundation soil improvement." *Chinese J. Geotech. Eng.*, 16(2), 22–28 (in Chinese).

Chen, Y. J., and Zhang, S. L. (1989). "Test embankment dam of fracture grouting." *J. Geotech. Eng.*, 115(11), 1668–1672.

Closure to "Factors Affecting Long-Term Efficiency of Compensation Grouting in Clays" by S. K. A. Au, K. Soga, M. R. Jafari, M. D. Bolton, and K. Komiya

March 2003, Vol. 129, No. 3, pp. 254–262.
DOI: 10.1061/(ASCE)1090-0241(2003)129:3(254)

S. K. A. Au[1]; K. Soga[2]; M. R. Jafari[3]; M. D. Bolton[4]; and K. Komiya[5]

[1]Lecturer, City Univ. of Hong Kong, Dept. of Building and Construction, Hong Kong.
[2]Reader, Univ. of Cambridge, Engineering Dept., Cambridge CB2 1PZ, UK.
[3]Senior Geotechnical Engineer, STV Inc., New York, NY 10003.
[4]Professor, Univ. of Cambridge, Dept. of Engineering, Cambridge, CB2 1PZ, UK.
[5]Professor, Chiba Institute of Technology, Dept. of Civil Engineering, Chiba, Japan.

The writers thank the discusser for providing additional insights into the experimental data presented in the paper. Generally speaking, we support the discusser's comments and it appears there are no conflicting statements to our original discussion. However, the writers would like to clarify several points in response to the discusser's comments.

Inducement of Fracture Grouting

The writers agree with the discusser that the occurrence of different grouting modes are influenced by various factors including grout properties, soil properties, soil state, and injection methods. Possible interactions of these factors in relation to fracture initiation and orientation are discussed extensively in Au (2001). In particular, the effect of the injection rate is presented in Soga et al. (2003).

Process of Fracture Grouting

The process of soil fracturing by grouting deserves proper interpretation using theories of soil mechanics, rather than a simple conceptual interpretation made by the discusser. For instance, the "lower compressibility of the clay" should imply a heavily overconsolidated clay in which tensile fracture is possible by elastic deformation upon injection rather than plastic yielding. Normally consolidated clays yield at the early stage of the deformation and therefore it is difficult to see how plastic yielding initiates a fracture. A possible explanation is that the increase in a plastic shear failure zone creates shear bands or an unstable state around the injection cavity. This leads to a localized microscale crack and the injected fluid can penetrate into the crack to produce local tensile stresses at the crack tips.

Effect of Grout Viscosity and Soil Compressibility of Final Grout Efficiency

The discusser's statement implies that the change in stress induced by grouting controls grout bleeding and soil consolidation. This is not correct. The consolidation is caused by the excess pore pressures generated during injection. The change in grout-induced stress state is the outcome of stress relaxation associated with the bleeding and hardening of the grout as well as the change in effective stresses of the soil during consolidation rather than the cause as implied by the discusser.

The high final grout efficiencies measured in overconsolidated clay specimens are not only due to its large yield stress and less compressibility, but also due to interesting pattern of excess pore pressure generation and dissipation observed in Figs. 5 and 7. The negligible decrease in grout efficiency in the long-term for the overconsolidated clays is because (1) the compression due to dissipation of the positive excess pore pressures generated near the injection is small (more or less on the reloading line); and (2) the shear induced negative excess pore pressure away from the injection leads swelling as shown in Fig. 7.

Effect of Stress State on Grout Vein Orientation and Final Grout Efficiency

In order to heave the soil by vertical fractures, it is necessary to shear more volume of soil by higher pressures compared to the condition with horizontal fractures. Hence, a dramatic decrease in grout efficiency with time is observed in specimens with vertical fractures. The low grout efficiencies measured in the balloon expansion tests of the normally consolidated clay specimens are mainly due to dissipation of shear induced excess pore pressures.

Effect of Volume Proportion of Grout on Final Grout Efficiency

The writers consider that the ratio V_g/V_s given by the discusser can lead to unnecessary confusions when interpreting our data. As given in the paper, the grout efficiency is defined as the ratio of the heave volume achieved (i.e., volume *increment* of soil medium with injected grout) to the volume of injected grout. The soil volume is not considered at this stage. Once the heave volume is known, it is possible to consider this volume in relation to the volume of the treatment zone and decide whether the injection volume is enough or not to achieve the compensation effect. Hence, the grout efficiency and the soil volume should be treated separately. The effect of radial boundary on grout efficiency shown in Fig. 16 is therefore the consequence of the grouting process interacting with the radial boundary. It is not because of the differences in initial soil volume as stated by the discusser. As discussed in the original paper, the radial boundary effect can be considered to be equivalent to performing simultaneous multiple injections. Although the actual injection in the field does not resemble this process, the multiple injection tests presented in Soga et al. (2004) show that a better grout efficiency can be obtained by injecting grout at multiple locations simultaneously rather than sequentially. Further details of multiple grouting effects are given in Soga et al. (2004).

Negative Final Grout Efficiency

As presented in the introduction of the paper, there are several reported field cases in which the injection of grout in soft clay actually resulted in settlements in the long-term even though heave was achieved in the short-term. Hence, the negative efficiencies observed in our laboratory experiments do happen in the field as well.

In summary, fracture initiation in soil requires careful examination of interaction between pore fluid pressure and soil deformation as discussed in the paper and in this closure. However, the actual mechanisms of fracture development in a soil are considered to be more complex. They may involve plastic deformation at the crack tip, soil rate effects, penetration of injection fluid into the cracks, and permeation of injection fluid from cracks to the soil medium. If the clay is overconsolidated, the negative pore pressure generated by shearing in front of the crack may lead to cavitation and dry cracks can develop in front of penetrating injection fluid. Further investigation is needed.

References

Au, S. K. A. (2001). "Fundamental study of compensation grouting in clay." PhD thesis, Univ. of Cambridge, Cambridge, U.K.

Soga, K., Au, S. K. A., and Bolton, M. D. (2003). "Effect of injection rate on soil-grout behavior for compensation grouting." *Proc., Grouting and Grout Treatment, Geotechnical Special Publication No. 120*, Vol. 1, ASCE, Reston, Va., 845–856.

Soga, K., Au, S. K. A., Jafari, M. R., and Bolton, M. D. (2004). "Laboratory investigation of multiple grout injections into clay." *Geotechnique*, 54(2), 81–90.

付録

APPENDIX

2017 年 8 月 2 日、千葉工業大学の学長だった私は、千葉工業大学とチュラロンコン大学工学部との間で学生交流や共同研究等を行うための大学間交流協定締結の交渉のために、単身チュラロンコン大学を訪ねました。
チュラロンコン大学の学長や工学部長らとの交渉は友好的、成功裏に終始し、早期に協定締結のための準備を始めることになりました。
すると、交渉が終了した直ぐ後、同席していた若い准教授が、本書にある Géotechnique と ASCE の論文のコピーを私のところに持ってきて、論文に私のサインが欲しいと言いました。この予期せぬ嬉しいハプニングによって、会場は大いに盛り上がり、急遽論文へのサイニングセレモニーを行いました。

その後、2018 年 6 月 19 日にチュラロンコン大学にて、千葉工業大学とチュラロンコン大学工学部との間に大学間交流協定が締結されました。 私は、チュラロンコン大学工学部のためにもう一つのサインをしました。

令和 5 年 11 月 22 日
小 宮 一 仁

On 2nd August 2017, when I was serving as the president of Chiba Institute of Technology, I visited Chulalongkorn University alone, and I negotiated conclusion of a Memorandum of Understanding (MOU) between Chiba Institute of Technology (CIT) and Faculty of Engineering of Chulalongkorn University (Chula Engineering) for student exchange and joint research etc with the President and Deans of Chulalongkorn University.
My negotiations for the conclusion of the MOU were amicable and successful, and it was decided to begin preparations for the conclusion of the MOU as soon as possible.
Then, just after the negotiations were finished, a young associate professor, who was at the meeting, came up to me. He had copies of the Géotechnique and ASCE papers which were included in this book and he wanted my signature on these papers. Due to this unexpected and happy happening, the attendees of the meeting were very excited, and a signing ceremony was hurriedly held in which I signed the papers he had brought.

After that, on 19 June 2018, the MOU was signed between CIT and Chula Engineering. I have signed another for Chula Engineering in the MOU signing ceremony.

Kazuhito Komiya
22nd November 2023

2017 年 8 月 2 日のサイニングセレモニー
The signing ceremony on 2 August 2017

2018 年 6 月 19 日のサイニングセレモニー
The signing ceremony on 19 June 2018